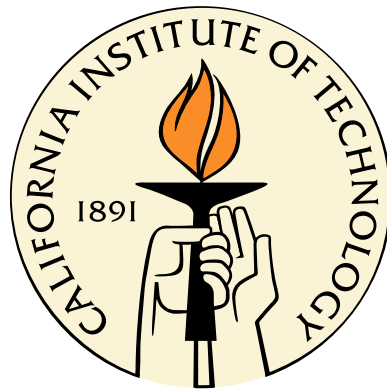# Cosmological Consequences of Dark Matter Interactions and Vacuum Fluctuations

Thesis by

Kimberly K. Boddy

In Partial Fulfillment of the Requirements

for the Degree of

Doctor of Philosophy



California Institute of Technology

Pasadena, California

2014

(Defended 21 May 2014)

To Tim, my love, for everything.

# Acknowledgments

First, I would like to thank my advisor, Sean Carroll, for taking a chance on an experimentalist gone astray. His door is always open, making it quite convenient to walk across the hall and start discussing research on a whim. He has an easygoing personality and showed great patience with all the physics nits that I insisted needed picking.

I want to thank the UCI crowd for the welcome they extended to me during my visits. Thanks in particular to Annika Peter, who is a wonderfully supportive and kindhearted person. The commutes to Irvine were significantly better with company! Also, thanks to my collaborators Jonathan Feng, Manoj Kaplinghat, and Tim Tait for all of their advice and guidance.

The friends and colleagues who have impacted both my physics work and my life outside of Caltech have given me an enormous amount of support and encouragement throughout the years. Most notably, Jonathan Arnold, Jenne Driggers, and Aaron Zimmerman are the ones with whom I took classes, studied for quals, discussed physics, competed to be the better TA, and spent countless hours hanging out outside of work. A tip of the hat to Nick Heinz—future DM and other half of our two-person book club—for always lending an ear. They are my buddy, pal, friend, and amigo. So team, what are we getting into later?

I am very appreciative of my parents, who provided the means for me to prioritize my academics while growing up and throughout college. They make a valiant effort to understand just what exactly it is that I do. Last but certainly not least, to my soon-to-be husband, Tim Hill: he has suffered me writing two theses now, has traveled back and forth across the country an absurd number of times for my sake, has listened to many of my research presentations (multiple times each), and is incredibly patient and supportive. He and our pup-dog, Baxter, mean the universe to me.

# Abstract

This thesis is divided into two parts: interacting dark matter and fluctuations in cosmology. There is an incongruence between the properties that dark matter is expected to possess between the early universe and the late universe. Weakly-interacting dark matter yields the observed dark matter relic density and is consistent with large-scale structure formation; however, there is strong astrophysical evidence in favor of the idea that dark matter has large self-interactions. The first part of this thesis presents two models in which the nature of dark matter fundamentally changes as the universe evolves. In the first model, the dark matter mass and couplings depend on the value of a chameleonic scalar field that changes as the universe expands. In the second model, dark matter is charged under a hidden $SU(N)$ gauge group and eventually undergoes confinement. These models introduce very different mechanisms to explain the separation between the physics relevant for freezeout and for small-scale dynamics.

As the universe continues to evolve, it will asymptote to a de Sitter vacuum phase. Since there is a finite temperature associated with de Sitter space, the universe is typically treated as a thermal system, subject to rare thermal fluctuations, such as Boltzmann brains. The second part of this thesis begins by attempting to escape this unacceptable situation within the context of known physics: vacuum instability induced by the Higgs field. The vacuum decay rate competes with the production rate of Boltzmann brains, and the cosmological measures that have a sufficiently low occurrence of Boltzmann brains are given more credence. Upon further investigation, however, there are certain situations in which de Sitter space settles into a quiescent vacuum with no fluctuations. This reasoning not only provides an escape from the Boltzmann brain problem, but it also implies that vacuum states do not uptunnel to higher-energy vacua and that perturbations do not decohere during slow-roll inflation, suggesting that eternal inflation is much less common than often supposed. Instead, decoherence occurs during reheating, so this analysis does not alter the conventional understanding of the origin of density fluctuations from primordial inflation.

# Contents

# List of Figures

# Part I

# Interacting Dark Matter

The standard model of cosmology describes a universe that is dominated by the vacuum energy $\Lambda$ and collisionless cold dark matter (CDM). The success of the $\Lambda$CDM model is based on its well-established record of describing the features of the large-scale structure observed in the universe. On smaller scales, however, the picture is much less clear. $N$-body simulations of collisionless CDM appear to disagree with observations on small scales (*e.g.*, the core-cusp problem, the missing-satellites problem, and the too-big-to-fail problem). These discrepancies motivate models of dark matter with properties that differ significantly from the standard paradigm.

The particle physics properties of dark matter are important for three distinct aspects of its behavior: they determine how the initial abundance of dark matter arose, they govern how the dark matter distribution evolves and influences structure formation, and they delineate the possible ways in which dark matter may be detected. Of course, these three roles are not typically independent, since they all depend on the prescribed interactions between the dark matter particles themselves and also between dark matter and the Standard Model (SM). These connections often provide a powerful motivation for particular dark matter candidates—for example, the freezeout abundance of weakly-interacting massive particles (WIMPs) points to new physics at the weak scale, which in turn leads to an attractive connection between dark matter and proposed solutions to the hierarchy problem, such as weak-scale supersymmetry. Although weak-scale annihilations of dark matter yield the observed relic abundance, weak dark matter interactions are negligible during structure formation, resulting still in the aforementioned discrepancies on small scales.

The particular solution to the small-scale structure problems we focus on here is to give the dark matter substantial interactions beyond the weak scale. Dark matter with mass $m_X$ may have large annihilation cross sections of $\langle \sigma v \rangle \sim 3 \times 10^{-19}(m_X/\text{GeV})$ cm$^3$/s, which soften halo cusps [1] (but do not address more recent astrophysical anomalies that can be explained with self-interacting dark matter). The clear obstacle to simple implementations of this idea is that the annihilation cross section is far too large to obtain the correct relic abundance, which requires a weak-scale cross section of $\langle \sigma v \rangle \sim 3 \times 10^{-27}$ cm$^3$/s. In Chapter 1, we consider a mechanism that allows the dark matter annihilation cross section to increase between freezeout and structure formation [2]. The dark matter properties depend on a "chameleon" scalar field, whose value in turn depends on the local matter density. As the universe expands, the matter density decreases and the scalar field value changes. By choosing appropriate forms for the effective potential of the chameleon, the dark matter annihilation and scattering cross sections may increase many orders of magnitude between freezeout and today.

Alternatively, if dark matter is self-interacting (able to scatter elastically with itself) [3–7], simulations show that the core sizes and central densities of dwarf spheroidal galaxies, low-surface-brightness spirals, and galaxy clusters can all be brought in line with observations [8–11]. Modifying $\Lambda$CDM to incorporate self-interacting dark matter (SIDM), sometimes called the $\Lambda$SIDM model, is

consistent with constraints from the Bullet Cluster, measurements of dark matter halo shapes, and subhalo survival requirements. To make the simulations and observations consistent, the ratio of the dark matter self-interaction cross section to its mass should be in the range $\sigma/m_X \sim 0.1$–$10$ cm$^2$/g. The requirement of such strong self-interactions eliminates from consideration all of the most studied dark matter candidates, including WIMPs, axions, and sterile neutrinos. However, these scattering cross sections are nuclear scale (1 cm$^2$/g $\simeq 1.78$ barn/GeV), while annihilations need to be weak scale for the correct relic abundance. In Chapter 2, we consider dark matter charged under a hidden non-abelian SU($N$) gauge symmetry [12]. In the early universe, the dark matter is an SU($N$)-charged particle that is able to satisfy the relic abundance constraint; in the late universe, the dark matter is a confined, composite particle that is able to have large interaction cross sections to satisfy the small-scale constraints.

# Chapter 1

# Dark Matter with Density-Dependent Interactions

## 1.1   Introduction

We explore the idea that the dark matter cross section might be much larger now than it was at freezeout, due to the evolution of a background field. In a cosmological context, the evolution of background fields can assert a significant influence on the properties of dark matter as a function of spatial location or cosmic epoch [13–22]. A straightforward way to achieve such effects is to invoke a light scalar field that interacts with dark matter and/or ordinary matter as well as through its own potential, and whose expectation value feeds into the dark matter properties. A popular scenario along these lines is the "chameleon mechanism," which acts to screen light, cosmologically-relevant degrees of freedom to protect them from precision local tests of gravity [23–27].

We consider dark matter that interacts through a gauge symmetry with a coupling constant that depends on a chameleonlike scalar field (the effects of chameleon vector bosons on laboratory experiments were considered in [28]). Just as the properties of a cosmologically-relevant scalar can be drastically modified in the presence of local density inhomogeneities or after evolving over cosmic time, so too may the interactions of dark matter be modified. We are able to find a model in which the late-time interaction strength is considerably higher than that at freezeout—although admittedly, this behavior does not seem generic.

We begin by reexamining the conventional story of dark matter freezeout according to the Boltzmann equation, but with the additional ingredient that the dark matter properties are evolving with time. We then look at specific models featuring a Dirac dark matter particle and a U(1) gauge symmetry that is spontaneously broken, along with a chameleon scalar field. We study the cosmological evolution of this coupled system and calculate the dark matter properties, including annihilation and scattering cross sections. Finally, we exhibit numerical solutions to a specific model, showing that the annihilation cross section can increase substantially during cosmic evolution.

## 1.2 The General Picture: Evolving Dark Matter in the Early Universe

Before discussing specific models, let us first consider how the usual story of dark matter freezeout might be modified if the annihilation cross section depends on the dynamics of another field. In the next section, we will explore Lagrangians that couple the dark matter to a scalar field that affects its interaction cross sections. For simplicity, we work in a flat Friedmann-Robertson-Walker (FRW) universe, described by the metric $ds^2 = -dt^2 + a^2(t) \times (dx^2 + dy^2 + dz^2)$, with scale factor $a(t)$.

The decoupling of dark matter takes place in the early universe in the radiation-dominated regime, in which particles with masses $m \ll T$ are the dominant component of the cosmic energy budget. To a good approximation, we may therefore ignore contributions from nonrelativistic species in thermal equilibrium, with the radiation and approximate the energy density as

$$\rho_{\mathrm{R}} = \frac{\pi^2}{30} g_* T^4 \tag{1.1}$$

and the entropy density as

$$s = \frac{2\pi^2}{45} g_{*S} T^3 \ , \tag{1.2}$$

where, as usual,

$$g_* = \sum_{i=\text{bosons}} g_i \left(\frac{T_i}{T}\right)^4 + \frac{7}{8} \sum_{i=\text{fermions}} g_i \left(\frac{T_i}{T}\right)^4 \tag{1.3}$$

$$g_{*S} = \sum_{i=\text{bosons}} g_i \left(\frac{T_i}{T}\right)^3 + \frac{7}{8} \sum_{i=\text{fermions}} g_i \left(\frac{T_i}{T}\right)^3 \tag{1.4}$$

and $g_i$ is the number of internal degrees of freedom for particle species $i$.

For $T \gtrsim 300$ GeV, $g_{*S} = g_* = 106.75$, which includes all particles in the SM. When $100$ MeV $\gtrsim T \gtrsim 1$ MeV, the electron and positron are relativistic, so $g_{*S} = g_* = 10.75$. At the temperature of the CMB today, $T_0 = 2.725$ K, $g_{*S,0} = 3.91$, and $g_{*,0} = 3.36$.

Consider a dark sector that was in thermal equilibrium with the visible sector at some very high temperature scale, below which they decouple effectively enough to consider each sector separately to be in equilibrium. The visible sector is at temperature $T$ with entropy density $s(T)$, while the dark sector is at temperature $T_d$ with entropy density $s_d(T_d)$. The expansion of the universe is governed by both sectors with

$$g_*^{\text{tot}}(T) = g_*(T) + g_*^d(T_d) \left(\frac{T_d}{T}\right)^4 \ , \tag{1.5}$$

but quantities in the dark sector (for example, the dark matter annihilation cross section and number

density) are determined by $T_d$ [29].

Since the entropy in each sector is conserved independently, the assumption that the two sectors were in equilibrium at some unification scale at time $t_u$ allows us to express the dark bath temperature in terms of the visible bath temperature at some later time $t$ via

$$\frac{g_{*S}^d(t)}{g_{*S}(t)}\frac{T_d^3(t)}{T^3(t)} = \frac{g_{*S}^d(t_u)}{g_{*S}(t_u)} \; . \tag{1.6}$$

All SM particles contribute at $t_u$ to give $g_{*S}(t_u) = 106.75$, and all dark particles contribute to $g_{*S}^d(t_u)$. In what follows, we will use the temperature of the visible sector and convert $T_d$ to $T$ as needed. For convenience we write

$$\xi(t) = \frac{T_d(t)}{T(t)} = \left(\frac{g_{*S}(t)}{g_{*S}^d(t)}\frac{g_{*S}^d(t_u)}{g_{*S}(t_u)}\right)^{1/3} \; . \tag{1.7}$$

The success of big bang nucleosynthesis (BBN) and the structure of the cosmic microwave background (CMB) power spectrum place tight bounds on any new relativistic degrees of freedom in the dark sector. The limit on the effective number of light neutrino species is $N_\nu = 3.24 \pm 1.2$ at the 95% confidence level (C.L.) [30], which gives

$$g_*^d \xi^4(t_{\text{BBN}}) = \frac{7}{8} \times 2 \times (N_\nu - 3) \leq 2.52 \quad (95\% \text{ C.L.}) \tag{1.8}$$

for 3 light SM neutrino species [31]. The 5-year WMAP data [32] also bounds the number of neutrino species by $N_\nu = 4.4 \pm 1.5$ at the 65% C.L., and the 7-year WMAP data [33] places a tighter lower limit of $N_\nu > 2.7$ at the 95% C.L.

### 1.2.1 The Boltzmann Equation

Let us assume the dark matter $\psi$ is a stable particle that annihilates with a thermalized annihilation cross section $\langle\sigma v\rangle$. The general Boltzmann equation governing the number density $n$ of a particle of mass $m$ is

$$\dot{n} + 3Hn + \langle\sigma v\rangle\,(n^2 - n_{\text{EQ}}^2) = 0 \; , \tag{1.9}$$

where $H$ is the Hubble parameter

$$H = \frac{\dot{a}}{a} = \sqrt{\frac{8}{3}\pi G\rho_R} = \sqrt{\frac{4\pi^3 G g_*^{\text{tot}}}{45}}\,T^2 \; , \tag{1.10}$$

$n_{\text{EQ}}$ is the equilibrium number density

$$n_{\text{EQ}} \approx \frac{g}{(2\pi)^3}\int d^3\vec{p}\, e^{-E/T_d} = \frac{g}{2\pi^2}m^2\xi T K_2\left(\frac{m}{\xi T}\right) \; , \tag{1.11}$$

and $K_2$ is the modified Bessel function of the second kind of order two. Generalizing the traditional treatment, we allow for the possibility that the mass of the dark matter $\tilde{m}_\psi(\phi)$ is a function of a real scalar chameleon field $\phi$, and denote $\phi$-dependent masses and couplings with a tilde.

It is convenient to scale out the effects of the expansion of the universe by defining

$$Y \equiv \frac{n_\psi}{s} \tag{1.12}$$

($n_\psi(x)$ and $Y(x)$ are taken to be independent of $\phi$) and to use a new independent variable, related to the cosmic time $t$ through

$$x(t) \equiv \frac{m_T}{T(t)} , \tag{1.13}$$

where $m_T$ is some constant mass scale. In the usual derivation, $m_T$ is chosen to coincide with the dark matter mass; however, since our dark matter has varying mass, we use this constant parameter instead. Defining

$$b = \sqrt{\frac{45}{4\pi^3 G}} \frac{1}{m_T} \tag{1.14}$$

allows us to write

$$\frac{dx}{dt} = \frac{m_T}{bx} \sqrt{g_*^{\text{tot}}} , \tag{1.15}$$

which can be used to rewrite the Boltzmann equation for the dark matter as

$$Y'(x) + \frac{B}{x^2}(Y^2 - Y_{\text{EQ}}^2) = 0 . \tag{1.16}$$

Here a prime denotes a derivative with respect to $x$, and

$$B = \langle \sigma v \rangle \frac{2\pi^2}{45} \frac{g_{*S}}{\sqrt{g_*^{\text{tot}}}} b m_T^2 , \tag{1.17}$$

which may depend implicitly on $\phi$ in our model via a $\phi$ dependence in the cross section. Note that, in terms of these new variables, the equilibrium term is

$$Y_{\text{EQ}} = \frac{45g}{(2\pi^2)^2 g_{*S}} \left(x \frac{\tilde{m}_\psi(\phi)}{m_T}\right)^2 \xi K_2 \left(\frac{x}{\xi} \frac{\tilde{m}_\psi(\phi)}{m_T}\right) , \tag{1.18}$$

with $g = 2$ for Dirac dark matter.

At this level, it remains to specify $Y(x_i)$, the initial condition for $Y$. We consider $\Delta \equiv Y - Y_{\text{EQ}}$, the departure from equilibrium, which obeys [34]

$$\Delta' = -Y_{\text{EQ}}' - \frac{B}{x^2}\Delta(2Y_{\text{EQ}} + \Delta) . \tag{1.19}$$

At early times $(1 < x \ll x_f)$, $Y$ tracks $Y_{\text{EQ}}$ extremely closely such that $\Delta$ and $|\Delta'|$ are small. Note

that in the non-relativistic approximation, $T \ll \tilde{m}_\psi(\phi)$,

$$Y_{\text{EQ}} \sim x^{3/2} e^{-(x/\xi)(\tilde{m}_\psi(\phi)/m_T)} \; , \tag{1.20}$$

so $Y_{\text{EQ}}'/Y_{\text{EQ}} \approx -\tilde{m}_\psi(\phi)/\xi m_T$ and $\Delta' \approx 0$. Thus, the required initial condition is

$$Y(x_i) = Y_{\text{EQ}}(x_i) + \frac{x_i^2 \tilde{m}_\psi(\phi_i)}{2B\xi m_T} \; , \tag{1.21}$$

where $B(\phi_i)$ and $\tilde{m}_\psi(\phi_i)$ are evaluated at the initial value $\phi_i = \phi(x_i)$.

After the freezeout value $x_f$, $Y(x)$ will asymptotically approach a constant value $Y_\infty$. The energy density of non-relativistic dark matter today is then

$$\begin{aligned} \rho_0 &= \tilde{m}_\psi(\phi_0) n_\psi(x_0) = \tilde{m}_\psi(\phi_0) Y_\infty s_0 \\ &= \tilde{m}_\psi(\phi_0) Y_\infty \frac{2\pi^2}{45} g_{*S,0} T_0^3 \; . \end{aligned} \tag{1.22}$$

Having generalized the usual treatment of dark matter as a fluid to the case in which there is a chameleon field determining the dark matter properties, we now turn to specific examples of particle physics models in which these phenomena might arise.

## 1.3 Gauged Dark Matter

Consider dark matter to consist of a Dirac fermion $\psi$, charged under a dark U(1) gauge group with gauge boson $A_\mu$, and a dark Higgs field $\Phi$ that spontaneously breaks the U(1). We also introduce a chameleonlike field $\phi$ that is a real scalar field with properties that depend on the dark matter energy density. The chameleon couples to the other particles in the dark sector by entering into the dark matter mass $\tilde{m}_\psi(\phi)$, the U(1) coupling $\tilde{f}(\phi)$, and other couplings described below. We consider only an isolated dark sector so that we may investigate the properties of this simple model without the complications of coupling to the visible sector.

### 1.3.1 A Toy Model for Varying Coupling

As a first step, let us consider the QED Lagrangian with a real scalar field $\phi$, but in which we allow the coupling constant $e$ to vary as a function of spacetime [35]. Specifically, it can vary as a function of $\phi$. Let us write the new coupling as $\tilde{f}(\phi)$. The Lagrangian is

$$\mathcal{L}_{\text{QED}\phi} = -\frac{1}{2} \partial_\mu \phi \partial^\mu \phi - V(\phi) - \frac{1}{4\tilde{f}^2(\phi)} F^{\mu\nu} F_{\mu\nu} + i\bar{\psi}\slashed{\partial}\psi - m_\psi \bar{\psi}\psi - \bar{\psi}\gamma^\mu \psi A_\mu \; , \tag{1.23}$$

where $F_{\mu\nu} = \partial_\mu A_\nu - \partial_\nu A_\mu$. Making the redefinition $A_\mu \to \tilde{f}(\phi) A_\mu$, we obtain

$$\mathcal{L}_{\text{QED}\phi} = -\frac{1}{2}\partial_\mu\phi\partial^\mu\phi - V(\phi) + i\bar{\psi}\slashed{\partial}\psi - m_\psi\bar{\psi}\psi - \tilde{f}(\phi)\bar{\psi}\gamma^\mu\psi A_\mu - \frac{1}{4\tilde{f}^2}\left[\partial^\mu(\tilde{f}A^\nu) - \partial^\nu(\tilde{f}A^\mu)\right]^2 . \quad (1.24)$$

Both Lagrangians are equivalent, but now the gauge transformation reads

$$\tilde{f}(\phi)A_\mu \to \tilde{f}(\phi)A_\mu + \partial_\mu\omega \quad (1.25\text{a})$$

$$\psi \to e^{-i\omega}\psi \quad (1.25\text{b})$$

$$\bar{\psi} \to e^{+i\omega}\bar{\psi} . \quad (1.25\text{c})$$

If we can neglect factors of $(\partial_\mu\tilde{f}/\tilde{f})$ compared to all other mass scales in the theory (except the Planck mass), then the Lagrangian simplifies to the approximately gauge-invariant form

$$\mathcal{L}_{\text{QED}\phi} \approx -\frac{1}{2}\partial_\mu\phi\partial^\mu\phi - V(\phi) - \frac{1}{4}F^{\mu\nu}F_{\mu\nu} + i\bar{\psi}\slashed{\partial}\psi - m_\psi\bar{\psi}\psi - \tilde{f}(\phi)\bar{\psi}\slashed{A}\psi \quad (1.26)$$

with U(1) current

$$j^\mu(x) = \tilde{f}(\phi)\bar{\psi}\gamma^\mu\psi . \quad (1.27)$$

## 1.3.2 The Cosmological Equations of Motion

We now include gravity and a complex dark Higgs field $\Phi$ to break the U(1) symmetry and to give the dark gauge field a mass. We allow for a varying dark matter mass by using the effective mass parameter $\tilde{m}_\psi(\phi)$, and in the spirit of effective field theory, we also allow all couplings [not just the U(1) coupling $\tilde{f}(\phi)$] to depend on $\phi$.

Neglecting factors of $(\partial_\mu\tilde{f}/\tilde{f})$, the action is

$$S \approx \int d^4x\sqrt{-g}\left[\frac{\mathcal{R}}{16\pi G} - \frac{1}{2}g^{\mu\nu}\nabla_\mu\phi\nabla_\nu\phi - V(\phi) - (D_\mu\Phi)^\dagger D^\mu\Phi - V_0(\Phi)\right.$$
$$\left. - \frac{1}{4}F^{\mu\nu}F_{\mu\nu} + i\bar{\psi}\slashed{D}\psi - \tilde{m}_\psi(\phi)\bar{\psi}\psi\right] , \quad (1.28)$$

where the gauge covariant derivative is $D_\mu = \nabla_\mu + i\tilde{f}(\phi)A_\mu$. The equations of motion for the fields are

$$\left(i\slashed{D} - \tilde{m}_\psi(\phi)\right)\psi = 0 \quad (1.29)$$

$$\Box\phi - V'(\phi) - \tilde{m}'_\psi(\phi)\bar{\psi}\psi - \tilde{f}'(\phi)\bar{\psi}\slashed{A}\psi = 0 , \quad (1.30)$$

where a prime denotes differentiation with respect to $\phi$. Let us assume that the universe is dark-charge symmetric, so the average charge current density is negligible compared to the dark matter

number density [see (1.34) below]. Thus, the term proportional to $\tilde{f}'/\tilde{f}$ should be small compared to the one containing $\tilde{m}'/\tilde{m}$, given that $\tilde{f}'/\tilde{f} \sim \tilde{m}'/\tilde{m}$ to within a few orders of magnitude—a condition we will enforce later. We may write this last equation as

$$\Box\phi - V'(\phi) - \tilde{m}'_\psi(\phi)\bar{\psi}\psi \approx 0 \ . \tag{1.31}$$

We calculate the energy-momentum tensor for $\psi$ by varying the action with respect to the metric. Taking care to correctly handle the nontrivial metric dependence of the covariant derivative [36], we have

$$T^{(\psi)}_{\mu\nu} = -\frac{i}{2}\left[\bar{\psi}\gamma_{(\mu}\nabla_{\nu)}\psi - (\nabla_{(\mu}\bar{\psi})\gamma_{\nu)}\psi\right] + \tilde{f}(\phi)\bar{\psi}\gamma_{(\mu}A_{\nu)}\psi \ , \tag{1.32}$$

where we have integrated by parts and used the field equation of motion. Taking the trace, we obtain

$$\begin{aligned}
g^{\mu\nu}T^{(\psi)}_{\mu\nu} &= -\frac{i}{2}\left[\bar{\psi}\overset{\rightarrow}{\nabla}\!\!\!\!/\,\psi - \bar{\psi}\overset{\leftarrow}{\nabla}\!\!\!\!/\,\psi\right] + \tilde{f}(\phi)\bar{\psi}A\!\!\!/\psi \\
&= -\frac{1}{2}\left[\bar{\psi}i(\overset{\rightarrow}{\nabla}\!\!\!\!/ + i\tilde{f}(\phi)A\!\!\!/)\psi - \bar{\psi}i(\overset{\leftarrow}{\nabla}\!\!\!\!/ - i\tilde{f}(\phi)A\!\!\!/)\psi\right] \\
&= -\tilde{m}_\psi(\phi)\bar{\psi}\psi \ ,
\end{aligned} \tag{1.33}$$

where again we have used the Dirac equation for $\psi$ and $\bar{\psi}$ to obtain the last line. If we model the dark matter as nonrelativistic dust, its pressure is zero, and the trace of the stress tensor is approximately given by $-\rho_\psi$. Thus,

$$\rho_\psi = \tilde{m}_\psi(\phi)\bar{\psi}\psi \ . \tag{1.34}$$

As a final step in this section, we use this result to rewrite the $\phi$ equation of motion (1.31) as

$$\Box\phi - V'_{\text{eff}}(\phi) = 0 \ , \tag{1.35}$$

where the effective potential is

$$\begin{aligned}
V_{\text{eff}} &= V(\phi) + \tilde{m}_\psi(\phi)n_\psi \\
&= V(\phi) + \tilde{m}_\psi(\phi)Y(x)\frac{2\pi^2}{45}g_{*S}\left(\frac{m_T}{x}\right)^3 \ .
\end{aligned} \tag{1.36}$$

## 1.4   Chameleon Behavior

With a complete model in place, we now turn to a detailed investigation of the dynamics. We first examine the chameleon field, which is central to the effect we seek. Assuming that $\phi$ is homogeneous

and isotropic, the equation of motion becomes

$$\ddot{\phi} + 3H\dot{\phi} + V'(\phi) + \tilde{m}'_\psi(\phi)n_\psi = 0 \ . \tag{1.37}$$

It is convenient for seeking numerical solutions to work with a dimensionless variable

$$P \equiv \frac{\phi}{m_T} \tag{1.38}$$

and to use $x$ as our independent variable. The equation of motion is then

$$P''(x) + \frac{2}{x}P'(x) + \frac{b^2 x^2}{m_T^3 g_*^{\text{tot}}} \frac{dV}{d\phi}\bigg|_{\phi=Pm_T} + \frac{2\pi^2 b^2}{45x} \frac{g_{*S}}{g_*^{\text{tot}}} \frac{d\tilde{m}_\psi}{d\phi}\bigg|_{\phi=Pm_T} Y(x) = 0 \ . \tag{1.39}$$

We choose the initial conditions for $\phi$ to begin at the minimum of its effective potential and to move with the same initial velocity as the changing minimum. The minimum $\phi_{\text{min}}$ solves the equation $V'_{\text{eff}}(\phi_{\text{min}}) = 0$, so one of the initial conditions for this equation can be obtained by evaluating this expression at $x_i$, using the relevant value for $Y(x_i)$ from (1.21). Furthermore, since $\phi_{\text{min}}$ is a function of $x$, the initial velocity is found simply by taking a derivative and using the Boltzmann equation to obtain the relevant value for $Y'(x_i)$.

### 1.4.1 Exponential Potentials

Our goal here is to work out a single example model that exhibits the effects we are investigating, while at the same time remaining compatible with experimental constraints. For simplicity, we will choose exponential functions, which also have the nice feature that observables approach a fixed asymptotic value at late times.

With these comments in mind, we therefore choose the form of the effective potential and U(1) coupling to be

$$V(\phi) = \Lambda^4 e^{-\phi/m_1} \tag{1.40a}$$

$$\tilde{m}_\psi(\phi) = m_\psi \left(1 - A_2 e^{-\phi/m_2}\right) \tag{1.40b}$$

$$\tilde{f}(\phi) = e \left(1 + A_3 e^{-\phi/m_3}\right)^{-3} , \tag{1.40c}$$

where $\Lambda$ and $m_\psi$ are constants with dimensions of mass, and $e$ and $A_2$, $A_3 > 0$ are dimensionless. The term with $A_2$ is necessary to incorporate the properties of $\psi$ into the equation of motion for $\phi$. The possibility for $A_3 = 0$ (constant gauge coupling) is viable, but we are specifically interested in increasing the cross section for $\psi$ as the universe expands. We choose this form for $\tilde{f}$ so that both the annihilation and scattering cross sections, which we calculate below, increase with time.

The largest energies of the particles in our theory are of order $m_\psi$ for nonrelativistic dark matter, since all other particles should be lighter than the dark matter to allow for annihilation. We therefore require $m_2$, $m_3 \gg m_\psi$ to suppress higher-dimensional operators involving derivatives of $\tilde{m}_\psi$ and $\tilde{f}$ when we expand the action. Additionally, we need $m_1 \gtrsim \Lambda$ to suppress higher-dimensional operators in the self-couplings of $\phi$.

The effective potential in (1.36) is now

$$V_{\text{eff}}(\phi) = \Lambda^4 e^{-\phi/m_1} + m_\psi(1 - A_2 e^{-\phi/m_2})Y(x)\frac{2\pi^2}{45}g_{*S}\left(\frac{m_T}{x}\right)^3 \ , \tag{1.41}$$

possessing a critical point at

$$\phi_{\text{min}} = -\frac{m_1 m_2}{m_2 - m_1}\ln\left(A_2\frac{m_1}{m_2}\frac{m_\psi m_T^3}{\Lambda^4}\frac{Y}{x^3}\right) \ , \tag{1.42}$$

which is real and finite. In order to generate a mass for the excitations of $\phi$, we require this critical point to be a minimum, which holds for $m_2 > m_1$. The minimum moves with a speed

$$\frac{d\phi_{\text{min}}}{dx} = -\frac{m_1 m_2}{m_2 - m_1}\left(Y\frac{dY}{dx} - \frac{3}{x}\right) \ , \tag{1.43}$$

which is positive ($\phi_{\text{min}}$ increases with $x$). Finally, we identify the initial conditions for $\phi$:

$$\phi(x_i) = -\frac{m_1 m_2}{m_2 - m_1}\ln\left(A_2\frac{m_1}{m_2}\frac{m_\psi m_T^3}{\Lambda^4}\frac{Y(x_i)}{x_i^3}\right) \ , \tag{1.44}$$

$$\frac{d\phi}{dx}(x_i) = -\frac{m_1 m_2}{m_2 - m_1}\left(Y(x_i)\frac{dY}{dx}(x_i) - \frac{3}{x_i}\right)$$

$$= \frac{m_1 m_2}{m_2 - m_1}\left(\frac{3}{x_i} + \frac{\tilde{m}_\psi}{\xi m_T}\frac{Y_{\text{EQ}}(x_i) + (x_i^2\tilde{m}_\psi)/(4B\xi m_T)}{Y_{\text{EQ}}(x_i) + (x_i^2\tilde{m}_\psi)/(2B\xi m_T)}\right) \ . \tag{1.45}$$

To ensure $\tilde{m}_\psi > 0$, we require $\phi > m_2\ln(A_2)$ for all $\phi$ relevant for our calculation.

## 1.4.2 An Attractor Solution

A particularly interesting and simple possible evolution for the chameleon field is for it to begin at the minimum of the effective potential, and then to adiabatically track this minimum as it evolves cosmologically. This attractor solution [37] is achieved if the physical mass of the chameleon satisfies

$$m_{\phi,\text{ph}} = \sqrt{V''_{\text{eff}}(\phi_{\text{min}})} \gg H \ . \tag{1.46}$$

If (1.46) holds during radiation dominance, when

$$H_R = \frac{m_T}{b}\sqrt{g_*^{\text{tot}}}x^{-2} \ , \tag{1.47}$$

we can then avoid solving the coupled differential equations (1.16) and (1.37) and simply use the expression for $\phi_{\min}$ for the evolution of $\phi$. Similarly, if (1.46) holds during matter domination, when

$$H_M = H_0 \left( \frac{x_0}{x} \right)^{3/2} \, , \tag{1.48}$$

then we can easily determine $\phi_0$, the value of $\phi$ today, which is needed to calculate the values of the $\phi$-dependent parameters today.

Under the approximation that $m_2 \gg m_1$,

$$\tilde{m}_{\phi,\mathrm{ph}} \approx \left( A_2 \frac{2\pi^2}{45} \frac{m_\psi m_T^3}{m_1 m_2} \right)^{1/2} Y^{1/2} g_{*S}^{1/2} x^{-3/2} \, . \tag{1.49}$$

It follows that $H_R$ decreases more rapidly than $\tilde{m}_{\phi,\mathrm{ph}}$ with time, whereas during matter domination, $H_M$ and $\tilde{m}_{\phi,\mathrm{ph}}$ have the same $x$ dependence. We will verify later that these attractor solutions exist by numerically solving all the relevant equations of motion.

## 1.5 Particle Physics Interactions and Constraints

In the adiabatic regime described above, we now have all the ingredients necessary to understand the cosmological evolutions of the fields. We next turn to the particle physics phenomenology of the model. To do so, we rewrite the action (1.28) without gravity to give the Lagrangian

$$\begin{aligned}
\mathcal{L} \approx &-\frac{1}{2}\partial_\mu \phi \partial^\mu \phi - V(\phi) - (D_\mu \Phi)^\dagger (D^\mu \Phi) - V_0(\Phi) \\
&-\frac{1}{4}F^{\mu\nu}F_{\mu\nu} + i\bar{\psi}\slashed{\partial}\psi - \tilde{m}_\psi(\phi)\bar{\psi}\psi - \tilde{f}(\phi)\bar{\psi}\slashed{A}\psi \, ,
\end{aligned} \tag{1.50}$$

where $D_\mu = \partial_\mu + i\tilde{f}(\phi)A_\mu$.

### 1.5.1 Breaking the Dark U(1) Symmetry

The potential of the dark Higgs field $\Phi$ is chosen so that this field acquires a vacuum expectation value (VEV)

$$\langle 0|\Phi(x)|0\rangle = \frac{\mathsf{v}}{\sqrt{2}} \, . \tag{1.51}$$

Decomposing $\Phi$ into two real scalar fields via

$$\Phi(x) = \frac{1}{\sqrt{2}}(\mathsf{v} + h(x))e^{-i\chi(x)/\mathsf{v}} \, , \tag{1.52}$$

we can then use unitary gauge $\chi(x) = 0$ to rewrite the kinetic term for $\Phi$ as

$$-(D_\mu \Phi)^\dagger D^\mu \Phi = -\frac{1}{2}\partial^\mu h \partial_\mu h - \frac{1}{2}\tilde{f}^2(\phi)(\mathsf{v}+h)^2 A^\mu A_\mu \ . \tag{1.53}$$

The Goldstone boson is eaten to give the dark U(1) gauge boson a mass, $\tilde{M}_A(\phi) = \tilde{f}(\phi)\mathsf{v}$. A typical choice for the dark Higgs potential is

$$V_0(\Phi) = \frac{1}{4}\tilde{\lambda}_h(\phi) \left[ \Phi^\dagger \Phi - \frac{1}{2}\mathsf{v}^2 \right]^2 \ , \tag{1.54}$$

which, when expanded about the VEV, yields

$$V_0(h) = \frac{1}{4}\tilde{\lambda}_h(\phi)\mathsf{v}^2 h^2 + \frac{1}{4}\tilde{\lambda}_h(\phi)\mathsf{v}h^3 + \frac{1}{16}\tilde{\lambda}_h(\phi)h^4 \ . \tag{1.55}$$

The mass of the physical dark Higgs particle $h$ is therefore

$$\tilde{m}_h(\phi) = \sqrt{\frac{\tilde{\lambda}_h(\phi)}{2}}\mathsf{v} \ , \tag{1.56}$$

and we see that the masses of the $A$ and $h$ fields are then related by

$$\tilde{M}_A(\phi) = \tilde{f}(\phi)\sqrt{\frac{2}{\tilde{\lambda}_h(\phi)}}\tilde{m}_h(\phi) \ . \tag{1.57}$$

Since the relative sizes of $\tilde{f}(\phi)$ and $\tilde{\lambda}_h(\phi)$ are unrestricted, in principle the relative masses of $A$ and $h$ are not fixed. However, in order to simplify the analysis, we will impose the hierarchy $\tilde{m}_h(\phi) > 2\tilde{M}_A(\phi)$ for all relevant $\phi$ so that $h$ has a tree-level decay channel to $A$.

Our Lagrangian at this stage is

$$\begin{aligned}
\mathcal{L} = &-\frac{1}{2}\partial_\mu\phi\partial^\mu\phi - V(\phi) - \frac{1}{2}\partial_\mu h\partial^\mu h - \frac{1}{4}\tilde{\lambda}_h(\phi)\mathsf{v}^2 h^2 - \frac{1}{4}\tilde{\lambda}_h(\phi)\mathsf{v}h^3 - \frac{1}{16}\tilde{\lambda}_h(\phi)h^4 \\
&-\frac{1}{4}F^{\mu\nu}F_{\mu\nu} - \frac{1}{2}\tilde{M}_A^2(\phi)A^\mu A_\mu + i\bar{\psi}\slashed{\partial}\psi - \tilde{m}_\psi(\phi)\bar{\psi}\psi - \tilde{f}(\phi)\bar{\psi}\gamma^\mu A_\mu\psi \\
&-\frac{1}{4}\left[2\tilde{f}^2(\phi)\right]h^2 A^\mu A_\mu - \frac{1}{2}\left[2\tilde{f}(\phi)\tilde{M}_A(\phi)\right]hA^\mu A_\mu \ .
\end{aligned} \tag{1.58}$$

What remains is to incorporate the fact that $\phi$ is adiabatically tracking the minimum of its effective potential. We expand $\phi(x) = \phi_c(t) + \eta(x)$ around its classical value and recall that $m_2$ and $m_3$ are
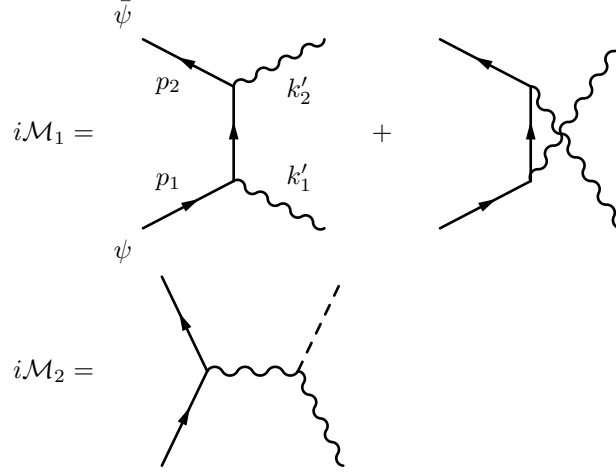
Figure 1.1: Tree-level $\psi$ annihilation diagrams. The massive vector boson $A$ is a wavy line, and the scalar $h$ is a dashed line. Annihilations to $A + A$ and $h + h$ via $\eta$-exchange and annihilations to final-state $\eta$ particles are suppressed by large-mass factors.

sufficiently large to suppress irrelevant terms of $\mathcal{O}(\eta)$ or higher. The Lagrangian (1.58) becomes

$$
\begin{aligned}
\mathcal{L} = &-\frac{1}{2}\partial_\mu\eta\partial^\mu\eta - \frac{1}{2}\partial_\mu h\partial^\mu h - \frac{1}{4}F^{\mu\nu}F_{\mu\nu} + i\bar{\psi}\slashed{\partial}\psi - \left[V(\phi_c) + \frac{1}{2}V''(\phi_c)\eta^2 + \mathcal{O}(\eta^3)\right] \\
&-\frac{1}{4}\left[\tilde{\lambda}_h(\phi_c) + \mathcal{O}(\eta)\right]\mathsf{v}^2 h^2 - \frac{1}{6}\left[\frac{3}{2}\tilde{\lambda}_h(\phi_c) + \mathcal{O}(\eta)\right]\mathsf{v}h^3 - \frac{1}{24}\left[\frac{3}{2}\tilde{\lambda}_h(\phi_c) + \mathcal{O}(\eta)\right]h^4 \\
&-\frac{1}{2}\left[\tilde{M}_A^2(\phi_c) + \mathcal{O}(\eta)\right]A^\mu A_\mu - \left[\tilde{f}(\phi_c) + \mathcal{O}(\eta)\right]\bar{\psi}\gamma^\mu A_\mu\psi \\
&-\left[\tilde{m}_\psi(\phi_c) + \tilde{m}'_\psi(\phi_c)\eta + \mathcal{O}(\eta^2)\right]\bar{\psi}\psi \\
&-\frac{1}{4}\left[2\tilde{f}^2(\phi_c) + \mathcal{O}(\eta)\right]h^2 A^\mu A_\mu - \frac{1}{2}\left[2\tilde{f}(\phi_c)\tilde{M}_A(\phi_c) + \mathcal{O}(\eta)\right]hA^\mu A_\mu .
\end{aligned}
\tag{1.59}
$$

## 1.5.2   The Dark Matter Annihilation Cross Section

Our central goal is to understand how the dependence of dark matter cross sections on the chameleon field changes the standard dark matter creation, evolution, and detection story. To this end, we next turn to the calculation of the dark matter annihilation cross section. The relevant Feynman rules can be found in Appendix 1.A.

We assume that the dark matter is the heaviest particle in the dark sector, such that $\tilde{m}_\psi \gg \tilde{m}_h$, $\tilde{M}_A$. Then, the lowest order, tree-level processes for $2 \to 2$ dark matter annihilation are shown in Fig. 1.1, and their amplitudes are

$$
\mathcal{M}_1 = i\epsilon_{1'}^\mu\epsilon_{2'}^\nu\bar{v}_2\left[\tilde{f}^2(\phi_c)\left(\gamma_\nu\Delta_\psi(p_1 - k_1')\gamma_\mu + \gamma_\mu\Delta_\psi(p_1 - k_2')\gamma_\nu\right)\right]u_1
\tag{1.60a}
$$

$$
\mathcal{M}_2 = i\epsilon_{1'\nu}\bar{v}_2\tilde{f}^2(\phi_c)\tilde{M}_A(\phi_c)\gamma_\mu\Delta_A^{\mu\nu}(p_1 + p_2)u_1 .
\tag{1.60b}
$$
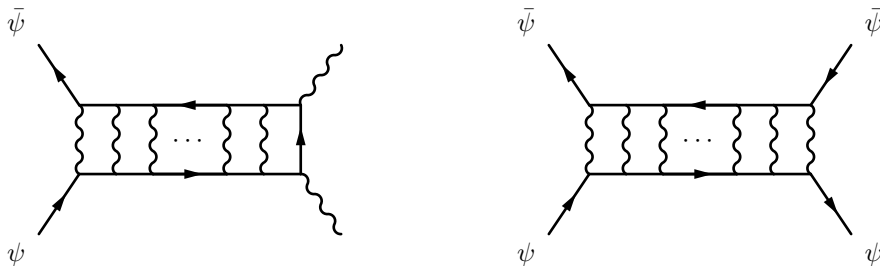
Figure 1.2: Ladder diagrams for dark matter annihilation (left) and scattering (right).

Working in the center-of-mass frame and in the nonrelativistic limit, we obtain

$$\sigma_1 v \approx \frac{\tilde{f}^4(\phi_c)}{16\pi \tilde{m}_\psi^2(\phi_c)} \tag{1.61a}$$

$$\sigma_2 v \approx \frac{\tilde{f}^4(\phi_c)}{256\pi \tilde{m}_\psi^2(\phi_c)} \ , \tag{1.61b}$$

where $v$ is the relative velocity of the incoming particles. Since $\sigma_2 v$ is an order of magnitude smaller than $\sigma_1 v$, we neglect it and only consider interactions between the dark matter and gauge bosons. We see that $\sigma_1$ is an $S$-wave cross section, so it is a simple task to carry out the thermal averaging required in the Boltzmann equation. Note, however, that if thermal averaging is needed (following [38]), we must use the dark sector temperature $T_d$ in the expression

$$\langle \sigma v \rangle = \frac{1}{(n_\psi^{\text{EQ}}(T_d))^2} \frac{g^2}{2(2\pi)^4} \int_{4\tilde{m}_\psi^2}^{\infty} ds \ \sqrt{s} T_d K_1 \left( \frac{\sqrt{s}}{T_d} \right) (s - 4\tilde{m}_\psi^2)\sigma(s) \ . \tag{1.62}$$

### 1.5.3 Corrections to the Cross Section

We are interested in nonrelativistic dark matter, for which the relative velocities are much less than the speed of light. It is well known that for sufficiently low velocities, nonperturbative effects can have a large impact on the annihilation and scattering cross sections; and ladder diagrams, such as the ones shown in Fig. 1.2, must be included in the calculation.

#### 1.5.3.1 The Annihilation Cross Section

In the case of annihilation, performing this summation is equivalent to solving the Schrödinger equation in quantum mechanical scattering theory [39], and we obtain the Sommerfeld enhancement [40] for annihilations (for detailed reviews in the context of dark matter, see, for example, [41–43]). We consider the annihilation cross section $\sigma_0$ for a pointlike interaction near $r = 0$ in perturbative field

theory. For small velocities, the attractive Yukawa potential

$$V(r) = -\frac{\tilde{\alpha}}{r} e^{-\tilde{M}_A r} \ , \tag{1.63}$$

where $\tilde{\alpha} = \tilde{f}^2(\phi_c)/4\pi$, distorts the wave function at the origin and cannot be ignored. Including the potential will enhance the annihilation cross section to $\sigma = \sigma_0 S_k$ by the Sommerfeld enhancement factor $S_k$. Let us define the dimensionless parameters

$$\epsilon_v = \frac{v}{\tilde{\alpha}} \quad \text{and} \quad \epsilon_A = \frac{\tilde{M}_A}{\tilde{\alpha} \tilde{m}_\psi} \ , \tag{1.64}$$

where $v$ is the velocity of each annihilating particle in the center of mass frame. In the case of a massless gauge boson with a Coulomb potential, it is possible to solve the Schrödinger equation analytically to obtain the Sommerfeld enhancement.

For a massive gauge boson, the situation is more complicated, since the attractive potential has a finite range that limits the enhancement from being arbitrarily large for very low velocities. In the regime $\epsilon_A \ll \epsilon_v^2$, we recover the Coulomb case. At the crossover point $\epsilon_v \sim \epsilon_A$ (or equivalently $\tilde{m}_\psi v \sim \tilde{M}_A$), the de Broglie wavelength of the dark matter becomes comparable to the range of the interaction. At lower velocities with $\epsilon_A \gg \epsilon_v^2$, the Yukawa potential cannot be ignored. As $v \to 0$, the de Broglie wavelength increases to a value larger than the interaction range; thus, the enhancement saturates at

$$S_k \sim \frac{1}{\epsilon_A} \sim \frac{\tilde{\alpha} \tilde{M}_A}{\tilde{m}_\psi} \ . \tag{1.65}$$

Furthermore, zero-energy bound states may form for certain values of $\epsilon_A$, giving resonance regions with larger enhancements $\sim \epsilon_A/\epsilon_v^2$ until they are cut off by finite-width effects. In the early universe, freezeout typically occurs at velocities $v_f \sim 0.3$, so $\epsilon_v > 1$ and the Sommerfeld enhancement can be ignored. Note that there are no enhancements for $\epsilon_A > 1$.

To find the thermally averaged cross section, taking into account the Sommerfeld enhancement, we integrate $S_k$ using a Maxwellian distribution

$$F(v) = \frac{4}{\bar{v}^3 \sqrt{\pi}} v^2 e^{-v^2/\bar{v}^2} \ , \tag{1.66}$$

where $\bar{v}$ is the characteristic velocity of the astrophysical system of interest. Thus,

$$\langle \sigma v \rangle = (\sigma v)_{\text{s-wave}} \langle S_k \rangle \tag{1.67}$$

$$\langle S_k \rangle = \int_0^\infty dv \, F(v) S_k \ . \tag{1.68}$$

For the purposes of this paper, we choose to work in the $\epsilon_A > 1$ regime, and doing so has two

consequences. Practically, the calculation becomes much simpler, since we need not worry about the Sommerfeld enhancement at all. In addition, by de-emphasizing the Sommerfeld enhancement, we clarify the extent to which the novel effects developed in this paper can alone increase the cross section over time in areas of parameter space that the Sommerfeld enhancement cannot reach.

### 1.5.3.2 The Scattering Cross Section

To find the scattering cross section, we can use nonrelativistic quantum mechanics and sum over partial waves. The total cross section is

$$\sigma = \frac{4\pi}{k^2} \sum_{l=0}^{\infty} (2l+1) \sin^2 \delta_l ,$$
(1.69)

although a more useful quantity to compare to observational constraints is the transfer cross section,

$$\begin{aligned}
\sigma_{\mathrm{tr}} &= \int d\Omega \, (1 - \cos\theta) \frac{d\sigma}{d\Omega} \\
&= \frac{4\pi}{k^2} \sum_l [(2l+1) \sin^2 \delta_l - 2(l+1) \sin\delta_l \sin\delta_{l+1} \cos(\delta_{l+1} - \delta_l)] ,
\end{aligned}$$
(1.70)

which controls the rate at which energy is transferred between colliding particles. Following [44], analytic estimates for the cross section are

$$\sigma = \frac{4\pi}{\mu^2 v_{\mathrm{rel}}^2} (1 + L)^2$$
(1.71)

$$\sigma_{\mathrm{tr}} = \frac{4\pi}{\mu^2 v_{\mathrm{rel}}^2} (1 + L) ,$$
(1.72)

where $L = \mu v_{\mathrm{rel}} b_{\mathrm{max}}$ is the largest angular momentum needed to describe the interaction between two particles of reduced mass $\mu = \tilde{m}_\psi / 2$ that travel with a relative velocity $v_{\mathrm{rel}}$ and maximum relevant impact parameter $b_{\mathrm{max}}$. Note that these estimates are only valid for $L \gtrsim 1$. We estimate the impact parameter by solving

$$\frac{1}{2} \mu v_{\mathrm{rel}}^2 = \frac{\tilde{f}^2 / 4\pi}{b_{\mathrm{max}}} e^{-\tilde{M}_A b_{\mathrm{max}}} .$$
(1.73)

If we work in the $\epsilon_A > 1$ regime to avoid Sommerfeld enhancements, then we will also tend to avoid enhancements to the scattering cross section and can expect to be working in the Born limit. Simply taking the nonrelativistic limit of the perturbative cross section gives

$$\sigma = \frac{\tilde{f}^4(\phi_c) \tilde{m}_\psi^2(\phi_c)}{8\pi \tilde{M}_A^4(\phi_c)} = \frac{\tilde{m}_\psi^2(\phi_c)}{8\pi \mathsf{v}^4} .$$
(1.74)
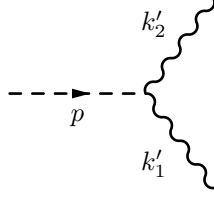
Figure 1.3: Tree-level $h$ decay.

Assuming that dark matter self-interactions are not needed[1] to explain the structure of dwarf galaxies [44], we use a conservative bound [45]

$$\sigma/\tilde{m}_\psi < 0.1 \ \mathrm{cm}^2/\mathrm{g} \qquad (1.75)$$

for characteristic velocities of 10 km/s. As we mention below, it would not be difficult to find parameters that violate this bound.

In the usual treatment of dark matter, constraints such as this one, obtained from present-day observations, can be directly applied to bounds on physics at freezeout or before. It is important to remember here that, in our model, the evolution of the chameleon field means that such a connection is far less direct, and such bounds typically do not apply in the early universe.

### 1.5.4 Dark Decays

The dark Higgs $h$ and the dark gauge boson $A$ are allowed to decay. As mentioned earlier, we assume $\tilde{m}_h(\phi_c) > 2\tilde{M}_A(\phi_c)$ so that $h$ has a tree-level decay channel to $A$, as shown in Fig. 1.3. Its decay width is

$$\Gamma_h = \frac{\tilde{f}^2(\phi_c)}{32\pi} \frac{\tilde{m}_h^3(\phi_c)}{\tilde{M}_A^2(\phi_c)} \sqrt{1 - \frac{4\tilde{M}_A^2(\phi_c)}{\tilde{m}_h^2(\phi_c)}} \left[ 1 - \frac{4\tilde{M}_A^2(\phi_c)}{\tilde{m}_h^2(\phi_c)} + 12\frac{\tilde{M}_A^4(\phi_c)}{\tilde{m}_h^4(\phi_c)} \right] . \qquad (1.76)$$

Although the $A$ particle is allowed to decay to $\eta$ particles, which are substantially smaller in mass, this occurs through a 1-fermion-loop process[2], as shown in Fig. 1.4. The amplitude is also suppressed by two factors of $m_2$ from the $\mathcal{O}(\eta^2)$ term in the expansion of $\tilde{m}_\psi(\phi)$. The nonzero amplitude in the limit of $\tilde{m}_\eta \ll \tilde{M}_A$, $\tilde{m}_\psi$ is

$$\mathcal{M} = -\frac{4i\pi^2 \tilde{f} \left(\tilde{m}'_\psi\right)^2}{\tilde{M}_A^2} k'_2 \cdot \epsilon^*(p) \left[ 4\tilde{m}_\psi \tilde{M}_A C_0[p^2, (p-k'_2)^2, k_2^2, \tilde{m}_\psi, \tilde{m}_\psi, \tilde{m}_\psi] \right.$$

$$\left. + (8\tilde{m}_\psi^2 + \tilde{M}_A^2) B_0[p^2, \tilde{m}_\psi, \tilde{m}_\psi] - 8\tilde{m}_\psi^2 B_0[k_2'^2, \tilde{m}_\psi, \tilde{m}_\psi] \right] , \qquad (1.77)$$

---

[1]Recent $N$-body simulations [8,9] support large self-interactions, which we discuss in Chapter 2.

[2]We use FeynCalc [46] to calculate the 1-loop $A$ decays.
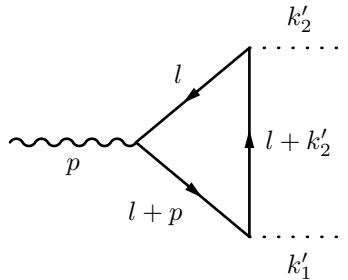
Figure 1.4: 1-loop $A$ decay.

where $B_0$ and $C_0$ are scalar Passarino-Veltman functions [47–50], defined via

$$B_0[p^2, m^2, m^2] = \frac{1}{i\pi^2} \int d^4 l \, \frac{1}{(l^2 + m^2)[(l+p)^2 + m^2]} \tag{1.78}$$

$$C_0[p^2, (p - p_1)^2, p_1^2, m, m, m] = -\frac{1}{i\pi^2} \int d^4 l \, \frac{1}{(l^2 + m^2)[(l+p)^2 + m^2][(l+p_1)^2 + m^2]} \,. \tag{1.79}$$

The $C_0$ integral is finite and, in the approximation $\tilde{m}_\psi \gg \tilde{M}_A \gg \tilde{m}_\eta$, reduces to

$$C_0[p^2, (p - k_2')^2, k_2'^2, \tilde{m}_\psi, \tilde{m}_\psi, \tilde{m}_\psi] \approx -\frac{1}{4\tilde{m}_\psi^2} \,. \tag{1.80}$$

The $B_0$ integral diverges, so we cut off the loop-momentum integral at some large scale. Using $m_3$ for this purpose, since we will often find it numerically to be the largest mass-suppression scale in our theory, we have

$$B_0[p^2, \tilde{m}_\psi, \tilde{m}_\psi] \approx B_0[k_2'^2, \tilde{m}_\psi, \tilde{m}_\psi] \approx 2 \ln\left(\frac{m_3}{\tilde{m}_\psi}\right) \,. \tag{1.81}$$

Putting everything together, the decay width of $A$ is then given by

$$\Gamma_A \approx \frac{1}{6\tilde{M}_A} \pi^2 \tilde{f}^2 \left(\frac{m_\psi A_2}{m_2}\right)^4 e^{-4\phi_c/m_2} \left[\ln\left(\frac{m_3}{\tilde{m}_\psi}\right)\right]^2 \,. \tag{1.82}$$

The $A$ bosons must decay efficiently enough not to contribute significantly to the energy density budget today. Though the decaying exponential makes meeting this criterion more difficult, there is still a small sample of parameter space for which the energy density of $A$ does not pose a problem.

## 1.6 Numerical Solutions

While we have described a number of ways to understand the evolution of the fields analytically, including, for example, the adiabatic approximation in which the chameleon tracks the minimum of its effective potential; ultimately, we are able to numerically solve[3] the relevant equations of motion

---

[3] We use Mathematica 8 to numerically solve the Boltzmann equation.

completely. To do so, of course, we must make sensible choices for our parameters to satisfy the various bounds and assumptions we have specified.

We need to implement the correct relationship between the dark sector temperature $T_d$ and that in the photon sector $T$, which in turn requires us to correctly enumerate the massless degrees of freedom at the relevant scales. At the unification scale, all of the dark particles ($\psi$, $A$, $h$, $\phi$) are relativistic, so $g_{*S}^d(t_u) = 8.5$. Around the epoch of dark matter freezeout, only $\psi$ is nonrelativistic, so $g_{*S}^d(t_f) = 5$. Thus, at freezeout, $\xi_f = 1.19$ for $g_{*S}(t_f) = 106.75$ or $\xi_f = 0.56$ for $g_{*S}(t_f) = 10.75$. With these numbers, the bound on the number of effective neutrino species in (1.8) is easily satisfied.

The model is insensitive to $\tilde{M}_A(\phi)$ and $\tilde{m}_h(\phi)$ at lowest order. We choose $\mathsf{v}$ such that $\bar{\psi}\psi \to AA$ is kinematically allowed today, while ensuring $\epsilon_A > 1$ and $\tilde{\alpha} < 1$. We must then check that $\tilde{M}_A(\phi_0)$ satisfies scattering cross section bounds. It is simplest to assume the attractor solution for $\phi$ and then later verify that it is in fact adhered to. The $A$ gauge bosons need to decay away before BBN so that their energy density is negligible. Finally, we must ensure that the evolution ends with the observed density of dark matter today. For this figure we use the bounds from the 7-year WMAP data [33], assuming a $\Lambda$CDM cosmology:

$$\Omega_{\mathrm{DM}}h^2 = \frac{\rho_0}{\rho_{c0}} = 0.1109 \pm 0.0056 \ . \tag{1.83}$$

Given these constraints, we numerically solve the Boltzmann equation and show a sample of parameter space in Fig. 1.5, resulting from a random, uniform scan over $m_\psi \in [0.1, 500]$ GeV; $m_1 \in [10^5, 10^7]$ GeV; $m_2 \in [5 \times 10^5, 5 \times 10^8]$ GeV; $m_3 \in [5 \times 10^5, 5 \times 10^8]$ GeV; $\Lambda \in [10, 10^3]$ GeV; $A_2 \in [0.1, 9.9]$; $A_3 \in [0.1, 10]$; and $e \in [0.01, \sqrt{4\pi}]$. The upper-left panel shows the coupling parameter $e$ vs the dark matter mass parameter $m_\psi$. The upper-right panel shows the annihilation cross section $\sigma v$ vs the scattering cross section $\sigma/\tilde{m}_\psi$, both evaluated at $x_0$ today. The bottom panels show the boost in annihilation cross section from freezeout to today and the scattering cross section today vs the mass parameter $m_\psi$. Again, there is flexibility when choosing $\mathsf{v}$ without affecting the evolution of $\phi$ and $Y$ at lowest order, so it is possible to obtain valid models for a scaled value of $\sigma/\tilde{m}_\psi$. Here, we show the largest possible scattering cross sections, while staying within the bound $\epsilon_A > 1$. As demonstrated in Fig. 1.6, only a small portion of the sampled parameter space fulfills the requirement that the $A$ gauge boson energy density is negligible by the time of BBN. While finding a set of parameters that satisfies all constraints is certainly possible, the effect of having very large increases in the annihilation cross section does not seem to be a general feature of the model.

As a concrete example, we show a specific model with the following parameter choices: $m_\psi = 123$ GeV; $m_T = m_\psi$; $m_1 = 38$ TeV; $m_2 = 500$ TeV; $m_3 = 500$ TeV; $\Lambda = 18$ GeV; $A_2 = 0.6$; $A_3 = 9.2$; $e = 0.96$; and $\mathsf{v} = 10$ GeV. These numbers comprise an optimistic set of parameter choices that satisfies all of our bounds and provides a large change of order $\sim 10^6$ in the annihilation
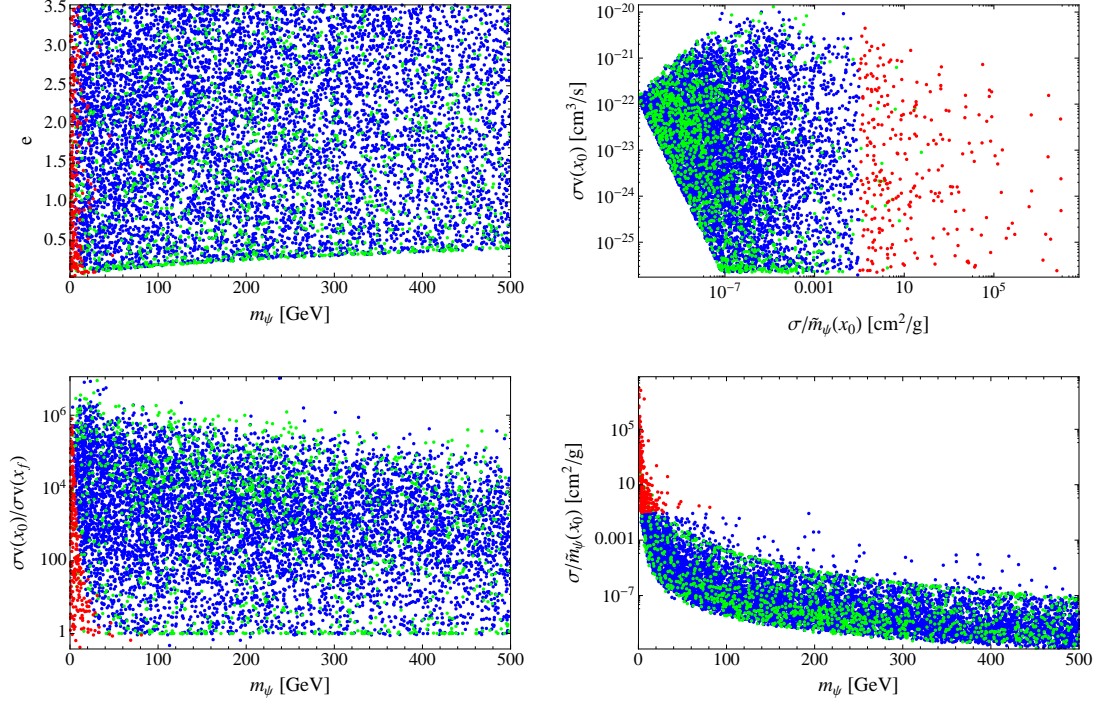
Figure 1.5: Scan of parameter space. Blue points indicate sets of parameters that satisfy all constraints, except (for most points) for having a negligible $A$ energy density. Red points do not satisfy the scattering cross section bound $\sigma/\tilde{m}_\psi < 0.1$ cm$^2$/g. Green points do not satisfy the adiabatic condition in (1.46) and should be solved with the coupled differential equations.

cross section over the history of the universe. Our choice for the value of $\mathsf{v}$ gives $\epsilon_A = 1.07$ today, so we can ignore the Sommerfeld enhancement. Larger values of $\mathsf{v}$ work equally well; increasing $\mathsf{v}$ increases $\epsilon_A \sim \mathsf{v}$ and decreases $\sigma/\tilde{m}_\psi \sim \mathsf{v}^{-4}$. The dark matter relic density is $\Omega_\psi h^2 = 0.1097$, within a standard deviation of the observed value. The scattering cross section today is $4.9 \times 10^{-4}$ cm$^2$/g, well below the conservative limit in (1.75). We must also check that these parameters satisfy the assumptions we have made in writing down the model. For example, we neglected terms with $\partial_\mu \tilde{f}/\tilde{f}$, and here we note that $\dot{\tilde{f}}/\tilde{f} \sim 10^{-9}$–$10^{-6}$ GeV, which is much smaller than other mass terms in the perturbative expansion. The adiabatic approximation is satisfied with $H/m_{\phi,\mathrm{ph}} \sim 10^{-11}$ throughout the evolution of $\phi$. Finally, we use the decay width of the $A$ particles to determine that they have decayed away in the time from freezeout to BBN, so they do not contribute to the energy budget we observe from the CMB.

The results for the evolution of $\phi$, $Y$, the dark matter mass $\tilde{m}_\psi$, and the coupling $\tilde{f}$ as a function of $T = m_T/x$ are shown in Fig. 1.7. We also show the annihilation and scattering cross sections in Fig. 1.8. The scattering cross section quickly approaches its asymptotic value by the time of dark matter freezeout, while the annihilation cross section still grows orders of magnitude from freezeout to now. This difference is due to the scattering cross section, $\sigma/\tilde{m}_\psi \propto \tilde{m}_\psi/\mathsf{v}^4$, and the annihilation
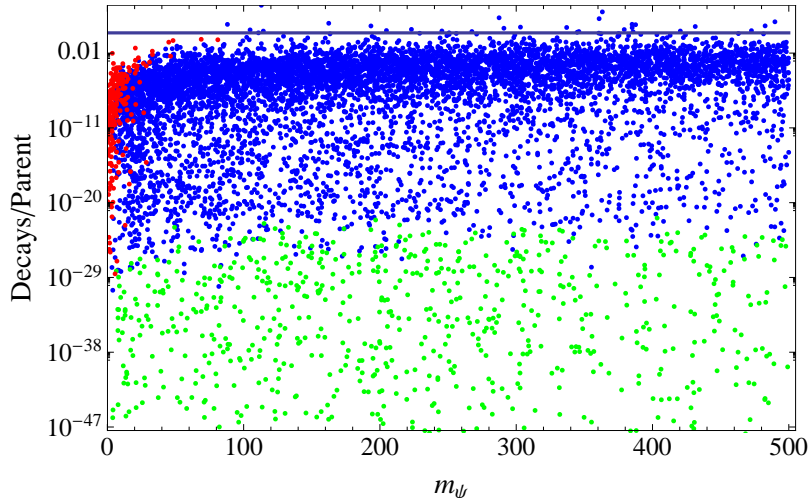
Figure 1.6: The number of $A$ decays per particle between freezeout and BBN. Points above the horizontal line at 1 indicate that all $A$ particles should have decayed and thus do not contribute significantly to the energy budget of the universe.

cross section, $\sigma v \propto \tilde{f}^4/\tilde{m}_\psi^2$, depending differently on $\phi$ via $\tilde{m}_\psi$ and $\tilde{f}$. We choose the form of $\tilde{f}$ to force the annihilation cross section to grow more slowly, whereas the scattering cross section has no such term countering its growth. With these particular choice of parameters, the scattering cross section is too small to have interesting astrophysically observable consequences.

As shown in Fig. 1.5, there are other choices of parameters that will still give a boost to the annihilation cross section while yielding a larger scattering cross section to match new simulation bounds [8, 9]; however, again, most of the plotted parameter space is restricted from the $A$ energy density requirement. One option for increasing the viable parameter space is to relax the requirement that $\epsilon_A > 1$ and to work in the regime of Sommerfeld enhancements; our model would still provide significant increases in the cross sections, and Sommerfeld enhancements would serve to further increase the boosts. Another clear option is to open an alternative decay channel for $A$.

## 1.7    Conclusions

In this paper we have investigated the possibility that the properties of dark matter depend crucially on the dynamics of a chameleon field—a scalar field whose cosmological evolution depends not only on its bare potential, but also on the local density of other matter (such as dark matter itself) in the universe. We have shown that such a coupling allows the annihilation cross section (for example) of the dark matter particles to change by several orders of magnitude between freezeout and today, while remaining consistent with all observational constraints. We have presented a general formalism to describe how this change might happen, and have provided a specific particle physics example in which all relevant quantities can be calculated. While there are significant observational and
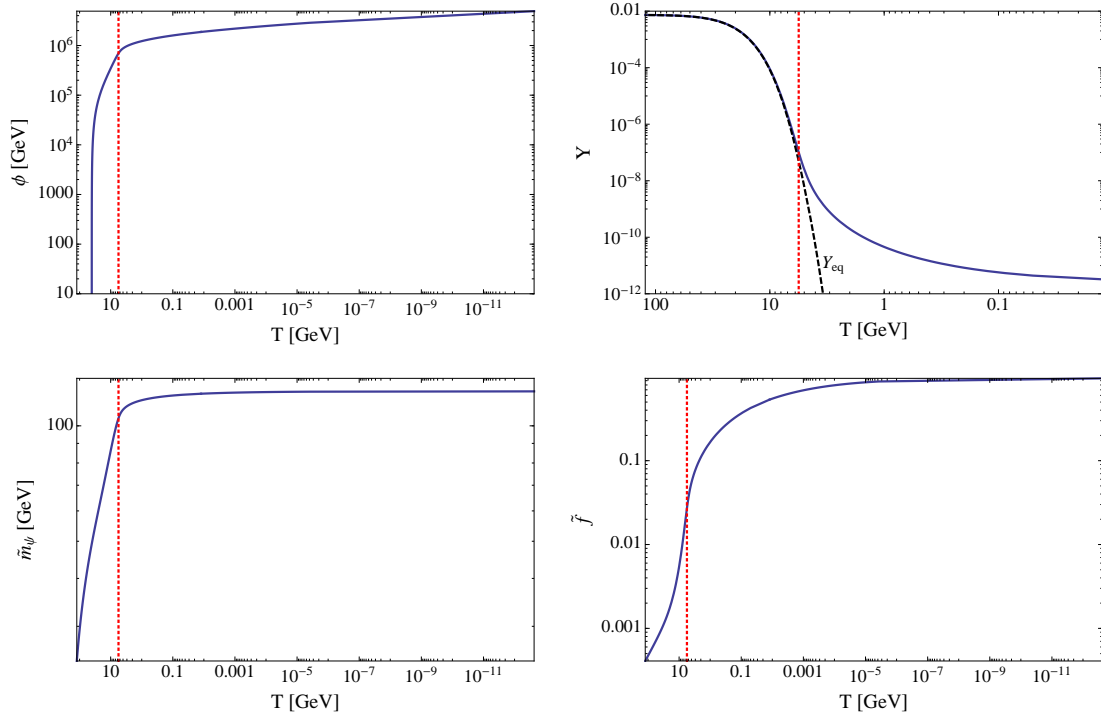
Figure 1.7: The evolution of $\phi$ (upper left), $Y$ (upper right), $\tilde{m}_\psi$ (lower left), and $\tilde{f}$ (lower right) as a function of $T$ in GeV for the model with $m_\psi = 123$ GeV. The red dotted line indicates the approximate dark matter freezeout temperature.

theoretical constraints on models of this type, it is nevertheless possible for the cross section to evolve in such a way that there may be interesting implications for the detection of dark matter and for its dynamical effects on late-universe astrophysics.

There are, of course, other possible complications to this idea that are beyond the scope of the current paper, but that provide interesting avenues for future study. One natural step is to couple our model directly to the SM. One way to achieve this coupling is to directly add the dark U(1) to the current SM gauge group [51]. Another possibility is to couple to the SM through U(1) kinetic mixing [52,53]. This extension of our model should be able to easily accommodate the relevant particle physics constraints [54–57], while easily allowing for decays of the dark gauge boson to SM particles well before BBN. The dark matter annihilations would still be dominated by the channel $\bar{\psi}\psi \to AA$, since annihilation to SM particles would be suppressed by the small coupling parameter for the U(1) mixing. However, it is a more delicate issue to decide what a natural route would be to couple the visible and dark scalar sectors, particularly with regards to coupling the chameleon to normal matter.

Finally, we did not attempt a careful analysis of the effect of late-universe inhomogeneities on the chameleon field or the dark matter properties on which it depends. In the specific models we considered, it seems as if such effects would be small, but a more careful examination is warranted.
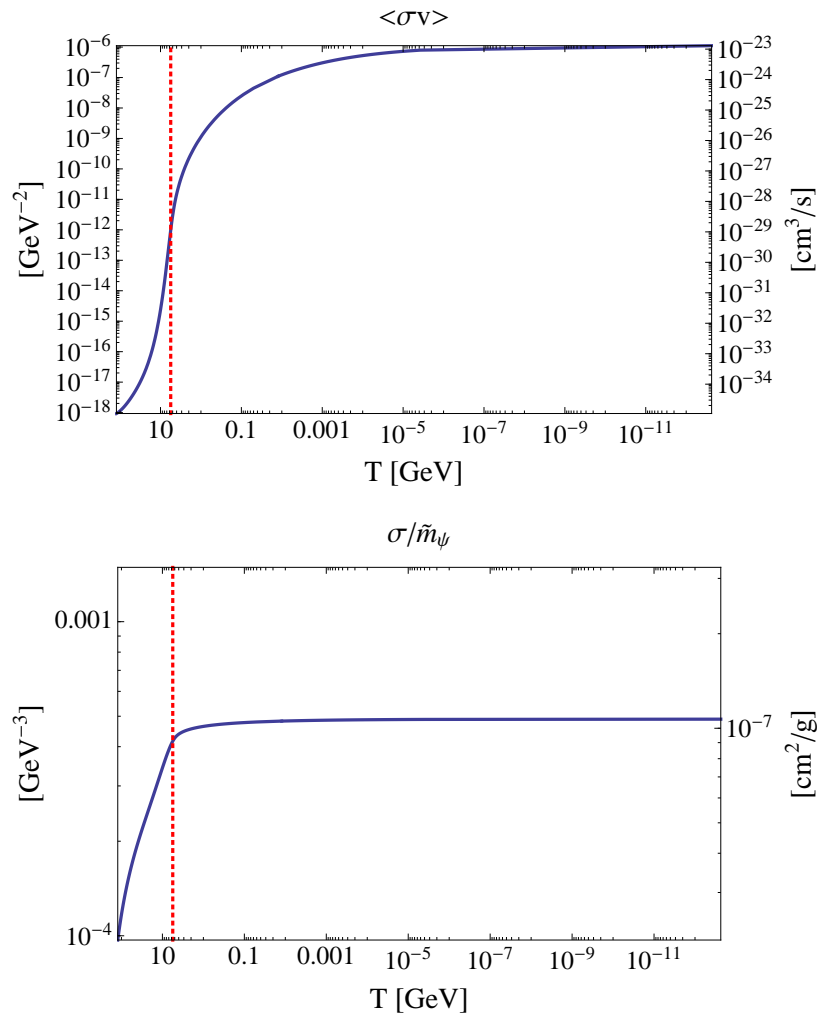
Figure 1.8: The evolution of the annihilation cross section $\langle \sigma v \rangle$ (top) and the scattering cross section $\sigma/\tilde{m}_\psi$ (bottom) as a function of $T$ in GeV with $m_\psi = 123$ GeV. The red dotted line indicates the approximate dark matter freezeout temperature.

# Appendix

## 1.A  Feynman Rules

The Feynman rules are shown in Fig. 1.A.1. All of these diagrams have higher-order corrections that involve $\eta$ particles.

$$= \Delta_h(p) = \frac{-i}{p^2 + \tilde{m}_h^2}$$

$$= -i\tilde{f}\gamma^\mu$$

$$= \Delta_\psi(p) = -i\frac{-\not{p} + \tilde{m}_\psi}{p^2 + \tilde{m}_\psi^2}$$

$$= -i\tilde{m}_\psi'$$

$$= \Delta_A^{\mu\nu}(p) = -i\frac{g^{\mu\nu} + p^\mu p^\nu/\tilde{M}_A^2}{p^2 + \tilde{M}_A^2}$$

$$= -2i\tilde{f}\tilde{M}_A g^{\mu\nu}$$

$$= \Delta_\eta(p) = \frac{-i}{p^2 + \tilde{m}_\eta^2}$$

$$= -i\frac{3}{2}\tilde{\lambda}_h \mathsf{v}$$

$$= -2i\tilde{f}^2 g^{\mu\nu}$$

$$= -i\frac{3}{2}\tilde{\lambda}_h$$
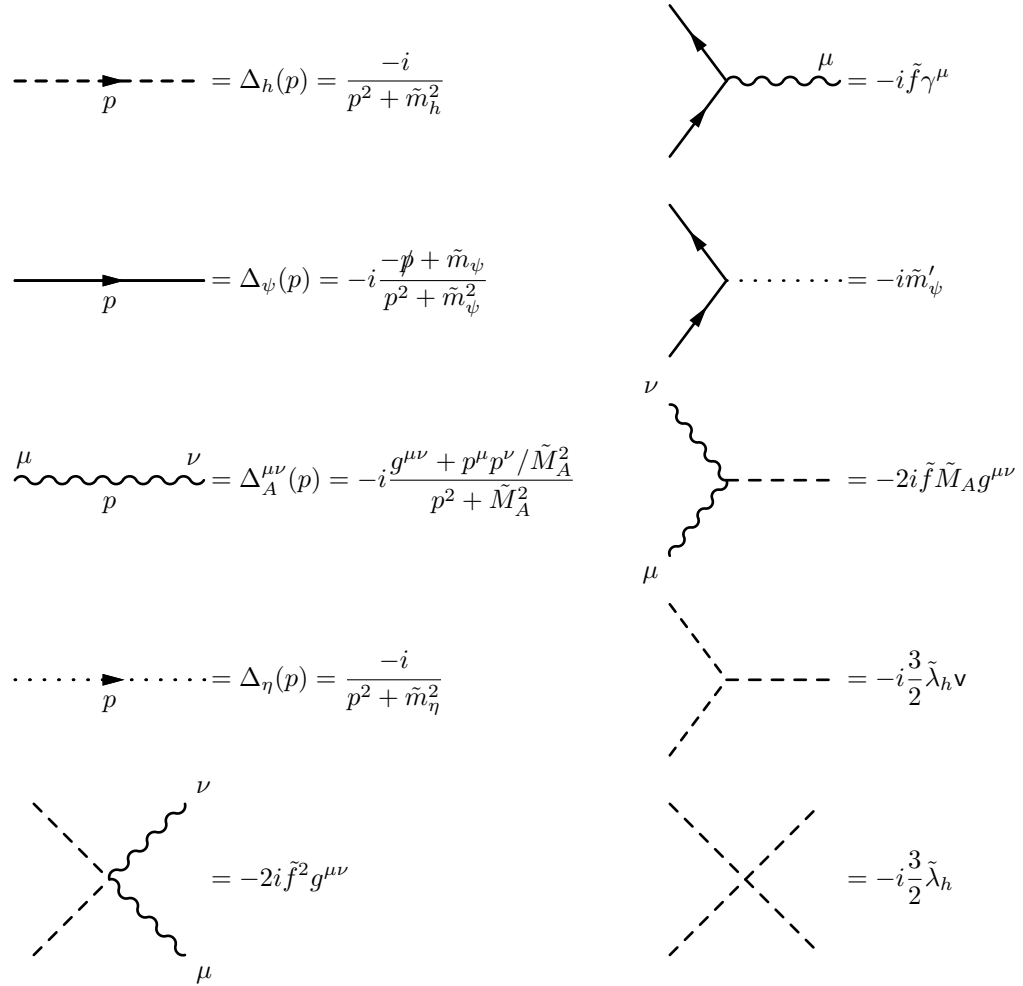
Figure 1.A.1: Feynman rules for $h$ (dashed), $\psi$ (solid), $A_\mu$ (wavy), and $\eta$ (dotted). We include the Yukawa interaction with $\psi$ and $\eta$, which is relevant for the 1-loop $A$-decay amplitude in (1.77), but other $\eta$-interaction vertices are not shown. All parameters labeled by a tilde are evaluated at $\phi_c$.

# Chapter 2

# Self-Interacting Dark Matter from a Non-Abelian Hidden Sector

## 2.1 Introduction

We consider self-interacting dark matter with cross sections of $\sigma/m \sim 0.1$–$10\ \mathrm{cm}^2/\mathrm{g}$, which are on par with nuclear-scale cross sections. The possibility that dark matter has color and interacts through the strong interactions of the SM is highly constrained, for example, by searches for anomalous isotopes in sea water [58–60]. However, dark matter may self-interact through non-Abelian forces (such as a dark analogue of QCD) in a hidden sector. As we will show below, this setup is straightforwardly realized in even the simplest such hidden sectors, with $\mathrm{SU}(N)$ gauge symmetry and no additional matter content. For confinement scales $\Lambda \sim 100$ MeV, the hidden gluons confine to form glueballs, and the resulting glueball dark matter has the required self-interactions. For hidden sectors that are roughly the same temperature as the visible sector, the glueball relic density is generically too large, but the desired relic density may be obtained by adjusting the relative temperatures of the hidden sector and visible sector, as we discuss below.

This hidden glueball scenario for self-interacting dark matter is remarkably simple, but it is decoupled from the visible sector, both in the technical sense and in the sense that it is not motivated by any of the well-known problems of the SM. In addition, the correct relic density is arranged by tuning a free parameter, the ratio of hidden to visible sector temperatures, and so the scenario cannot be claimed to naturally produce the right thermal relic density, as in the case of WIMPs. At first sight, it might appear difficult to enhance the model to accommodate all of these desirable features, especially since the WIMP miracle requires weak-scale annihilation cross sections, whereas the required self-interactions naturally suggest strong interactions.

In fact, however, we will show that all of these features are present in a supersymmetric version of the hidden glueball scenario, in which the hidden sector is a supersymmetric pure gauge theory. In this model, the dark matter is a $\sim 10$ TeV hidden gluino, which freezes out in the early universe
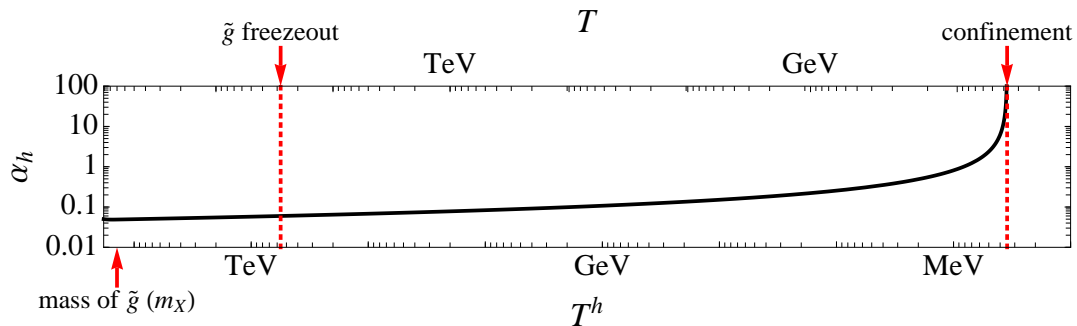
Figure 2.1: Example timeline of events in the supersymmetric pure $SU(N)$ theory without connectors, in terms of the hidden- and visible-sector temperatures $T^h$ and $T$. The hidden-sector coupling $\alpha_h$ is shown as a function of these temperatures. It is weak at gluino freezeout but grows as the temperature drops, leading to confinement and the formation of glueballino and glueball dark matter at a temperature $\sim \Lambda$. The scenario is described in detail in §2.6, and the chosen parameters are represented by the yellow dot in Fig. 2.5.

when the temperature is high. At freezeout, the theory is weakly coupled, but as the universe cools and expands, the theory confines, forming hidden glueballinos and glueballs. The glueballinos strongly interact via exchange of the hidden glueballs with the required self-interaction cross section. This scenario is straightforwardly accommodated in anomaly-mediated supersymmetry breaking (AMSB) scenarios [61, 62], which provide a connection to the problems of the SM, and also allow the glueballinos to naturally inherit the correct relic density through the WIMPless miracle [29, 63], a possibility discussed previously in [64–66]. For related work on strongly-interacting hidden sectors and dark matter, see [67–75].

Of course, the supersymmetric models also contain glueballs, which, as in the nonsupersymmetric case, may be dark matter. As we will see, in different regions of the AMSB parameter space, the dark matter may be dominantly glueballinos, dominantly glueballs, or a mixture of the two. For the case where the dark matter is dominantly glueballinos, we detail two possibilities. In the first case, the hidden sector is coupled to the visible sector only indirectly through the supersymmetry breaking mechanism. Since this coupling is extremely weak, the sectors can have different temperatures, and the glueball relic density may be very small for cold hidden sectors. An example cosmological timeline of events in this case is given in Fig. 2.1.

In the second case, the hidden sector is coupled to the visible sector through connector fields. The visible and hidden sectors, therefore, have the same temperature at early times, leading *a priori* to too-large glueball relic densities. Decays of glueballs are in conflict with big bang nucleosynthesis (BBN) and other astrophysical and particle constraints. Instead, we rely on a novel nonthermal process in the early universe to deplete the gluon density, thereby suppressing the glueball density after confinement. In this case, the gluons annihilate into singlet right-handed neutrinos with $\sim$ 1 GeV
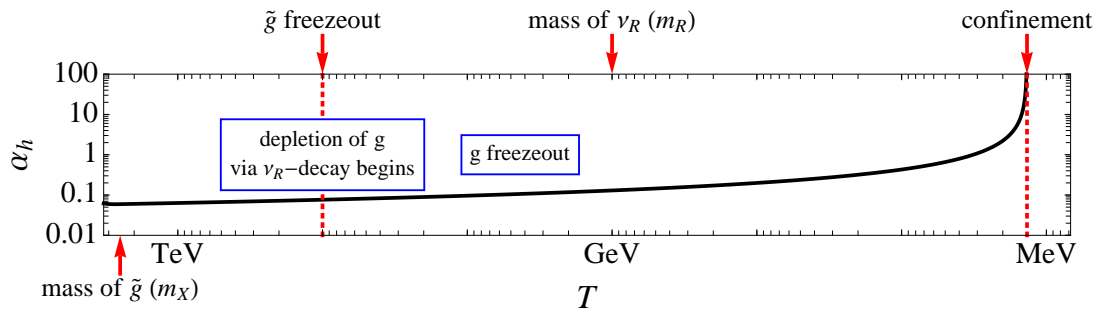
Figure 2.2: As in Fig. 2.1, but for supersymmetric pure SU(N) theory *with* connectors. Since the hidden and visible sectors communicate efficiently in the early universe, they share a temperature $T$. The gluon population is depleted through annihilations to and the subsequent decays of the $\nu_R$ in the visible sector, and the resulting scenario has pure glueballino dark matter. The scenario is described in detail in §2.7, and the chosen parameters are represented by the yellow dot in Fig. 2.8.

mass, and we reduce the hidden gluon density by forcing the right-handed neutrinos to decay into SM particles more quickly than they can annihilate back into hidden gluons. A representative timeline for this case is shown in Fig. 2.2.

This chapter is organized as follows. In §2.2, we review the astrophysical evidence for self-interacting dark matter. In §2.3, we begin with the simplest possible case: nonsupersymmetric pure gauge hidden sectors and glueball dark matter. We discuss glueball self-interactions and relic densities and determine the preferred parameters for this simple model. We then move to supersymmetric models with pure gauge hidden sectors and glueballino dark matter. In §2.4, we review the calculation of the glueballino self-interaction cross section, and in §2.5, we discuss the glueballino relic density and the realization of the WIMPless miracle in the AMSB framework. Finally, with this groundwork, we present full AMSB models of glueballino/glueball dark matter without and with connectors in §2.6 and §2.7, respectively. We conclude in §2.8.

Lastly, we make a quick note on naming conventions. In the rest of this chapter, we follow the literature: glueballinos denote gluino-gluon bound states, while gluinoballs denote gluino-gluino bound states. In addition, unless otherwise stated, "gluon," "gluino," "glueball," and "glueballino" refer to hidden sector particles and are denoted by $g$, $\tilde{g}$, gb, and gbino, respectively.

## 2.2 Astrophysical Evidence for Self-Interacting Dark Matter

The $\Lambda$CDM model is quite successful in describing large-scale structure. The predictions of the standard six-parameter $\Lambda$CDM cosmology match remarkably well to the latest measurements of the cosmic microwave background (CMB) by WMAP [76] and Planck [77] at large multipoles of the power spectrum. Additionally, CDM fits the dark matter power spectrum very well [78], using

observations of luminous red galaxy clustering in the Sloan Digital Sky Survey [79].

Despite these agreements on large scales, observations of small-scale structures indicate that CDM is insufficient. Challenges to the ΛCDM paradigm arise largely from tensions between observation and cosmological simulations. Simulations of CDM create dark matter halos with density profiles that have steep, inverse-power-law behaviors (cusps) towards the center of the halo [80–84]. Conversely, observations show that low-surface-brightness spiral galaxies (LSBs) [85–92], satellite dwarf galaxies [91, 93], and galaxy clusters [94–99] exhibit constant-density cores. In addition to the core-cusp discrepancy [100], the simulated central densities of halos are too high. By matching the luminosity function of the Milky Way to the Aquarius simulations [101], the brightest subhalos in the Milky Way are a factor of 5 less massive than predicted [102, 103]. If ΛCDM is correct, we are left to explain this "too big to fail" problem in which the largest subhalos of the Milky Way do not luminesce; otherwise, some additional physics is needed in simulations to decrease the central densities of these overly-massive halos.

To address these concerns with ΛCDM, there are a few generic possibilities to consider [104]: adding feedback from baryons in simulations [105–107], warm dark matter (WDM) [108–110], and self-interacting dark matter [5, 7, 111]. Feedback exists and should be included in simulations, but there may not be enough energy to eject a sufficient amount of mass from the halo center to solve the too-big-to-fail problem [103]. WDM tends to be too efficient in wiping out structure, leaving too few subhalos in the Milky Way [112]. Additionally, lower bounds on WDM masses from Lyman-$\alpha$ forest measurements constrain the ability of WDM to solve the core-cusp problem over the full range of astrophysical scales needed [113, 114]. Even with its mass unconstrained, WDM still leaves dwarf halos cuspy, though it does lower the central densities [115].

On the other hand, self-interacting dark matter can soften halo cores and lower central densities, while preserving large-scale structure [5] and satisfying bounds of $\sigma/m \lesssim 1$ cm$^2$/g from the Bullet Cluster [116]. Indeed, simulations with constant dark matter cross section-to-mass ratios in the range 0.1–1 cm$^2$/g show that self-interactions can bring theory in line with observations of both halo profiles and shapes [8, 9]. Velocity-dependent self-interactions widen this range to 0.1–10 cm$^2$/g and can also soften cores and reduce the density of the brightest satellites to solve the too-big-to-fail problem [10, 11].

With these results from simulation, dark matter with self-interactions is a strong contender within particle physics to be a solution to the small-scale formation woes in astrophysics. From a particle physics perspective, we will see that self-scattering is a quite reasonable and perhaps even generic property for dark matter to possess.

## 2.3  Glueball Dark Matter

The simplest construction resulting in dark matter that is a composite of a strongly-interacting hidden sector is a pure Yang-Mills gauge theory. At large energy scales, the theory consists of a weakly coupled set of massless gluons whose couplings are described by the gauge coupling. The theory is expected to confine at low energies at a scale $\Lambda$, where the gauge coupling becomes strong enough that perturbation theory breaks down [117–123]. At this point, it develops a mass gap, and the low energy physics is described by a set of glueball states whose masses are characterized by $\Lambda$ through dimensional transmutation.

At very low energies $\ll \Lambda$, the physics is described by an effective field theory composed of the the low-lying glueball states. In the absence of any coupling to the SM, the lightest of these states will be effectively stable.[1] The detailed mass spectrum (and spins) of these states depends on the underlying choice of theory and is further clouded by strong coupling, which leaves results based on perturbation theory suspect. Generically, one expects the glueball spectrum to have a lowest-lying element whose mass is $\mathcal{O}(\Lambda)$, which, following the guidance of QCD, we take to be a $J^{CP} = 0^{++}$ state [124, 125]. There will also be a collection of excited states with various spins and whose mass splittings are roughly multiples of $\Lambda$.

### 2.3.1  Glueball Self-Interactions

The various glueball states will interact with one another as a residual of the strong dynamics that bind them. Dimensional analysis dictates that the interactions among them will be proportional to $\Lambda$ to an appropriate power, with dimensionless coefficients characterized by naïve dimensional analysis (NDA) [126, 127]. For example, a description of a scalar glueball state $\phi_0$ would look like

$$\mathcal{L}_{\mathrm{gb}} = \frac{1}{2}\partial_\mu \phi_0 \partial^\mu \phi_0 - \frac{1}{2}m^2 \phi_0^2 + \frac{A}{3!}\phi_0^3 + \frac{\lambda}{4!}\phi_0^4 + \dots \ , \tag{2.1}$$

where NDA would suggest that for the lowest-lying state $m \simeq \Lambda$, and $A \simeq (4\pi)\Lambda$, $\lambda \simeq (4\pi)^2$, and the +... indicates interaction terms in the form of higher-dimensional operators that are suppressed by powers of $\Lambda$. Interactions involving the various glueball excited states can be formulated in a similar way.

For energies $\ll \Lambda$, the physics should be well described by an effective field theory composed of the lightest glueball. At kinetic energies of order $\Lambda$, more of the lowest-lying states become accessible and need to be included in the effective theory. At energies $\gg \Lambda$, the physics is described by the interactions of the gluons together with the structure functions that describe their distribution inside of the glueballs.

---

[1]Note that gravitational interactions will mediate very suppressed decays to light SM particles, but these are irrelevant for $\Lambda \ll M_{\mathrm{pl}}$.

Although it is clear that glueballs are strongly self-interacting, it is very difficult to make precise predictions for the scattering rate, given our general ignorance concerning strongly-coupled theories. The expected cross section will be characterized by the confinement scale and strong coupling,

$$\sigma\left(\text{gb gb} \to \text{gb gb}\right) \simeq \frac{4\pi}{\Lambda^2} \ , \tag{2.2}$$

which can also be understood from the geometric size of the glueballs, whose radius is $\sim 1/\Lambda$.

### 2.3.2 Glueball Relic Density

If the glueballs are stable on the scale of the age of the universe, they will contribute to the total observed dark matter relic density. At early times, when their temperature is $T_h \gg \Lambda$, the hidden sector is represented by a plasma of gluons whose comoving relativistic number density is given by

$$Y_\infty = \frac{n_g}{s} = \left.\frac{[\zeta(3)/\pi^2]g_{\text{eff}}T^{h3}}{(2\pi^2/45)g_{*S}T^3}\right|_{t_f} = \frac{45\zeta(3)}{2\pi^4}\xi_f^3\frac{g_{\text{eff}}}{g_{*S}(t_f)} \ , \tag{2.3}$$

where $s$ is the entropy in the visible sector, $\xi_f \equiv T^h/T$ is the ratio of temperatures in the hidden and visible sectors, $\zeta(3) \approx 1.202$ is the zeta function, and $g_{\text{eff}} = 2(N^2 - 1)$ for an SU($N$) gauge theory. We use an early time $t_f$ (which we will identify with the time of gluino freezeout in the supersymmetric models discussed below) as a reference point. The quantity $Y_\infty$ remains constant as the universe expands.

As the hidden sector temperature $T^h$ cools below the critical temperature $T^c \sim \Lambda$ [128], there is a transition to the confined phase, and the energy density of the gluon plasma is converted into glueballs. The result is that after confinement, the universe is filled with nonrelativistic glueballs whose comoving number density is the same as that of the gluons up to factors of $\mathcal{O}(1)$. Consequently, today the glueballs are nonrelativistic with a relic density

$$\Omega_{\text{gb}} \sim \frac{Y_\infty s_0 \Lambda}{\rho_{c0}} \ . \tag{2.4}$$

This expression assumes that there are no number-changing processes, but the glueballs may interact through a dimension-5 operator to give $3 \to 2$ scatterings [3]. We ignore this possibility here and leave it for future work.

### 2.3.3 Viable Glueball Parameters

Glueball dark matter is thus primarily characterized by two quantities: the confinement scale $\Lambda$, which simultaneously controls the dark matter mass and its self-interaction cross section, and $\xi_\Lambda$, the ratio of temperatures of the hidden and visible sectors at the time of confinement. Also relevant

## Glueball Dark Matter
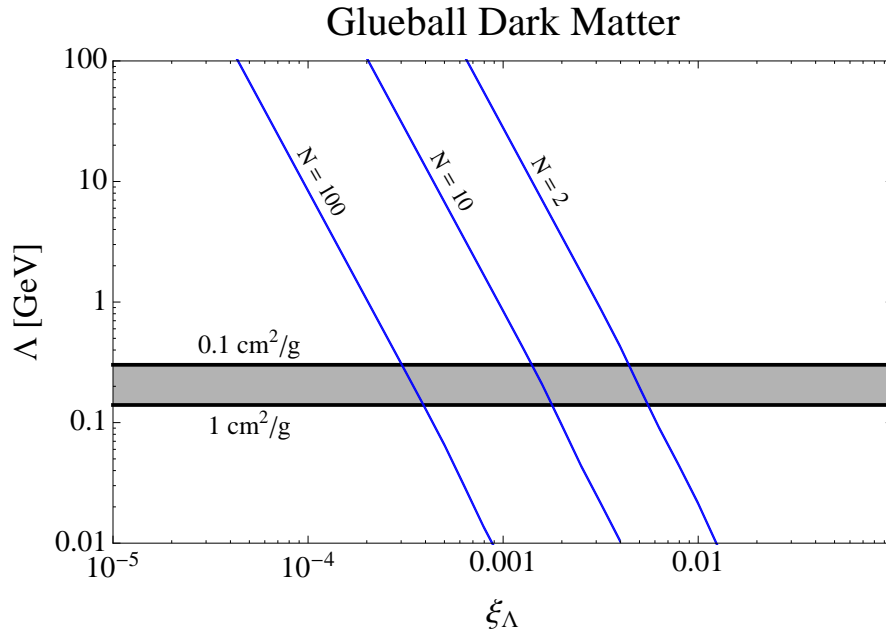


Figure 2.3: *Glueball dark matter* in the case of a nonsupersymmetric pure gauge $SU(N)$ hidden sector. The self-interaction cross section and relic density are given in the $(\xi_\Lambda, \Lambda)$ plane, where $\Lambda$ is the confinement scale in the hidden sector and $\xi_\Lambda \equiv T^h/T$ is the ratio of hidden to visible sector temperatures at the time that $T^h = \Lambda$. The self-interaction cross section is in the range $\langle \sigma_T \rangle / m_X = 0.1$–$1$ cm$^2$/g in the shaded region. The glueball relic density is $\Omega_{\rm gb} = \Omega_{\rm DM} \simeq 0.23$ on the diagonal contours for the number of colors $N$ indicated.

is the number of gluon degrees of freedom; for an $SU(N)$ gauge theory, $g_{\rm eff} = 2(N^2 - 1)$. In Fig. 2.3, we show the parameter space in the $(\xi_\Lambda, \Lambda)$ plane. The scattering cross section is independent of $\xi_\Lambda$, which together with the choice of $N$ controls the relic density of glueballs. The scattering cross sections of interest suggest $\Lambda \sim 100$ MeV, amusingly close to $\Lambda_{\rm QCD} \approx 300$ MeV. Note that since the cross section is constant, the acceptable upper limit from simulations is $1$ cm$^2$/g, in particular, to stay within cluster constraints. This limit will increase to $10$ cm$^2$/g for velocity-dependent cross sections, which we begin discussing in §2.4. The relic density requires the hidden-sector temperature to be a few orders of magnitude below the visible temperature at the time of confinement.

## 2.4 Glueballino Self-Interactions

The simplest extension to the pure gauge hidden sector discussed in §2.3 is to add a massive (mass $m_X \gg \Lambda$) gauge adjoint Majorana fermion to the theory, resulting in a spectrum with two types of composites: the bosonic glueballs with a mass $\sim \Lambda$ and the fermionic states with masses $\sim m_X$ [129–132]. Each sector contains excited states whose mass splittings are again characterized by $\Lambda$. In the absence of further ingredients, the massive fermionic states are stable because of Lorentz invariance, and this construction allows one to realize a situation where the dark matter

is (mostly) composed of the heavy composite fermions that self-interact via exchange of the much lighter glueballs, naturally realizing two widely separated energy scales. This dark sector is identical to a softly broken $N = 1$ supersymmetric gauge theory, and can be considered the supersymmetric version of the model of §2.3. In that language, the composite fermions are glueballino states.

The self-interactions of glueballinos are dominated by the exchange of glueballs. At low energies, when the kinetic energy available is $\lesssim \Lambda$, the scattering will be elastic. If there is sufficient kinetic energy,

$$\frac{1}{2} m_X v^2 \geq \Lambda \ , \tag{2.5}$$

inelastic scattering into excited states and glueball emission becomes possible, leading to novel effects, such as additional rapid halo cooling. The inelastic effects are not modeled in the $\Lambda$SIDM simulations and so are not well understood. For the remainder of this work, we focus on the elastic scattering regime and comment later in this section on systems where this approximation breaks down.

NDA suggests that the coupling between glueballs and glueballinos is $\alpha \sim 1$. Even for elastic scattering, there will be a large number of distinct glueball states, which are capable of mediating self-interactions of the glueballinos, but the dominant contribution arises from the lightest glueball states, which mediate the longest range interactions. Thus, we model the induced potential between two glueballinos as an attractive Yukawa interaction with a range $\Lambda$ and strength $\alpha \sim 1$:

$$V(r) = -\frac{\alpha}{r} \exp(-\Lambda r) \ . \tag{2.6}$$

It is common to use the transfer cross section

$$\sigma_T = \int d\Omega (1 - \cos\theta) \frac{d\sigma}{d\Omega} \tag{2.7}$$

to compare predictions to observations and simulations. We have numerically solved the Schrödinger equation to calculate $\sigma_T$, following the methods of [133]. See Appendix 2.A for details of the calculation. For the astrophysical systems of interest, to achieve the desired cross sections of 0.1–10 cm$^2$/g with $m_X \gtrsim$ TeV, the parameters must be in the classical scattering regime, $m_X v \gg \Lambda$. Scattering from Yukawa potentials has been studied in this regime in the context of classical, complex plasmas [134–136], and simple analytic fits to numerical results for the transfer cross section have been derived. These plasma physics results may be applied directly to the present dark matter case [137] (in fact, they describe the dark matter model exactly, whereas the Yukawa potentials are only an approximation to screened Coulomb interactions in the plasma physics context), and we have checked that these agree well with our numerical results.

Within a galactic halo or cluster, the dark matter particles have a velocity distribution that we

take to be Maxwell-Boltzmann:

$$f(v_i) = \left(\pi v_0^2\right)^{-3/2} e^{-v_i^2/v_0^2} , \tag{2.8}$$

where $v_0$ is the mode and $\langle v_i^2 \rangle = (3/2)v_0^2$ is the square of the three-dimensional velocity dispersion. This distribution is expected for cross sections of $\sigma/m = 1.0$ cm$^2$/g and above [138]; for the slightly lower cross sections that are still of interest to us, the distribution may be modified, but we do not expect this possibility to impact our results significantly. Simulations [8] show that $\langle v_i^2 \rangle \approx (1.2\,V_{\mathrm{max}})^2$, where $V_{\mathrm{max}}$ is the peak circular velocity of a given system, and thus $v_0 \approx 0.98\,V_{\mathrm{max}}$. The astrophysical systems of interest have values of $V_{\mathrm{max}}$ in the ranges 20–50 km/s for dwarfs, 50–130 km/s for LSBs, and 700–1000 km/s for clusters. We make a simplistic estimate for the dark matter escape velocity, $v_{\mathrm{esc}}^2 = 2v_0^2$, so that the largest relative velocity between particles is $2\sqrt{2}v_0$. For two scattering dark matter particles with velocities $\vec{v}_1$ and $\vec{v}_2$, the velocity-averaged transfer cross section is

$$\begin{aligned}
\langle \sigma_T \rangle &= \int \frac{d^3 v_1\, d^3 v_2}{(\pi v_0^2)^3} e^{-v_1^2/v_0^2} e^{-v_2^2/v_0^2} \sigma_T(|\vec{v}_1 - \vec{v}_2|) \\
&= \int_0^{2\sqrt{2}v_0} \frac{d^3 v}{(2\pi v_0^2)^{3/2}} e^{-v^2/2v_0^2} \sigma_T(v) .
\end{aligned} \tag{2.9}$$

Note that although the escape velocity may be an underestimate here, increasing it by a factor of 10 changes $\langle \sigma_T \rangle$ only at the 1% level.

The thermally-averaged transfer cross section, then, depends on four parameters: $m_X$, $\Lambda$, $\alpha$, and $V_{\mathrm{max}}$. In Fig. 2.4, we plot the ratio $\langle \sigma_T \rangle/m_X$ in the $(m_X, \Lambda)$ plane for $\alpha = 1$ and three representative characteristic velocities: $V_{\mathrm{max}} = 40$ km/s for dwarfs, $V_{\mathrm{max}} = 100$ km/s for LSBs, and $V_{\mathrm{max}} = 1000$ km/s for clusters. For masses $m_X \sim 1$ TeV and $\Lambda \sim 10$ MeV, we achieve transfer cross sections around the targeted range between 0.1 cm$^2$/g and 1.0 cm$^2$/g for all three systems under consideration. The transfer cross section decreases as a function of $v$ in the classical regime; thus, systems with larger characteristic velocities have smaller cross sections, all else being equal. The LSB line at 0.1 cm$^2$/g, for instance, lies below that for dwarfs, because a larger interaction range (smaller $\Lambda$) is needed to counter its larger velocity to give the same $\sigma_T$ as the dwarfs. Toward the lower values of $m_X$, the scattering exhibits resonant behavior due to the formation of quasibound states [133], analogous to Sommerfeld enhancements in annihilations.

The region below the straight magenta lines in Fig. 2.4 is where the dark matter typically has $(1/2)m_X v^2 > \Lambda$, and modifications from inelastic scattering processes can be important. We urge the reader to keep in mind that while in this region, the classical elastic scattering cross section (for our assumed Yukawa potential) falls below about $3\pi/\Lambda^2$, and we expect other energy-exchange mechanisms to become important in dark matter halos. Note that for clusters ($v \sim 3 \times$
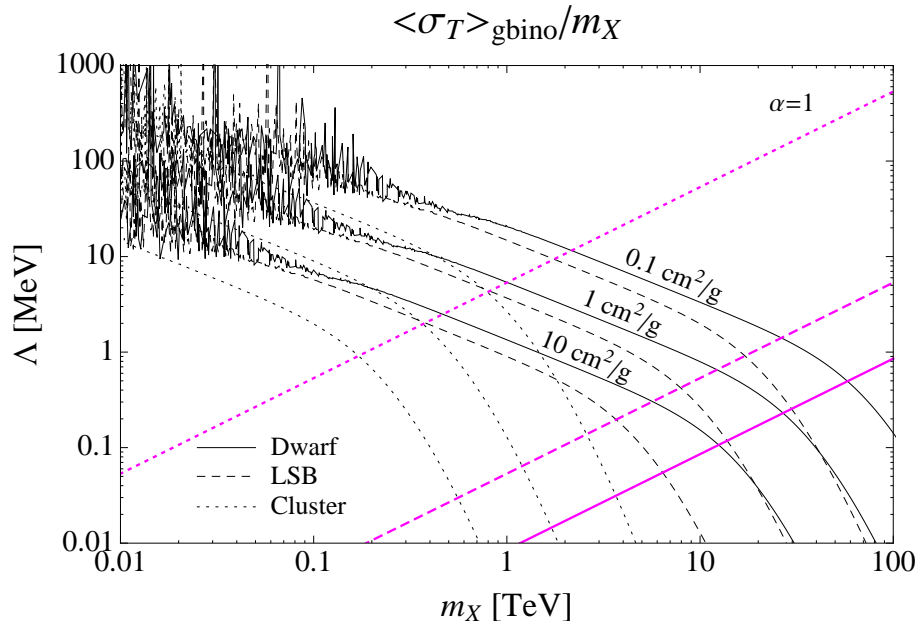
Figure 2.4: The ratio of the thermally-averaged transfer cross section to dark matter mass $\langle\sigma_T\rangle/m_X$ in the $(m_X, \Lambda)$ plane for $\alpha = 1$ and three different astrophysical systems: dwarf galaxies ($V_{\max} = 40$ km/s, solid), LSBs ($V_{\max} = 100$ km/s, dashed), and clusters ($V_{\max} = 1000$ km/s, dotted). For each system, three values of the cross section are shown: $0.1$ cm$^2$/g (top), $1$ cm$^2$/g (middle), and $10$ cm$^2$/g (bottom). The region below the straight magenta lines shows where inelastic processes may modify the picture based on elastic scattering for each type of system.

$10^{-3}$), the inelastic region is a substantial portion of the interesting parameter space: $(m_X/\text{TeV}) \gtrsim (\Lambda/10 \text{ MeV})$. The elastic glueballino scattering curves plotted for clusters in Fig. 2.4 and other figures are far from the whole story. We expect new astrophysical phenomenology, especially in clusters of galaxies, that deserves separate consideration.

## 2.5 Glueballino Relic Density

One goal of supersymmetrizing the pure gauge hidden sectors considered in §2.3 is to revive the possibility of dark matter with naturally the right relic density, as in the case of WIMPs, but now for self-interacting dark matter. In this section, we first review the machinery required to calculate a glueballino relic density from the freezeout of thermal relic gluinos. We then discuss the possibility of realizing the correct thermal relic density through the WIMPless miracle in AMSB models [64].

### 2.5.1 Gluino Freezeout

In a supersymmetric pure gauge hidden sector, the gluinos are initially in equilibrium with a thermal bath of gluons at a hidden-sector temperature $T^h$. As the universe cools below the gluino mass $m_X$, however, the gluinos freeze out. The gluino is the lightest supersymmetric particle in the hidden

sector, and we will assume it is stable. In the absence of couplings to the visible sector, stability is guaranteed by Lorentz symmetry, as the gluino is the only fermion in the hidden sector.

The gluino relic density is determined by the usual thermal freezeout analysis, but with the slight extra complication that it occurs in a hidden sector with a temperature that may differ from the visible sector. For $S$-wave annihilation, the relic density of a thermal relic in a hidden sector is [29]

$$\Omega_X \approx \frac{s_0}{\rho_{c0}} \frac{3.79 x_f}{(g_{*S}/\sqrt{g_*^{\text{tot}}}) M_{\text{pl}} \langle \sigma v \rangle} \ , \tag{2.10}$$

where $s_0$ is the entropy of the visible sector today, $x_f \equiv m_X/T_f$, $\rho_{c0}$ is the critical density today, and $g_*^{\text{tot}} = g_* + \xi_f^4 g_*^h$ at freezeout.

We now discuss the various quantities entering (2.10). For the annihilation process $\tilde{g}\tilde{g} \to gg$, we use an $S$-wave cross section

$$\langle \sigma v \rangle = k_N \frac{\pi \alpha_X^2}{m_X^2} \ , \tag{2.11}$$

where $\alpha_X = g_h^2(m_X)/4\pi$ is the fine-structure constant with a corresponding hidden-gauge coupling $g_h$ evaluated at the scale $m_X$, and $k_N$ is an $\mathcal{O}(1)$ $N$-dependent coefficient, which we simply set to 1. Additionally, we set $x_f = 25\xi_f$, which is a good approximation for a large set of parameters [29]. Given this, $\Omega_X$ scales approximately linearly with $\xi_f$. The latest Planck results give a value of $\Omega_{\text{DM}} h^2 = 0.1196 \pm 0.0031$ from a six-parameter fit to the $\Lambda$CDM model [77].

To determine the number of relativistic degrees of freedom in the visible and hidden sectors, note that, although the hidden and visible sectors need to interact gravitationally, they do not necessarily have to communicate otherwise, even at high energies. Thus, the sector temperatures are generically unrelated, and the ratio $\xi = T^h/T$ parameterizes this difference. The comoving entropies in the visible and hidden sector are independently conserved, and the values of $\xi$ at different times $t_i$ and $t_f$ are related by

$$\frac{g_{*S}^h(t_i)}{g_{*S}(t_i)} \xi_i^3 = \frac{g_{*S}^h(t_f)}{g_{*S}(t_f)} \xi_f^3 \ . \tag{2.12}$$

The effective numbers of relativistic degrees of freedom associated with the entropy (energy) density in the visible and hidden sectors are $g_{*S}$ and $g_{*S}^h$ ($g_*$ and $g_*^h$), respectively. As we will see, for most of the parameter space of interest, the gluinos freeze out at visible-sector temperatures at or above $T_{\text{SM}} \approx 300$ GeV, so that all SM particles are relativistic and $g_{*S} = g_* = 106.75$. Although there may be Minimal Supersymmetric Standard Model (MSSM) superpartners with low enough masses to contribute to $g_*$ at freezeout, we assume the contribution is negligible, with most of the visible supersymmetric-partner spectrum being above $m_X$. For the gluons and gluinos,

$$g_*^h = g_{*S}^h = \begin{cases} 4(N^2 - 1) & T^h \gtrsim m_X \\ 2(N^2 - 1) & m_X \gtrsim T^h > \Lambda \ . \end{cases} \tag{2.13}$$

## 2.5.2 The WIMPless Miracle and AMSB

As noted above, the gluino thermal relic density has the parametric dependence

$$\Omega_X \sim \frac{1}{\langle \sigma v \rangle} \sim \frac{m_X^2}{\alpha_X^2} \ . \tag{2.14}$$

For weak-scale masses and weak-interaction coupling strengths, $\Omega_X$ is of the desired size; this co-incidence is the essence of the WIMP miracle. For the hidden sector, we have great freedom in choosing the parameters $m_X$ and $\alpha_X$, and may simply choose them to yield the correct relic density. However, it is preferable if the correct mass-to-coupling ratio is fixed in a noncontrived way. This fixing is a property of models that realize the WIMPless miracle [29, 63], where the dark matter mass and coupling are not set individually, but the ratio $m_X^2/\alpha_X^2$ is set to the desired value by the model framework.

Supersymmetric models with AMSB [61,62] provide a particularly nice realization of the WIMP-less miracle [64–66]. In AMSB, the MSSM is sequestered from the supersymmetry-breaking sector, so the gaugino masses in the visible sector do not receive any tree-level contributions and are instead generated by the Weyl anomaly, leading to

$$m_v \sim \frac{\alpha_v}{4\pi} m_{3/2} \ , \tag{2.15}$$

where $m_{3/2}$ is the gravitino mass, $\alpha_v$ is a SM fine-structure constant, and $m_v$ is of the order of the weak scale, if these models are to address the gauge hierarchy problem. In any additional sequestered hidden sector of the theory, the hidden-sector superpartner masses will be given by a similar relation,

$$m_X \sim \frac{\alpha_X}{4\pi} m_{3/2} \ , \tag{2.16}$$

where $\alpha_X$ is the hidden sector's fine-structure constant. Since there is only one gravitino mass, $m_X/\alpha_X \sim m_v/\alpha_v$, and any hidden sector thermal relic in AMSB can be expected to have the desired relic density, even if $m_X$ and $\alpha_X$ differ, perhaps greatly, from the SM values.

The visible sector of AMSB models contains a stable thermal relic, the lightest neutralino. How-ever, the standard AMSB relations imply that this particle is the wino. Winos annihilate very efficiently, and must have masses around 2.7–3.0 TeV to be all of dark matter [139, 140]. The ther-mal relic density scales as $\sim m_{\tilde{W}}^{-2}$, and so for lighter and more natural values closer to the LEP2 experimental limit $m_{\tilde{W}} \gtrsim 100$ GeV [141,142], the wino thermal relic density is completely negligible. We will therefore neglect it below, and take it as additional motivation to develop AMSB models with viable hidden-sector dark matter candidates.

The particle spectrum in AMSB models is completely specified by quantum numbers, dimension-less couplings, and the gravitino mass. In the visible sector, the wino mass limit $m_{\tilde{W}} \gtrsim 100$ GeV

implies

$$m_{3/2} \gtrsim 37 \text{ TeV} . \tag{2.17}$$

In the hidden sector, at scales above $m_X$, the one-loop $\beta$-function coefficient is $b_H = -3N$ and the theory is asymptotically free. The gluino mass is

$$m_X = -b_H \frac{\alpha_X}{4\pi} m_{3/2} = 3N \frac{\alpha_X}{4\pi} m_{3/2} . \tag{2.18}$$

Below $m_X$, we have a nonsupersymmetric SU($N$) gauge theory with a $\beta$-function coefficient $b_L = -(11/3)N$. The theory is expected to confine at the scale

$$\Lambda \sim m_X \exp\left(\frac{-6\pi}{11N\alpha_X}\right) = m_X \exp\left(\frac{-9m_{3/2}}{22m_X}\right) . \tag{2.19}$$

With this relationship, the relic density in (2.10) becomes

$$\Omega_X \approx \frac{s_0}{\rho_{c0}} \frac{\left[g_* + 2(N^2 - 1)\xi_f^4\right]^{1/2}}{g_{*S}} \frac{3.79 \cdot 25\xi_f}{M_{\text{pl}}} \frac{9N^2}{16\pi^3} m_{3/2}^2 . \tag{2.20}$$

## 2.6 Glueballino/Glueball Dark Matter without Connectors

Given the results above, we can now present simple AMSB models of self-interacting dark matter. We begin by considering the simple case without connector fields, in which the visible and hidden sectors are decoupled. The visible sector is the MSSM; the tachyonic slepton problem is assumed to be solved in a way that does not impact the masses of the MSSM gauginos, and the wino is assumed to be the visible lightest supersymmetric particle (LSP), with negligible thermal relic density. The hidden sector is a pure SU($N$) gauge theory, consisting of gluinos and gluons, which confine to form glueballino and glueball dark matter.

There are only four independent parameters in the theory, which may be taken to be

$$m_X, \ \Lambda, \ N, \ \xi_f . \tag{2.21}$$

These determine $\alpha_X$ and $m_{3/2}$ through (2.19). In contrast to the model-independent discussion of §2.4, in AMSB models, renormalization group equations relate the high-scale parameters $m_X$ and $\alpha_X$ to the low-scale parameter $\Lambda$. In terms of these parameters, the glueball self-interaction cross section and relic density are determined as described in §2.3.1 and §2.3.2, and the glueballino self-interaction cross section and relic density are determined as described in §2.4 and §2.5.

We first present results for models with mostly glueballino dark matter in Fig. 2.5. We scan over the $(m_X, \Lambda)$ plane. At every point in this plane, we require that glueballinos make up 90%

(top panel) or 99.99% (bottom panel) of the dark matter, and glueballs make up the remaining 10%
or 0.01%. The constraints on $\Omega_{\text{gbino}}$ and $\Omega_{\text{gb}}$ determine $N$ and $\xi_f$; contours of constant $N$ and $\xi_f$
are shown. The lower bound of (2.17) excludes parameter space with low $m_X$. In the remaining
parameter space, $m_X/\Lambda \gtrsim 10^3$, which is more than sufficient to ensure $T_f^h > \Lambda$, so gluino freezeout
occurs in the weakly-interacting theory, and the thermal freezeout calculation is valid.

These relic density results for a particular glueballino density may be understood as follows. On
a given curve of constant $N$, larger dark matter masses imply larger thermal relic densities and so
require smaller values of $\xi_f$ to keep $\Omega_{\text{gbino}}$ fixed. Once $\xi_f$ decreases, a larger $\Lambda$ is required to keep
$\Omega_{\text{gb}}$ constant. Note also that for $\Lambda \sim$ MeV and $\xi_f \sim 1$, glueballs overclose the universe. To avoid
overclosure, $\xi_f$ must be lowered; and to have mostly glueballino dark matter, $m_X$ must be a bit
larger than the weak scale. In short, the presence of glueballs forces the model away from the *a
priori* most natural parameter space with low $m_X$ and $\xi_f \sim 1$. In the context of AMSB, however,
it is rather natural to assume that the hidden and visible sectors are separated at high scales and
$\xi_f \ll 1$. The WIMPless miracle is nicely realized in regions of parameter space with $\xi_f \sim 0.01$ and
$N \sim \mathcal{O}(1)$ for $\Omega_{\text{gbino}} = 0.9\,\Omega_{\text{DM}}$.

There are also differences between the 90% and 99.99% glueballino cases. The curves of constant
$N$ and constant $\xi_f$ shift as the relative amounts of glueball and glueballino dark matter change. By
focusing on a particular point in the $(m_X, \Lambda)$ plane and comparing (2.4) and (2.20), we find

$$\xi_f \sim \frac{\Omega_{\text{gb}}^{1/2}}{\Omega_{\text{gbino}}^{1/2}} \qquad \text{and} \qquad N \sim \frac{\Omega_{\text{gbino}}^{3/4}}{\Omega_{\text{gb}}^{1/4}} \tag{2.22}$$

for $N^2 \gg 1$. When the glueball density is reduced by 3 orders of magnitude, we expect $N$ to increase
by a factor of $10^{3/4} \sim 6$ and $\xi_f$ to decrease by a factor of $10^{3/2} \sim 30$, as shown in Fig. 2.5.

Of course, the goal is not simply to obtain a multicomponent model of dark matter with the
correct relic densities, but to obtain self-interacting dark matter. The regions with the preferred
self-interaction cross sections are also shown in Fig. 2.5. For values of $m_X \sim 10$ TeV, $\Lambda \sim 1$ MeV,
$2 \leq N \lesssim 10$, and $10^{-3} \lesssim \xi_f \lesssim 10^{-2}$, we find models that satisfy the relic density constraints and
also satisfy the scattering constraints for dwarfs and LSBs. Viable models also exist for lower values
of $m_X$ down to the LEP2 limit for larger $N$ and lower $\xi_f$. A representative model is one with
$m_X \simeq 14$ TeV, $\Lambda \simeq 0.35$ MeV, $N = 2$, and $\xi_f \simeq 0.02$; it is shown as a yellow dot in Fig. 2.5. For
these parameters, Fig. 2.1 shows how the dark matter coupling behaves from the scale $m_X$ down to
confinement.

Measurements of nuclei abundances and of the CMB place restrictions on the number of light
degrees of freedom $N_{\text{eff}}$ around the time of BBN that contribute to the expansion of the universe.
Results from Planck give $N_{\text{eff}} = 3.30 \pm 0.27$ [77]. An interesting question, then, is whether these
models also imply nonstandard values of $N_{\text{eff}}$. Once the hidden-sector temperature drops below the

confinement scale, glueballinos and glueballs form. Confinement occurs when the visible sector's temperature is

$$T_\Lambda = \frac{T_\Lambda^h}{\xi_\Lambda} \sim \frac{\Lambda}{\xi_\Lambda} = \frac{\Lambda}{\xi_f} \left( \frac{g_{*S}(t_f)}{g_{*S}(t_\Lambda)} \right)^{1/3} , \qquad (2.23)$$

using (2.12) with $g_{*S}^h(t_\Lambda) = g_{*S}^h(t_f)$. For the representative example parameters given above, the confinement scale is $T_\Lambda \sim 90$ MeV; confinement occurs well before BBN and structure formation, as expected. There is therefore no relativistic, massless species to act as the hidden-sector bath during BBN. At the time of BBN, the hidden-sector temperature is not well defined, and its contribution to $N_{\rm eff}$ is essentially zero.

We next consider the case of mostly glueball dark matter. To be concrete, we present the case of $\Omega_{\rm gb} = 0.9\,\Omega_{\rm DM}$ and $\Omega_{\rm gbino} = 0.1\,\Omega_{\rm DM}$ in Fig. 2.6. Once again, we show contours of constant $N$ and $\xi_f$, but now we include the glueball scattering constraints from Fig. 2.3, since glueballs are the dominant component of dark matter. The values of $m_X$ that satisfy relic and scattering constraints for a given $N$ are fairly similar to those in the case of mostly glueballino dark matter; however, the corresponding values of $\Lambda$ are a few orders of magnitude larger than the mostly glueballino case.

In Fig. 2.5 and Fig. 2.6, the fraction of glueballino to glueball dark matter is fixed. Of course, different values are possible. In Fig. 2.7, we fix $N = 2$ and vary $m_X$ and $\Lambda$; $\xi_f$ is set by the requirement that $\Omega_{\rm gbino} + \Omega_{\rm gb} = \Omega_{\rm DM}$. The results are presented in the $(\langle\sigma_T\rangle_{\rm gbino}/m_X, \langle\sigma_T\rangle_{\rm gb}/\Lambda)$ plane, where $V_{\rm max} = 40$ km/s, and contours of constant $\Omega_{\rm gbino}/\Omega_{\rm gb}$ are shown. Regions excluded by LEP2 and by cluster bounds are shaded.

Fig. 2.7 shows that the fraction of dark matter that is glueballinos may take almost any value in the parameter space. Of course, regions of parameter space that are overwhelmingly glueballino dominated and have too-large glueballino self-interactions are excluded, as are regions that are overwhelmingly glueball dominated with too-large glueball self-interactions. The parts of parameter space that are certainly excluded by these considerations are indicated, but the position of this boundary is somewhat uncertain and requires detailed $N$-body simulations (modeling both components of dark matter) to determine. The cluster constraints [9, 116] are relevant here because glueballs have a velocity-independent scattering cross section and these constraints dictate that glueballs must be the subdominant component of dark matter in all of the parameter space shown in Fig. 2.7.

Especially interesting, however, are the regions of parameter space with a subdominant component of dark matter that self-interacts very strongly. For example, the dark matter may be 99% glueballinos and 1% glueballs, but the glueballs may have $\langle\sigma_T\rangle_{\rm gb}/\Lambda \sim 10^5$–$10^{11}$ cm$^2$/g. Such possibilities are not ruled out by the constraints discussed so far but may have very interesting astrophysical implications.

It has been pointed out that, at early times before the halo has had time to form a core through

self-interactions, seed black holes can grow by accreting self-interacting dark matter [143]. In the mixed self-interacting dark matter scenario where one of the components has $\langle\sigma_T\rangle/m \gg 1\mathrm{cm}^2/\mathrm{g}$, this accretion can be highly enhanced. The possibility that supermassive black hole growth is seeded by the self-interactions of either the glueballs or glueballinos is an exciting prospect. There is not yet a clear picture of how $10^9$ $\mathrm{M}_\odot$ quasars are assembled already by $z \gtrsim 6$ within the standard $\Lambda$CDM cosmology. Models starting with the expected 100 $\mathrm{M}_\odot$ seeds require special assumptions about the mass accretion histories of these quasars [144], which become more strained as higher redshift quasars are found [145]. Self-interactions within the dark matter sector may have a big role to play in this story, as they generically enhance the early black hole accretion rate.

There is a tight correlation between the mass of supermassive black holes in the centers of galaxies and the velocity dispersion or luminosity of the bulge [146]. By requiring that the predicted masses of supermassive black holes are not overly large, it should also be possible to constrain the ratio $\Omega_{\mathrm{gb}}/\Omega_{\mathrm{gbino}}$ in mixed self-interacting dark matter models where $\langle\sigma_T\rangle_{\mathrm{gb}}/\Lambda$ is large. To correctly implement this constraint, many new features of our simple model and their astrophysical consequences will have to be worked out. We highlight a few of these below.

The details of capture of glueballs by a seed black hole will differ significantly from the treatment in [143]. The black hole capture depends sensitively on the density profile of glueballs, which is tightly correlated with the potential well of the galaxy, which in turn is dominated by glueballinos. In particular, although an isolated strongly self-interacting dark matter halo will undergo core collapse, it is not true when the strongly self-interacting component (glueballs) is a small fraction of the dark matter.

A complicating factor is that the glueballs and glueballinos will scatter off of each other. Each collision will change the velocity of glueballs by $\mathcal{O}(1)$, but the velocity of glueballinos will only change by $\Lambda/m_X \ll 1$. The glueballino-glueball scattering cross section should be of the order the geometric cross section ($\sim 1/\Lambda^2$), and thus this effect could be important if the number density of glueballinos is much larger than that of glueballs (either because of a small $\Omega_{\mathrm{gb}}/\Omega_{\mathrm{gbino}}$ or as glueballs are depleted due to accretion by the black hole). Conversely, this scattering could also have an impact on the glueballino density profile if the number density of glueballs is large enough to overcome the small momentum transfer.

Another important effect, relevant for halo properties as well as black hole growth, is cooling. We have focused on elastic collisions in this chapter, but as mentioned previously, there are also inelastic processes leading to cooling through the emission of glueballs. Cooling will funnel more glueballs into the inner regions (modulo angular momentum constraints) and increase the black hole accretion rate. Note that, unlike the baryons, competing effects from star formation and subsequent heating by UV photons are not relevant for glueballs.

As an extreme example, one could assume that all of the glueballs are bound up in the central

supermassive black hole. In this case, we can use measured ratios of the black hole masses to halo masses to put an upper limit on $\Omega_{\rm gb}/\Omega_{\rm gbino}$. For the Milky Way, this ratio is $\sim 10^{-5}$, while for Andromeda the ratio is more like $10^{-4}$ (it should be kept in mind that the black hole will also accrete baryons and grow, so this estimate is a lenient upper bound). Rather than focus on the Local Group, one could look more generally at the black hole mass–virial mass relation for all galaxies, but as expected there is a lot of scatter in this relation [147].

To illustrate the effect of these constraints on the model parameter space, we have shown two possibilities in Fig. 2.5: one with $\Omega_{\rm gb}/\Omega_{\rm gbino} = 0.1$ (which may not be viable given the arguments above) and a second with $\Omega_{\rm gb}/\Omega_{\rm gbino} = 10^{-4}$. There is no impediment in making this ratio even smaller, although there is no natural reason to do so. In addition, as $\Omega_{\rm gb}/\Omega_{\rm gbino}$ is reduced, the regions with small $N$ move into the regime where inelastic process will be important for all relevant velocities (dwarfs to clusters).

## 2.7  Glueballino/Glueball Dark Matter with Connectors

Although a pure $\mathrm{SU}(N)$ hidden sector with no connectors can accommodate both early universe and structure formation constraints, it is interesting to consider the possibility of connector fields that allow communication between the hidden and visible sectors. Such scenarios may have, of course, a larger number of testable implications. In addition, as we will see, if the connectors mediate annihilation or decays to the visible sector, the viable parameter space may be significantly altered.

If the hidden and visible sectors communicate, we expect the temperatures of the two sectors to coincide nearly until kinetic decoupling at confinement. If glueballs are stable, they will generically overclose the universe, and so there must be a mechanism to reduce the glueball density. Let us assume that this mechanism exists and reduces the glueball relic density to a negligible level. We can then immediately determine the consequences for the parameter space. For a given point in the $(m_X, \Lambda)$ plane with $\xi_f = 1$, there are contours of constant $N$ on which $\Omega_{\rm gbino} = \Omega_{\rm DM}$. These are shown in Fig. 2.8, along with the self-interaction constraints. We see that the LEP2 bound excludes all but the $N \leq 4$ possibilities, but now, for small $N$, the allowed values of $m_X$ are much reduced and more natural relative to the case without connectors.

A straightforward way to eliminate glueballs is through decays, but other constraints render this scenario unacceptable. The glueballs have a mass around 1 to 10 MeV, so possible decay products will be photons, electrons, and neutrinos. Decays to photons will typically take too long and happen well after BBN. If too much energy and entropy is injected into the visible sector at $T \lesssim 1$ MeV, there is an unacceptably large contribution to $N_{\rm eff}$. Decays to electrons after 1 MeV face a similar problem, and, in addition, they can break up deuterium and ruin its BBN abundance (if the glueball is heavy enough). Decays to light neutrinos are problematic because glueballs can be produced in

supernovae, escape the neutrino sphere, and cool the supernovae too efficiently. If we attempt to adjust parameters to get around the difficulties with either electrons or neutrinos, then we encounter problems with $e^+e^-$ collider constraints. We are led to consider alternative processes to eliminate the glueball density.

Since decays after confinement are highly constrained, we investigate reducing the glueballino density by depleting the gluon density before confinement. The gluons may annihilate to SM particles via loop diagrams, but the reverse process needs to be suppressed. Let us introduce a right-handed neutrino $\nu_R$. The $\nu_R$ is a SM gauge singlet with a mass $m_R \sim$ GeV and could be one of the sterile states in a seesaw mechanism to produce neutrino masses. Our goal is for the gluons to annihilate into right-handed neutrinos, which then decay quickly into SM particles before they can annihilate back into gluons.

To implement this scenario, we postulate that there is a connector field $C$ with a mass $m_C$ that allows communication between the hidden and visible sector. The connector has a Yukawa interaction $\lambda_R C \bar{\nu}_R \nu_R$ in the visible sector, and a gauge interaction with the gluons with strength $g_h$ in the hidden sector. Integrating out the connector produces the effective interaction

$$\mathcal{L} \sim \frac{1}{16\pi^2} \frac{\lambda_R^2 g_h^2}{m_C^3} G_{\mu\nu}^h G^{h\,\mu\nu} \bar{\nu}_R \nu_R \ . \tag{2.24}$$

This interaction leads to an annihilation cross section,

$$\langle \sigma v \rangle_{gg \to \bar{\nu}_R \nu_R} \sim \frac{\lambda_R^4 g_h^4}{8\pi(16\pi^2)} \frac{T^4}{m_C^6} \equiv \sigma_0 z^{-4} \ , \tag{2.25}$$

where $z = m_R/T$. Note that the annihilation of gluons into right-handed neutrinos is subdominant to the annihilation rate of gluons into gluinos and can be ignored in the gluino freezeout calculations. The right-handed neutrino decays with a rate

$$\Gamma_R \sim \frac{g_\nu^2}{4\pi} \frac{m_R^2}{T} \equiv \Gamma_0 z \tag{2.26}$$

into SM particles at tree level with a coupling strength $g_\nu$. As long as the neutrino decay rate is much faster than the gluon annihilation into neutrinos (and both are faster than the Hubble expansion), the gluons cannot maintain their equilibrium density and their energy is transferred to SM particles. The depletion terminates no later than $\sim m_R$, when any surviving right-handed neutrinos freeze out, and the gluon density decreases subsequently only due to Hubble expansion.

To give a concrete example, consider the following parameters: $N = 2$, $m_X = 2.5$ TeV, $\Lambda \simeq 1.4$ MeV, $m_C = 0.5$ TeV, $m_R = 1$ GeV, $g_h = 1.1$, $\lambda_R = 1.6$, and $g_\nu = 0.1$. The output glueball relic density is $\sim 5\%$ of the total dark matter abundance. We find this result by numerically solving the

coupled Boltzmann equations for the gluons and right-handed neutrinos:

$$Y_g'(z) = -z^{-6}\sigma_0 \frac{s(m_R)}{H(m_R)} \left(Y_g^2 - Y_R^2\right) \tag{2.27}$$

$$Y_R'(z) = -z^{-6}\sigma_0 \frac{s(m_R)}{H(m_R)} \left(Y_R^2 - Y_g^2\right) - z^2 \frac{\Gamma_0}{H(m_R)} Y_R \;, \tag{2.28}$$

where $s(m_R)$ and $H(m_R)$ are the entropy and Hubble rate at $T = m_R$. The initial conditions $Y_R(z_f)$ and $Y_g(z_f)$ are given by (2.3) at dark matter freezeout, $z_f = 25 m_R/m_X$. These differential equations tend to be fairly stiff, so in certain regions of parameter space, it is beneficial to decouple the equations. We may do so if the neutrino decay term dominates, allowing us to approximate $Y_R$ as exponentially decaying. Solving the decoupled differential equation yields results that are numerically similar (typically within 10%) to solving the full set of coupled equations when the decay term dominates.

There are few constraints on this mechanism. Prior to confinement, a large amount of entropy is transferred from the gluons to light SM particles. Since the right-handed neutrinos are still relativistic, there is no entropy nonthermally deposited into the visible sector. All the right-handed neutrino decay products fall into equilibrium with the bath well before BBN. With a nonzero glueball density, a concern might be that the glueballs will be able to decay to SM particles via off-shell right-handed neutrinos and nonthermally deposit entropy into the visible sector. If the right-handed neutrino decays into a left-handed neutrino and the Higgs, then we expect the glueball decay rate into $\bar{\nu}_L \nu_L e^+ e^- e^+ e^-$ to be

$$\Gamma_{\text{gb}} \sim y_e^4 g_\nu^4 \frac{\Lambda^{19}}{m_C^6 m_h^8 m_R^4} \;, \tag{2.29}$$

where $y_e$ is the electron Yukawa coupling and $m_h$ is the mass of the Higgs. This decay rate is slow enough that the glueballs are essentially stable. Furthermore, they will not contribute significantly to $N_{\text{eff}}$, since they are nonrelativistic below 1 MeV; and they will not have a large impact on the expansion rate of the universe during BBN, given their small energy density. Our glueball depletion process is robust, and it is consistent with terrestrial and cosmic constraints [148].

## 2.8 Conclusions

We have explored the possibility that dark matter may be a composite particle, made up of bound states of a dark analogue of QCD in the hidden sector. Such constructions lead to rich and varied phenomena that are distinct from the WIMP scenario more typically considered. It also naturally leads to large self-interactions of the dark matter, which can explain several observational puzzles in the small-scale structure of the universe.

The simplest scenarios contain only dark gluons, which confine into glueballs with cosmologically

interesting scattering cross sections for confinement scales around 100 MeV. Arranging the correct relic density requires one to disconnect the temperatures in the hidden and visible sectors such that their ratio at confinement is $\sim 10^{-3}$.

A richer theory arises when one considers supersymmetric versions, for which the dark gluino mass provides a separate mass scale and (in AMSB) can provide the correct relic density of glueballinos via the WIMPless miracle. The phenomenology depends crucially on how connected the hidden sector is to the visible matter. If there are no light connecting particles, one can dial the balance of dark matter from glueballs to glueballinos by adjusting the relative temperatures of the hidden and visible sectors. These mixed scenarios are strongly-interacting analogues of atomic dark matter [149–153], and inspire further simulation of the galactic dynamics in cases where there are two components of dark matter with naturally very different mass scales and different self-interaction rates. Such simulations would be very helpful to better understand the observational limits on these theories. For clusters, another important issue is the fact that the dark matter may have enough energy to scatter inelastically, bringing the details of the dark composite sector to the forefront of the physics; further work is needed to better understand the implications. We have also pointed out that our models have rich implications for the early growth of supermassive black holes. The mechanism by which $\sim 10^9 \, \mathrm{M}_\odot$ quasars are assembled as early as redshifts of 6–7 is a mystery, and self-interacting dark matter could have a major role to play in this story.

If the hidden and visible sectors are closely connected such that the temperatures remain comparable even at late times, the hidden glueballs will generically overclose the universe. We considered a depletion mechanism into right-handed neutrinos and found that it can efficiently remove hidden gluons before confinement. Self-interaction strengths required to explain the astrophysical puzzles on small scales are obtained for glueballino masses $\gtrsim 1$ TeV and confinement scales $\sim$ MeV.

The possibility of strong self-interactions in the dark sector is well motivated by observations of lower-than-expected dark matter densities in the centers of galaxies. A strongly-interacting hidden sector naturally realizes this possibility. Even in the simple models explored in this chapter, we have discovered new features that must be incorporated into numerical simulations to correctly predict the spatial distribution of dark matter in the central parts of structures from dwarf galaxies to clusters of galaxies.
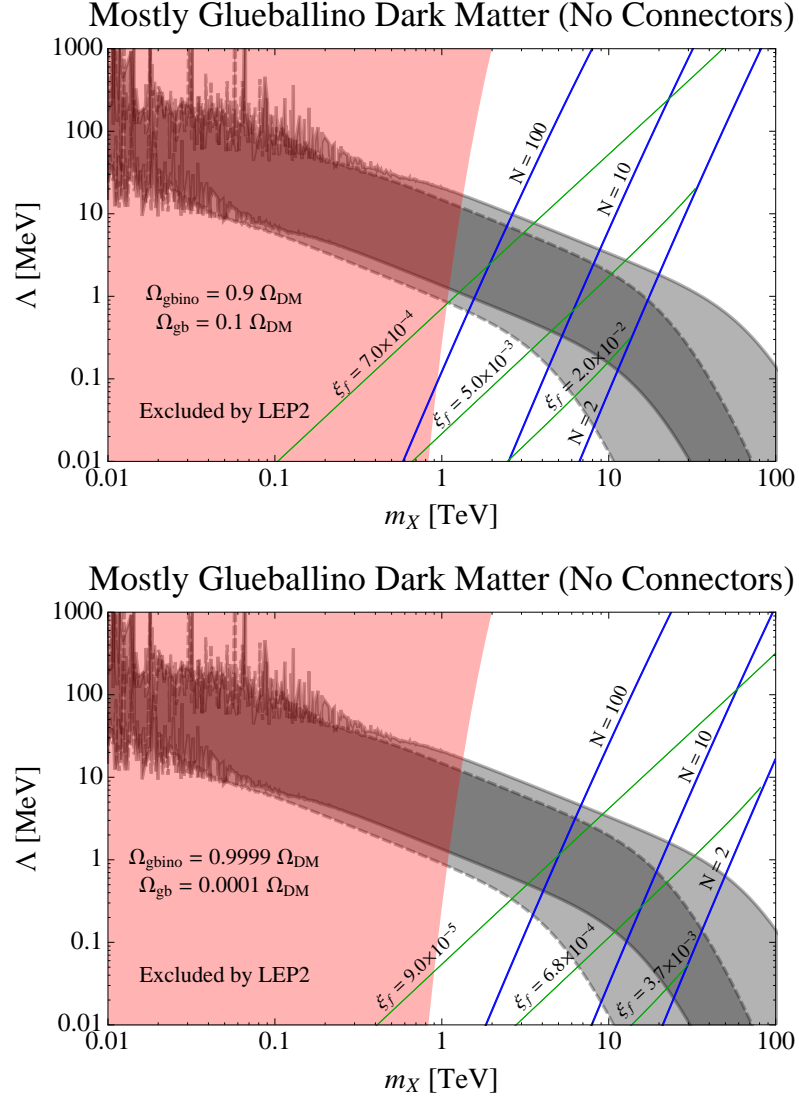
Figure 2.5: *Mostly glueballino dark matter in AMSB models with pure SU(N) hidden sectors without connectors.* Glueballinos make up 90% (top) or 99.99% (bottom) of the dark matter, and glueballs make up the remaining portion. For a point in the $(m_X, \Lambda)$ plane, these constraints on the relic densities determine $N$ and $\xi_f$; contours of constant $N$ and $\xi_f$ are shown. The gray shaded bands are from Fig. 2.4, and give the regions where the glueballino self-interaction cross section is in the preferred range. The red shaded region is excluded by null searches for visible-sector winos at LEP2. The yellow dot in the top panel defines a representative model with $m_X \simeq 14$ TeV, $\Lambda \simeq 0.35$ MeV, $N = 2$, and $\xi_f \simeq 0.02$.
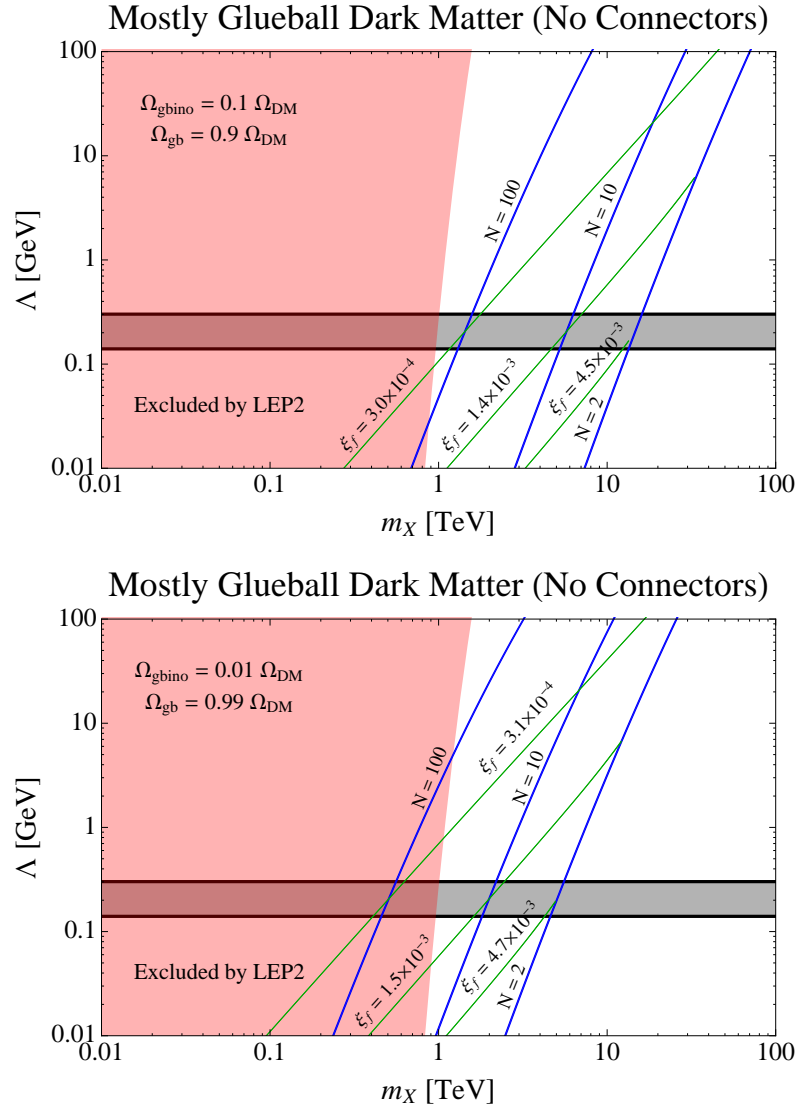
Figure 2.6: *Mostly glueball dark matter in AMSB models with pure SU(N) hidden sectors and no connectors.* Glueballs make up 90% (top) or 99% (bottom) of the dark matter, and glueballinos make up the remaining portion. For a point in the $(m_X, \Lambda)$ plane, these constraints on the relic densities determine $N$ and $\xi_f$; contours of constant $N$ and $\xi_f$ are shown. The gray shaded band is from Fig. 2.3, and gives the region where the glueball self-interaction cross section is in the preferred range. The red shaded region is excluded by null searches for visible-sector winos at LEP2.
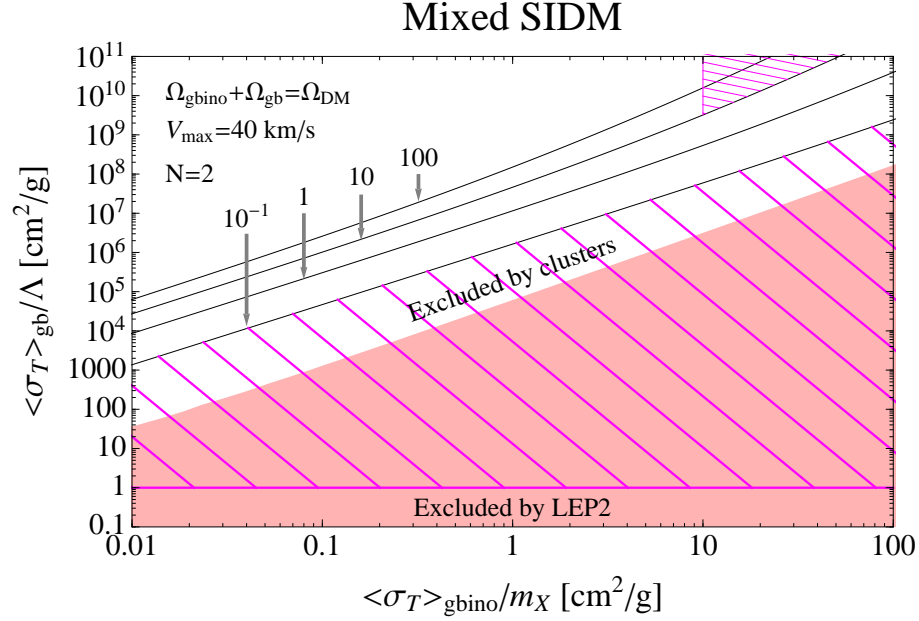
Figure 2.7: *Mixed dark matter without connectors to the SM.* We show curves of constant $\Omega_{\text{gbino}}/\Omega_{\text{gb}}$ in the $(\langle\sigma_T\rangle_{\text{gbino}}/m_X, \langle\sigma_T\rangle_{\text{gb}}/\Lambda)$ plane, for $N = 2$ and considering dwarf systems with $V_{\text{max}} = 40$ km/s. The black curves have $\Omega_{\text{gbino}}/\Omega_{\text{gb}} = 0.1, 1, 10, 100$, as indicated. The bound from LEP2 is shown in the red shaded region. A stronger bound from clusters is shown in the lower hatched magenta region; since the glueball scattering cross section is the same on all scales, its value is limited for the dwarf systems to avoid violating bounds from cluster scales. We caution the reader that the bound may be stronger, and it is certainly not as sharp as indicated by the hatched region. The hatched magenta wedge near the upper right-hand portion of the graph represents an upper limit of 10 cm$^2$/g for the case of mostly glueballino dark matter, which will have important implications for cores in dwarfs galaxies and may be excluded by a comparison to the observed core sizes and densities (*e.g.*, [8, 11]).
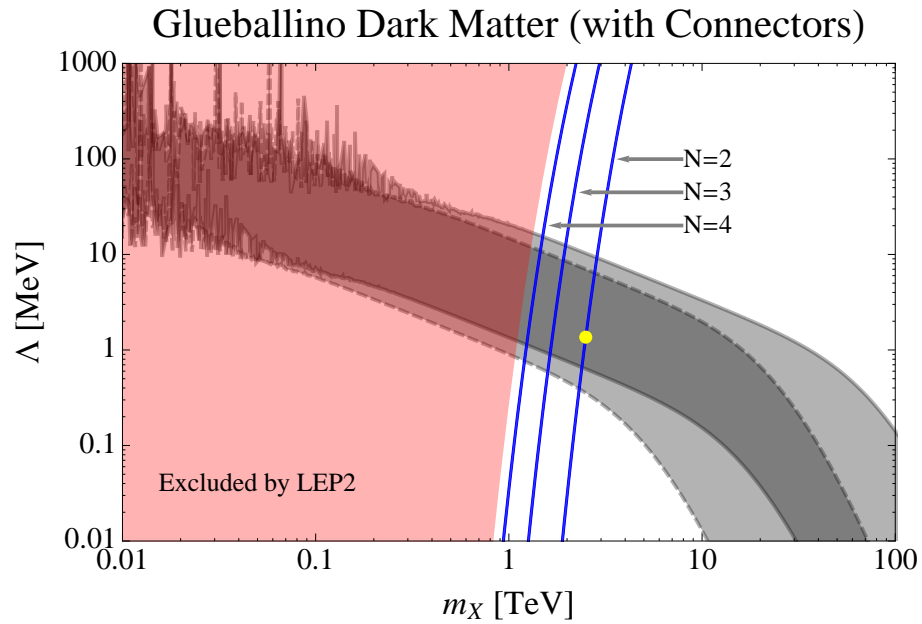
Figure 2.8: *Glueballino dark matter in AMSB models with pure SU(N) hidden sectors and connectors to the SM.* Glueballinos are assumed to make up all of the dark matter. The relic density constraints are given in the $(m_X, \Lambda)$ plane with $\xi_f = 1$; contours of constant $N$ are shown. The gray shaded bands are from Fig. 2.4 and give the regions where the glueballino self-interaction cross sections are in the preferred range. The red shaded region is excluded by null searches for visible-sector winos at LEP2. The yellow dot defines a representative model with $m_X \simeq 2.5$ TeV, $\Lambda \simeq 1.4$ MeV, and $N = 2$.

# Appendix

## 2.A   Solving the Schrödinger Equation for an Attractive Yukawa Potential

We are interested in the elastic scattering of fermionic glueballinos with mass $m_X$ via the exchange of scalar glueballs with mass $\Lambda$. The interaction strength is $\alpha = g^2/4\pi \approx 1$. This scenario is modeled as scattering from an attractive Yukawa potential

$$V(r) = -\frac{\alpha}{r} \exp(-\Lambda r) \ . \tag{2.30}$$

Note that if the exchange particle were a vector, we would have a combination of attractive $(\bar{X}X)$ and repulsive $(XX$ or $\bar{X}\bar{X})$ interactions. With a scalar mediator, only attractive interactions are possible. For convenience, we use the parameterization variables

$$R = \frac{m_X v}{\Lambda} \quad \text{and} \quad \beta = \frac{2\alpha\Lambda}{m_X v^2} \ , \tag{2.31}$$

where $v$ is the relative velocity of the scattering particles in the center-of-mass frame. The quantity $R$ compares the range of the interaction to the de Broglie wavelength of the scattering particle, and $\beta$ compares the potential and kinetic energy of the particle.

To make the connection between observation and simulation, it is common to use the transfer cross section (2.7). For a weak potential, it is straightforward to calculate the transfer cross section in the Born limit $(\alpha m_X \ll \Lambda)$:

$$\sigma_{T,\text{Born}} = \frac{2\pi}{\Lambda^2} \beta^2 \left[ \ln(1 + R^2) - \frac{R^2}{1 + R^2} \right] \ . \tag{2.32}$$

However, since $\alpha \approx 1$ and $m_X > \Lambda$, the Born limit is not applicable in our model. Instead, it is the nonperturbative regime that is relevant for this work, and the cross section receives large corrections for small $v$ [44, 133, 137, 154]. Within the nonperturbative regime, there are two important limits: the classical limit $(R \gg 1)$ and the quantum limit $(R \lesssim 1)$.

For the classical case, numerical studies for the Yukawa potential have been done in the context

of complex plasmas, and the following phenomenological forms of the transfer cross section agree well with the numerical results [134–136]:

$$\sigma_{T,\text{clas}} \simeq \begin{cases} \frac{4\pi}{\Lambda^2}\beta^2 \ln(1+\beta^{-1}) & \beta \lesssim 0.1 \\ \frac{8\pi}{\Lambda^2}\beta^2 \left(1 + 1.5\beta^{1.65}\right)^{-1} & 0.1 \lesssim \beta \lesssim 1000 \\ \frac{\pi}{\Lambda^2} \left(\ln \beta + 1 - \frac{1}{2}\ln^{-1}\beta\right)^2 & \beta \gtrsim 1000 \ . \end{cases} \tag{2.33}$$

Notice that for $\beta \gtrsim 1$, the transfer cross section changes slowly as a function of $v$. When $\beta \lesssim 1$, the transfer cross section approaches that for Rutherford scattering.

In the quantum limit, there are resonances due to zero energy bound state formation. It happens that the Yukawa potential may be approximated on very short or very long distance scales as the Hulthén potential

$$V_H(r) = -\alpha\delta\,\frac{e^{-\delta r}}{1 - e^{-\delta r}} \ . \tag{2.34}$$

The parameter $\delta$ can be set by matching to the wave function of the Yukawa potential. For $\delta = \kappa\Lambda$, matching to the Yukawa at $r \to 0$ gives $\kappa = \pi^2/6$ [155], whereas matching to the Yukawa at $r \to \infty$ gives $\kappa = \sqrt{2\zeta(3)}$ [133]. The advantage of the Hulthén potential is that it makes the Schrödinger equation analytically solvable for $l = 0$. Low partial waves dominate in the quantum limit, so the approximate analytic formula for the transfer cross section is [133]

$$\sigma_{T,\text{Hul}} = \frac{16\pi}{m_X^2 v^2}\sin^2\delta_0 \ , \tag{2.35}$$

where

$$\delta_0 = \arg\left[\frac{i\Gamma(iR/\kappa)}{\Gamma(\lambda_+)\Gamma(\lambda_-)}\right] \ , \tag{2.36}$$

$$\lambda_\pm \equiv 1 + \frac{iR}{2\kappa}\left(1 \pm \sqrt{1 - 2\beta\kappa}\right) \ . \tag{2.37}$$

In general, it is necessary to numerically solve the radial Schrödinger equation. Decomposing the scattering amplitude into partial waves, the transfer cross section may be written as

$$\sigma_T = \frac{4\pi}{k^2}\sum_{l=0}^{\infty}(l+1)\sin^2(\delta_{l+1} - \delta_l) \ , \tag{2.38}$$

where $\delta_l$ is the phase shift, determined by the asymptotic form of the wave function at $r \to \infty$, and $k = m_X v/2$ is the momentum of the reduced mass system. We refer the reader to [133] for details on numerically solving the differential equation, and we implement their algorithm for our work here, using the LSODA software from LLNL [156, 157] (all other calculations in this chapter were performed with Mathematica 8.0). Fig. 2.A.1 shows the numerical solutions of $\sigma_T k^2/4\pi$, scanning
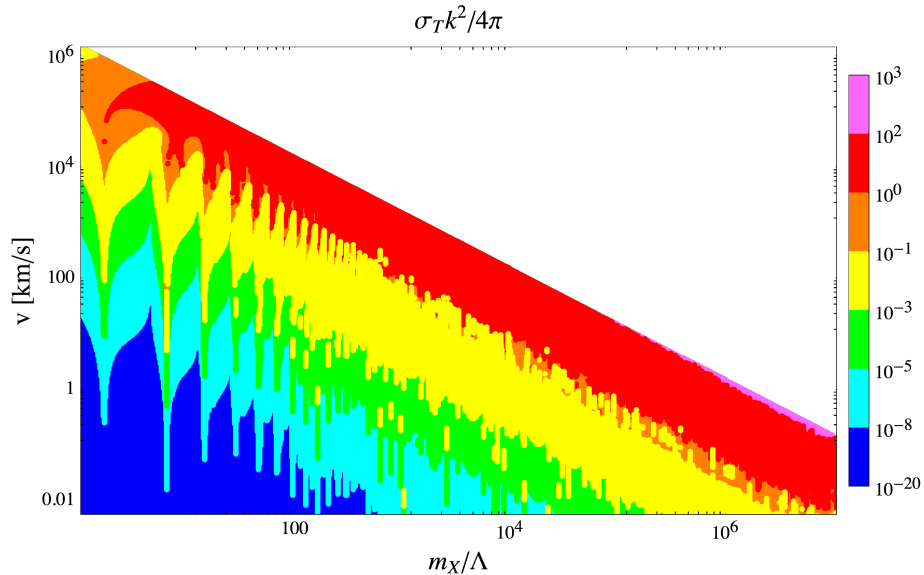
$$\sigma_T k^2/4\pi$$



Figure 2.A.1: Parameter scan to find numerically the transfer cross section. Values of $\sigma_T k^2/4\pi$ are color coded using the scale on the right. Parameter points with $R > 5$ have been excluded, since the computation becomes intensive in the classical regime, where many partial waves contribute. The peaking structure is the resonant behavior in the quantum limit. The Born regime occurs at lower $m_X/\Lambda$ and is not shown here.

the parameters $v$ and $m_X/\Lambda$.

To perform the integration for velocity averaging in (2.9), we match to the analytic expressions for the classical and quantum regimes, given in (2.33) and (2.35). For the sake of computation time, no set of parameters with $R > 5$ were used to numerically solve for $\sigma_T$, and we rely on the classical formulae. Given the ambiguity of $\kappa$ in the Hulthén potential, we scale $\kappa$ to match the numerical solution at low $v$ for a given mass ratio; however, uncertainties introduced in scaling have little effect, since velocities smaller than the ones shown in Fig. 2.A.1 will contribute very little to the integrals for $v_0 \geq 10$ km/s.

# Bibliography

[1] M. Kaplinghat, L. Knox, and M. S. Turner, "Annihilating the Cold Dark Matter Cusp Crisis," *Phys. Rev. Lett.* **85** (2000) 3335, `arXiv:astro-ph/0005210 [astro-ph]`.

[2] K. K. Boddy, S. M. Carroll, and M. Trodden, "Dark Matter with Density-Dependent Interactions," *Phys. Rev.* **D86** (2012) 123529, `arXiv:1208.4376 [astro-ph.CO]`.

[3] E. D. Carlson, M. E. Machacek, and L. J. Hall, "Self-Interacting Dark Matter," *Astrophys. J.* **398** (1992) 43.

[4] A. A. de Laix, R. J. Scherrer, and R. K. Schaefer, "Constraints of Selfinteracting Dark Matter," *Astrophys. J.* **452** (1995) 495, `arXiv:astro-ph/9502087 [astro-ph]`.

[5] D. N. Spergel and P. J. Steinhardt, "Observational Evidence for Selfinteracting Cold Dark Matter," *Phys. Rev. Lett.* **84** (2000) 3760, `arXiv:astro-ph/9909386 [astro-ph]`.

[6] B. D. Wandelt, R. Dave, G. R. Farrar, P. C. McGuire, D. N. Spergel, and P. J. Steinhardt, "Self-Interacting Dark Matter," in *Sources and Detection of Dark Matter and Dark Energy in the Universe*, Cline, D. B., ed., pp. 263–274. 2001. `arXiv:astro-ph/0006344 [astro-ph]`.

[7] C. Firmani, E. D'Onghia, V. Avila-Reese, G. Chincarini, and X. Hernandez, "Evidence of Self-Interacting Cold Dark Matter from Galactic to Galaxy Cluster Scales," *Mon. Not. R. Astron. Soc.* **315** (2000) L29, `arXiv:astro-ph/0002376 [astro-ph]`.

[8] M. Rocha, A. H. G. Peter, J. S. Bullock, M. Kaplinghat, S. Garrison-Kimmel, J. Oñorbe, and L. A. Moustakas, "Cosmological Simulations with Self-Interacting Dark Matter I: Constant Density Cores and Substructure," *Mon. Not. R. Astron. Soc.* **430** (2013) 81, `arXiv:1208.3025 [astro-ph.CO]`.

[9] A. H. G. Peter, M. Rocha, J. S. Bullock, and M. Kaplinghat, "Cosmological Simulations with Self-Interacting Dark Matter II: Halo Shapes vs. Observations," *Mon. Not. R. Astron. Soc.* **430** (2013) 105, `arXiv:1208.3026 [astro-ph.CO]`.

[10] M. Vogelsberger, J. Zavala, and A. Loeb, "Subhaloes in Self-Interacting Galactic Dark Matter Haloes," *Mon. Not. R. Astron. Soc.* **423** (2012) 3740, `arXiv:1201.5892 [astro-ph.CO]`.

[11] J. Zavala, M. Vogelsberger, and M. G. Walker, "Constraining Self-Interacting Dark Matter with the Milky Way's Dwarf Spheroidals," *Mon. Not. R. Astron. Soc.* **431** (2013) L20, `arXiv:1211.6426 [astro-ph.CO]`.

[12] K. K. Boddy, J. L. Feng, M. Kaplinghat, and T. M. P. Tait, "Self-Interacting Dark Matter from a Non-Abelian Hidden Sector," `arXiv:1402.3629 [hep-ph]`.

[13] J. Casas, J. Garcia-Bellido, and M. Quiros, "Scalar - Tensor Theories of Gravity with phi Dependent Masses," *Class. Quant. Grav.* **9** (1992) 1371, `arXiv:hep-ph/9204213 [hep-ph]`.

[14] G. W. Anderson and S. M. Carroll, "Dark Matter with Time Dependent Mass," in *Proceedings COSMO-97, 1st International Workshop on Particle Physics and the Early Universe, Ambleside, England, 1997*, L. Roszkowskip, ed., p. 227. World Scientific, Singapore, 1997. `arXiv:astro-ph/9711288 [astro-ph]`.

[15] L. Amendola, "Coupled Quintessence," *Phys. Rev.* **D62** (2000) 043511, `arXiv:astro-ph/9908023 [astro-ph]`.

[16] M. B. Hoffman, *Cosmological Constraints on a Dark Matter - Dark Energy Interaction*. PhD thesis, The University of Chicago, 2003. `arXiv:astro-ph/0307350 [astro-ph]`.

[17] G. R. Farrar and P. J. E. Peebles, "Interacting Dark Matter and Dark Energy," *Astrophys. J.* **604** (2004) 1, `arXiv:astro-ph/0307316 [astro-ph]`.

[18] R. Bean, E. E. Flanagan, and M. Trodden, "The Adiabatic Instability on Cosmology's Dark Side," *New J. Phys.* **10** (2008) 033006, `arXiv:0709.1124 [astro-ph]`.

[19] R. Bean, E. E. Flanagan, and M. Trodden, "Adiabatic Instability in Coupled Dark Energy-Dark Matter Models," *Phys. Rev.* **D78** (2008) 023009, `arXiv:0709.1128 [astro-ph]`.

[20] R. Bean, E. E. Flanagan, I. Laszlo, and M. Trodden, "Constraining Interactions in Cosmology's Dark Sector," *Phys. Rev.* **D78** (2008) 123514, `arXiv:0808.1105 [astro-ph]`.

[21] P. S. Corasaniti, "Slow-Roll Suppression of Adiabatic Instabilities in Coupled Scalar Field-Dark Matter Models," *Phys. Rev.* **D78** (2008) 083538, `arXiv:0808.1646 [astro-ph]`.

[22] T. Cohen, D. E. Morrissey, and A. Pierce, "Changes in Dark Matter Properties after Freeze-Out," *Phys. Rev.* **D78** (2008) 111701, `arXiv:0808.3994 [hep-ph]`.

[23] J. Khoury and A. Weltman, "Chameleon fields: Awaiting Surprises for Tests of Gravity in Space," *Phys. Rev. Lett.* **93** (2004) 171104, `arXiv:astro-ph/0309300 [astro-ph]`.

[24] J. Khoury and A. Weltman, "Chameleon Cosmology," *Phys. Rev.* **D69** (2004) 044026,
`arXiv:astro-ph/0309411 [astro-ph]`.

[25] P. Brax, C. van de Bruck, D. F. Mota, N. J. Nunes, and H. A. Winther, "Chameleons with
Field Dependent Couplings," *Phys. Rev.* **D82** (2010) 083503, `arXiv:1006.2796`
`[astro-ph.CO]`.

[26] R. Gannouji, B. Moraes, D. F. Mota, D. Polarski, S. Tsujikawa, *et al.*, "Chameleon Dark
Energy Models with Characteristic Signatures," *Phys. Rev.* **D82** (2010) 124006,
`arXiv:1010.3769 [astro-ph.CO]`.

[27] D. F. Mota and H. A. Winther, "Cosmology of Chameleons with Power-Law Couplings,"
*Astrophys. J.* **733** (2011) 7, `arXiv:1010.5650 [astro-ph.CO]`.

[28] A. Nelson and J. Walsh, "Chameleon Vector Bosons," *Phys. Rev.* **D77** (2008) 095006,
`arXiv:0802.0762 [hep-ph]`.

[29] J. L. Feng, H. Tu, and H.-B. Yu, "Thermal Relics in Hidden Sectors,"
*J. Cosmol. Astropart. Phys.* **0810** (2008) 043, `arXiv:0808.2318 [hep-ph]`.

[30] R. H. Cyburt, B. D. Fields, K. A. Olive, and E. Skillman, "New BBN Limits on Physics
Beyond the Standard Model from He-4," *Astropart. Phys.* **23** (2005) 313,
`arXiv:astro-ph/0408033 [astro-ph]`.

[31] L. Ackerman, M. R. Buckley, S. M. Carroll, and M. Kamionkowski, "Dark Matter and Dark
Radiation," *Phys. Rev.* **D79** (2009) 023519, `arXiv:0810.5126 [hep-ph]`.

[32] **WMAP** Collaboration, "Five-Year Wilkinson Microwave Anisotropy Probe (WMAP)
Observations: Data Processing, Sky Maps, and Basic Results," *Astrophys. J. Suppl.* **180**
(2009) 225, `arXiv:0803.0732 [astro-ph]`.

[33] D. Larson, J. Dunkley, G. Hinshaw, E. Komatsu, M. Nolta, *et al.*, "Seven-Year Wilkinson
Microwave Anisotropy Probe (WMAP) Observations: Power Spectra and WMAP-Derived
Parameters," *Astrophys. J. Suppl.* **192** (2011) 16, `arXiv:1001.4635 [astro-ph.CO]`.

[34] E. W. Kolb and M. S. Turner, *The Early Universe*. Frontiers in Physics. Addison-Wesley,
Reading, MA, 1990.

[35] C. L. Steinhardt, "Constraints on Field Theoretical Models for Variation of the Fine
Structure Constant," *Phys. Rev.* **D71** (2005) 043509, `arXiv:hep-ph/0308253 [hep-ph]`.

[36] N. D. Birrell and P. C. W. Davies, *Quantum Fields in Curved Space*. Cambridge Monographs
on Mathematical Physics. Cambridge University Press, 1984. First published 1982.
Reprinted 1989, 1992, 1994.

[37] P. Brax, C. van de Bruck, A.-C. Davis, J. Khoury, and A. Weltman, "Detecting Dark Energy in Orbit - The Cosmological Chameleon," *Phys. Rev.* **D70** (2004) 123518, `arXiv:astro-ph/0408415 [astro-ph]`.

[38] J. Edsjo and P. Gondolo, "Neutralino Relic Density including Coannihilations," *Phys. Rev.* **D56** (1997) 1879, `arXiv:hep-ph/9704361 [hep-ph]`.

[39] V. Berestetskii, E. Lifshitz, and L. Pitaevskii, *Quantum Electrodynamics*. Pergamon Press, Oxford; New York, 2 ed., 1982.

[40] A. Sommerfeld *Annalen der Physik* **403** (1931) 257.

[41] N. Arkani-Hamed, D. P. Finkbeiner, T. R. Slatyer, and N. Weiner, "A Theory of Dark Matter," *Phys. Rev.* **D79** (2009) 015014, `arXiv:0810.0713 [hep-ph]`.

[42] M. Lattanzi and J. I. Silk, "Can the WIMP Annihilation Boost Factor be Boosted by the Sommerfeld Enhancement?," *Phys. Rev.* **D79** (2009) 083523, `arXiv:0812.0360 [astro-ph]`.

[43] B. Robertson and A. Zentner, "Dark Matter Annihilation Rates with Velocity-Dependent Annihilation Cross Sections," *Phys. Rev.* **D79** (2009) 083525, `arXiv:0902.0362 [astro-ph.CO]`.

[44] M. R. Buckley and P. J. Fox, "Dark Matter Self-Interactions and Light Force Carriers," *Phys. Rev.* **D81** (2010) 083522, `arXiv:0911.3898 [hep-ph]`.

[45] S. Hannestad, "Can Dark Matter See Itself?," `arXiv:astro-ph/0008422 [astro-ph]`.

[46] R. Mertig, M. Bohm, and A. Denner, "FEYN CALC: Computer Algebraic Calculation of Feynman Amplitudes," *Comput. Phys. Commun.* **64** (1991) 345.

[47] G. 't Hooft and M. Veltman, "Scalar One Loop Integrals," *Nucl. Phys.* **B153** (1979) 365.

[48] G. Passarino and M. Veltman, "One Loop Corrections for e+ e- Annihilation into mu+ mu- in the Weinberg Model," *Nucl. Phys.* **B160** (1979) 151.

[49] M. Consoli, "One Loop Corrections To $e^+e^- \to e^+e^-$ in the Weinberg Model," *Nucl. Phys.* **B160** (1979) 208.

[50] A. Denner, "Techniques for Calculation of Electroweak Radiative Corrections at the One Loop Level and Results for W Physics at LEP-200," *Fortsch. Phys.* **41** (1993) 307, `arXiv:0709.1075 [hep-ph]`.

[51] P. Gondolo, P. Ko, and Y. Omura, "Light dark matter in leptophobic Z' models," *Phys. Rev.* **D85** (2012) 035022, `arXiv:1106.0885 [hep-ph]`.

[52] B. Holdom, "Two U(1)'s and Epsilon Charge Shifts," *Phys. Lett.* **B166** (1986) 196.

[53] J. L. Feng, M. Kaplinghat, and H.-B. Yu, "Sommerfeld Enhancements for Thermal Relic Dark Matter," *Phys. Rev.* **D82** (2010) 083525, `arXiv:1005.4678 [hep-ph]`.

[54] J. D. Bjorken, R. Essig, P. Schuster, and N. Toro, "New Fixed-Target Experiments to Search for Dark Gauge Forces," *Phys. Rev.* **D80** (2009) 075018, `arXiv:0906.0580 [hep-ph]`.

[55] B. Batell, M. Pospelov, and A. Ritz, "Probing a Secluded U(1) at B-factories," *Phys. Rev.* **D79** (2009) 115008, `arXiv:0903.0363 [hep-ph]`.

[56] M. Pospelov and A. Ritz, "Astrophysical Signatures of Secluded Dark Matter," *Phys. Lett.* **B671** (2009) 391, `arXiv:0810.1502 [hep-ph]`.

[57] M. Pospelov, "Secluded U(1) below the Weak Scale," *Phys. Rev.* **D80** (2009) 095002, `arXiv:0811.1030 [hep-ph]`. 14 pages, 2 figures.

[58] T. Hemmick, D. Elmore, T. Gentile, P. Kubik, S. Olsen, *et al.*, "A Search for Anomalously Heavy Isotopes of Low $Z$ Nuclei," *Phys. Rev.* **D41** (1990) 2074.

[59] P. Verkerk, G. Grynberg, B. Pichard, M. Spiro, S. Zylberajch, *et al.*, "Search for Superheavy Hydrogen in Sea Water," *Phys. Rev. Lett.* **68** (1992) 1116.

[60] T. Yamagata, Y. Takamori, and H. Utsunomiya, "Search for Anomalously Heavy Hydrogen in Deep Sea Water at 4000-m," *Phys. Rev.* **D47** (1993) 1231.

[61] L. Randall and R. Sundrum, "Out of this World Supersymmetry Breaking," *Nucl. Phys.* **B557** (1999) 79, `arXiv:hep-th/9810155 [hep-th]`.

[62] G. F. Giudice, M. A. Luty, H. Murayama, and R. Rattazzi, "Gaugino Mass without Singlets," *J. High Energy Phys.* **9812** (1998) 027, `arXiv:hep-ph/9810442 [hep-ph]`.

[63] J. L. Feng and J. Kumar, "The WIMPless Miracle: Dark-Matter Particles without Weak-Scale Masses or Weak Interactions," *Phys. Rev. Lett.* **101** (2008) 231301, `arXiv:0803.4196 [hep-ph]`.

[64] J. L. Feng and Y. Shadmi, "WIMPless Dark Matter from Non-Abelian Hidden Sectors with Anomaly-Mediated Supersymmetry Breaking," *Phys. Rev.* **D83** (2011) 095011, `arXiv:1102.0282 [hep-ph]`.

[65] J. L. Feng, V. Rentala, and Z. Surujon, "WIMPless Dark Matter in Anomaly-Mediated Supersymmetry Breaking with Hidden QED," *Phys. Rev.* **D84** (2011) 095033, `arXiv:1108.4689 [hep-ph]`.

[66] J. L. Feng, V. Rentala, and Z. Surujon, "WIMPless Dark Matter from an AMSB Hidden Sector with No New Mass Parameters," *Phys. Rev.* **D85** (2012) 055003, `arXiv:1111.4479 [hep-ph]`.

[67] G. D. Kribs, T. S. Roy, J. Terning, and K. M. Zurek, "Quirky Composite Dark Matter," *Phys. Rev.* **D81** (2010) 095001, `arXiv:0909.2034 [hep-ph]`.

[68] D. S. Alves, S. R. Behbahani, P. Schuster, and J. G. Wacker, "Composite Inelastic Dark Matter," *Phys. Lett.* **B692** (2010) 323, `arXiv:0903.3945 [hep-ph]`.

[69] A. Falkowski, J. Juknevich, and J. Shelton, "Dark Matter Through the Neutrino Portal," `arXiv:0908.1790 [hep-ph]`.

[70] M. Lisanti and J. G. Wacker, "Parity Violation in Composite Inelastic Dark Matter Models," *Phys. Rev.* **D82** (2010) 055023, `arXiv:0911.4483 [hep-ph]`.

[71] D. Spier Moreira Alves, S. R. Behbahani, P. Schuster, and J. G. Wacker, "The Cosmology of Composite Inelastic Dark Matter," *J. High Energy Phys.* **1006** (2010) 113, `arXiv:1003.4729 [hep-ph]`.

[72] K. Kumar, A. Menon, and T. M. Tait, "Magnetic Fluffy Dark Matter," *J. High Energy Phys.* **1202** (2012) 131, `arXiv:1111.2336 [hep-ph]`.

[73] J. M. Cline, Z. Liu, G. Moore, and W. Xue, "Composite Strongly Interacting Dark Matter," `arXiv:1312.3325 [hep-ph]`.

[74] J. Kang, M. A. Luty, and S. Nasri, "The Relic Abundance of Long-Lived Heavy Colored Particles," *J. High Energy Phys.* **0809** (2008) 086, `arXiv:hep-ph/0611322 [hep-ph]`.

[75] Y. Bai and P. Schwaller, "The Scale of Dark QCD," *Phys. Rev.* **D89** (2014) 063522, `arXiv:1306.4676 [hep-ph]`.

[76] **WMAP** Collaboration, "Nine-Year Wilkinson Microwave Anisotropy Probe (WMAP) Observations: Cosmological Parameter Results," *Astrophys. J. Suppl.* **208** (2013) 19, `arXiv:1212.5226 [astro-ph.CO]`.

[77] **Planck** Collaboration, "Planck 2013 Results. XVI. Cosmological Parameters," `arXiv:1303.5076 [astro-ph.CO]`.

[78] B. A. Reid, W. J. Percival, D. J. Eisenstein, L. Verde, D. N. Spergel, *et al.*, "Cosmological Constraints from the Clustering of the Sloan Digital Sky Survey DR7 Luminous Red Galaxies," *Mon. Not. R. Astron. Soc.* **404** (2010) 60, `arXiv:0907.1659 [astro-ph.CO]`.

[79] **SDSS** Collaboration, "The Seventh Data Release of the Sloan Digital Sky Survey,"
*Astrophys. J. Suppl.* **182** (2009) 543, arXiv:0812.0649 [astro-ph].

[80] J. F. Navarro, C. S. Frenk, and S. D. White, "The Assembly of Galaxies in a Hierarchically
Clustering Universe," *Mon. Not. R. Astron. Soc.* **275** (1995) 56, arXiv:astro-ph/9408067
[astro-ph].

[81] J. F. Navarro, C. S. Frenk, and S. D. White, "The Structure of Cold Dark Matter Halos,"
*Astrophys. J.* **462** (1996) 563, arXiv:astro-ph/9508025 [astro-ph].

[82] J. F. Navarro, C. S. Frenk, and S. D. White, "A Universal Density Profile from Hierarchical
Clustering," *Astrophys. J.* **490** (1997) 493, arXiv:astro-ph/9611107 [astro-ph].

[83] J. S. Bullock, T. S. Kolatt, Y. Sigad, R. S. Somerville, A. V. Kravtsov, A. A. Klypin, J. R.
Primack, and A. Dekel, "Profiles of Dark Haloes. Evolution, Scatter, and Environment,"
*Mon. Not. R. Astron. Soc.* **321** (2001) 559, arXiv:astro-ph/9908159 [astro-ph].

[84] R. H. Wechsler, J. S. Bullock, J. R. Primack, A. V. Kravtsov, and A. Dekel, "Concentrations
of Dark Halos from Their Assembly Histories," *Astrophys. J.* **568** (2002) 52,
arXiv:astro-ph/0108151 [astro-ph].

[85] R. A. Flores and J. R. Primack, "Observational and Theoretical Constraints on Singular
Dark Matter Halos," *Astrophys. J.* **427** (1994) L1, arXiv:astro-ph/9402004 [astro-ph].

[86] J. D. Simon, A. D. Bolatto, A. Leroy, L. Blitz, and E. L. Gates, "High-Resolution
Measurements of the Halos of Four Dark Matter-Dominated Galaxies: Deviations from a
Universal Density Profile," *Astrophys. J.* **621** (2005) 757, arXiv:astro-ph/0412035
[astro-ph].

[87] R. Kuzio de Naray, S. S. McGaugh, and W. de Blok, "Mass Models for Low Surface
Brightness Galaxies with High Resolution Optical Velocity Fields," *Astrophys. J.* **676** (2008)
920, arXiv:0712.0860 [astro-ph].

[88] A. A. Dutton, C. Conroy, F. C. d. Bosch, L. Simard, T. Mendel, *et al.*, "Dark Halo Response
and the Stellar Initial Mass Function in Early-Type and Late-Type Galaxies," *Mon. Not.
R. Astron. Soc.* **416** (2011) 322, arXiv:1012.5859 [astro-ph.CO].

[89] R. K. de Naray and K. Spekkens, "Do Baryons Alter the Halos of Low Surface Brightness
Galaxies?," *Astrophys. J.* **741** (2011) L29, arXiv:1109.1288 [astro-ph.CO].

[90] S.-H. Oh, W. de Blok, E. Brinks, F. Walter, and J. Kennicutt, Robert C., "Dark and
Luminous Matter in THINGS Dwarf Galaxies," *Astron. J.* **141** (2011) 193,
arXiv:1011.0899 [astro-ph.CO].

[91] P. Salucci, M. I. Wilkinson, M. G. Walker, G. F. Gilmore, E. K. Grebel, A. Koch, C. Frigerio Martins, and R. F. G. Wyse, "Dwarf Spheroidal Galaxy Kinematics and Spiral Galaxy Scaling Laws," *Mon. Not. R. Astron. Soc.* **420** (2012) 2034, `arXiv:1111.1165 [astro-ph.CO]`.

[92] G. Castignani, N. Frusciante, D. Vernieri, and P. Salucci, "The Density Profiles of Dark Matter Halos in Spiral Galaxies," *Natural Sci.* **4** (2012) 265, `arXiv:1201.3998 [astro-ph.CO]`.

[93] M. G. Walker and J. Penarrubia, "A Method for Measuring (Slopes of) the Mass Profiles of Dwarf Spheroidal Galaxies," *Astrophys. J.* **742** (2011) 20, `arXiv:1108.2404 [astro-ph.CO]`.

[94] D. J. Sand, T. Treu, G. Smith, and R. Ellis, "The Dark Matter Distribution in the Central Regions of Galaxy Clusters," *Astrophys. J.* **604** (2004) 88, `arXiv:astro-ph/0310703 [astro-ph]`.

[95] D. Sand, T. Treu, R. Ellis, G. Smith, and J.-P. Kneib, "Separating Baryons and Dark Matter in Cluster Cores: A Full 2D Lensing and Dynamic Analysis of Abell 383 and MS2137-23," *Astrophys. J.* **674** (2008) 711, `arXiv:0710.1069 [astro-ph]`.

[96] A. B. Newman, T. Treu, R. S. Ellis, D. J. Sand, J. Richard, P. J. Marshall, P. Capak, and S. Miyazaki, "The Distribution of Dark Matter Over Three Decades in Radius in the Lensing Cluster Abell 611," *Astrophys. J.* **706** (2009) 1078, `arXiv:0909.3527 [astro-ph.CO]`.

[97] A. B. Newman, T. Treu, R. S. Ellis, and D. J. Sand, "The Dark Matter Distribution in Abell 383: Evidence for a Shallow Density Cusp from Improved Lensing, Stellar Kinematic and X-ray Data," *Astrophys. J.* **728** (2011) L39, `arXiv:1101.3553 [astro-ph.CO]`.

[98] D. Coe, K. Umetsu, A. Zitrin, M. Donahue, E. Medezinski, *et al.*, "CLASH: Precise New Constraints on the Mass Profile of Abell 2261," *Astrophys. J.* **757** (2012) 22, `arXiv:1201.1616 [astro-ph.CO]`.

[99] K. Umetsu, E. Medezinski, M. Nonino, J. Merten, A. Zitrin, *et al.*, "CLASH: Mass Distribution in and around MACS J1206.2-0847 from a Full Cluster Lensing Analysis," *Astrophys. J.* **755** (2012) 56, `arXiv:1204.3630 [astro-ph.CO]`.

[100] W. de Blok, "The Core-Cusp Problem," *Advances in Astronomy* **2010** (2010) 789293, `arXiv:0910.3538 [astro-ph.CO]`.

[101] V. Springel, J. Wang, M. Vogelsberger, A. Ludlow, A. Jenkins, A. Helmi, J. F. Navarro, C. S. Frenk, and S. D. M. White, "The Aquarius Project: the subhalos of galactic halos," *Mon. Not. R. Astron. Soc.* **391** (2008) 1685, `arXiv:0809.0898 [astro-ph]`.

[102] M. Boylan-Kolchin, J. S. Bullock, and M. Kaplinghat, "Too Big to Fail? The Puzzling Darkness of Massive Milky Way Subhaloes," *Mon. Not. R. Astron. Soc.* **415** (2011) L40, arXiv:1103.0007 [astro-ph.CO].

[103] M. Boylan-Kolchin, J. S. Bullock, and M. Kaplinghat, "The Milky Way's Bright Satellites as an Apparent Failure of LCDM," *Mon. Not. R. Astron. Soc.* **422** (2012) 1203, arXiv:1111.2048 [astro-ph.CO].

[104] D. H. Weinberg, J. S. Bullock, F. Governato, R. K. de Naray, and A. H. G. Peter, "Cold Dark Matter: Controversies on Small Scales," arXiv:1306.0913 [astro-ph.CO].

[105] S.-H. Oh, C. Brook, F. Governato, E. Brinks, L. Mayer, *et al.*, "The Central Slope of Dark Matter Cores in Dwarf Galaxies: Simulations vs. THINGS," *Astron. J.* **142** (2011) 24, arXiv:1011.2777 [astro-ph.CO].

[106] F. Governato, A. Zolotov, A. Pontzen, C. Christensen, S. H. Oh, A. M. Brooks, T. Quinn, S. Shen, and J. Wadsley, "Cuspy No More: How Outflows Affect the Central Dark Matter and Baryon Distribution in Lambda CDM Galaxies," *Mon. Not. R. Astron. Soc.* **422** (2012) 1231, arXiv:1202.0554 [astro-ph.CO].

[107] A. B. Newman, T. Treu, R. S. Ellis, and D. J. Sand, "The Density Profiles of Massive, Relaxed Galaxy Clusters: II. Separating Luminous and Dark Matter in Cluster Cores," *Astrophys. J.* **765** (2013) 25, arXiv:1209.1392 [astro-ph.CO].

[108] S. Tremaine and J. Gunn, "Dynamical Role of Light Neutral Leptons in Cosmology," *Phys. Rev. Lett.* **42** (1979) 407.

[109] J. Bond, G. Efstathiou, and J. Silk, "Massive Neutrinos and the Large Scale Structure of the Universe," *Phys. Rev. Lett.* **45** (1980) 1980.

[110] K. A. Olive and M. S. Turner, "Cosmological Bounds on the Masses of Stable, Right-Handed Neutrinos," *Phys. Rev.* **D25** (1982) 213.

[111] C. Firmani, E. D'Onghia, G. Chincarini, X. Hernandez, and V. Avila-Reese, "Constraints on Dark Matter Physics from Dwarf Galaxies through Galaxy Cluster Haloes," *Mon. Not. R. Astron. Soc.* **321** (2001) 713, arXiv:astro-ph/0005001 [astro-ph].

[112] E. Polisensky and M. Ricotti, "Constraints on the Dark Matter Particle Mass from the Number of Milky Way Satellites," *Phys. Rev.* **D83** (2011) 043506, arXiv:1004.1459 [astro-ph.CO].

[113] U. Seljak, A. Makarov, P. McDonald, and H. Trac, "Can Sterile Neutrinos be the Dark Matter?," *Phys. Rev. Lett.* **97** (2006) 191303, arXiv:astro-ph/0602430 [astro-ph].

[114] M. Viel, G. Becker, J. Bolton, and M. Haehnelt, "Warm Dark Matter as a Solution to the Small Scale Crisis: New Constraints from High Redshift Lyman-alpha Forest Data," *Phys. Rev.* **D88** (2013) 043502, `arXiv:1306.2314 [astro-ph.CO]`.

[115] R. K. de Naray, G. D. Martinez, J. S. Bullock, and M. Kaplinghat, "The Case Against Warm or Self-Interacting Dark Matter as Explanations for Cores in Low Surface Brightness Galaxies," *Astrophys. J.* **710** (2010) L161, `arXiv:0912.3518 [astro-ph.CO]`.

[116] S. W. Randall, M. Markevitch, D. Clowe, A. H. Gonzalez, and M. Bradac, "Constraints on the Self-Interaction Cross-Section of Dark Matter from Numerical Simulations of the Merging Galaxy Cluster 1E 0657-56," *Astrophys. J.* **679** (2008) 1173, `arXiv:0704.0261 [astro-ph]`.

[117] D. D. Dietrich and F. Sannino, "Conformal Window of SU(N) Gauge Theories with Fermions in Higher Dimensional Representations," *Phys. Rev.* **D75** (2007) 085018, `arXiv:hep-ph/0611341 [hep-ph]`.

[118] T. Appelquist, A. Ratnaweera, J. Terning, and L. Wijewardhana, "The Phase Structure of an SU(N) Gauge Theory with N(f) Flavors," *Phys. Rev.* **D58** (1998) 105017, `arXiv:hep-ph/9806472 [hep-ph]`.

[119] V. Miransky and K. Yamawaki, "Conformal Phase Transition in Gauge Theories," *Phys. Rev.* **D55** (1997) 5051, `arXiv:hep-th/9611142 [hep-th]`.

[120] A. G. Cohen and H. Georgi, "Walking Beyond the Rainbow," *Nucl. Phys.* **B314** (1989) 7.

[121] T. Appelquist, K. D. Lane, and U. Mahanta, "On the Ladder Approximation for Spontaneous Chiral Symmetry Breaking," *Phys. Rev. Lett.* **61** (1988) 1553.

[122] E. Poppitz and M. Unsal, "Conformality or confinement (II): One-Flavor CFTs and Mixed-Representation QCD," *J. High Energy Phys.* **0912** (2009) 011, `arXiv:0910.1245 [hep-th]`.

[123] E. Poppitz and M. Unsal, "Conformality or Confinement: (IR)relevance of Topological Excitations," *J. High Energy Phys.* **0909** (2009) 050, `arXiv:0906.5156 [hep-th]`.

[124] S. Narison, "Masses, Decays and Mixings of Gluonia in QCD," *Nucl. Phys. Proc. Suppl.* **64** (1998) 210, `arXiv:hep-ph/9710281 [hep-ph]`.

[125] C. J. Morningstar and M. J. Peardon, "The Glueball Spectrum from an Anisotropic Lattice Study," *Phys. Rev.* **D60** (1999) 034509, `arXiv:hep-lat/9901004 [hep-lat]`.

[126] A. Manohar and H. Georgi, "Chiral Quarks and the Nonrelativistic Quark Model," *Nucl. Phys.* **B234** (1984) 189.

[127] A. G. Cohen, D. B. Kaplan, and A. E. Nelson, "Counting 4 pis in Strongly Coupled Supersymmetry," *Phys. Lett.* **B412** (1997) 301, `arXiv:hep-ph/9706275 [hep-ph]`.

[128] B. Lucini, M. Teper, and U. Wenger, "Properties of the Deconfining Phase Transition in SU(N) Gauge Theories," *J. High Energy Phys.* **0502** (2005) 033, `arXiv:hep-lat/0502003 [hep-lat]`.

[129] G. R. Farrar, "Phenomenology of Light Gauginos. 1. Motivation, Masses, Lifetimes and Limits," `arXiv:hep-ph/9508291 [hep-ph]`.

[130] S. Raby, "Gauge Mediated SUSY Breaking at an Intermediate Scale," *Phys. Rev.* **D56** (1997) 2852, `arXiv:hep-ph/9702299 [hep-ph]`.

[131] S. Raby and K. Tobe, "The Phenomenology of SUSY Models with a Gluino LSP," *Nucl. Phys.* **B539** (1999) 3, `arXiv:hep-ph/9807281 [hep-ph]`.

[132] M. R. Kauth, J. H. Kuhn, P. Marquard, and M. Steinhauser, "Gluinonia: Energy Levels, Production and Decay," *Nucl. Phys.* **B831** (2010) 285, `arXiv:0910.2612 [hep-ph]`.

[133] S. Tulin, H.-B. Yu, and K. M. Zurek, "Beyond Collisionless Dark Matter: Particle Physics Dynamics for Dark Matter Halo Structure," *Phys. Rev.* **D87** (2013) 115007, `arXiv:1302.3898 [hep-ph]`.

[134] S. A. Khrapak, A. V. Ivlev, G. E. Morfill, and S. K. Zhdanov, "Scattering in the attractive yukawa potential in the limit of strong interaction," *Phys. Rev. Lett.* **90** (2003) 225002. `http://link.aps.org/doi/10.1103/PhysRevLett.90.225002`.

[135] S. Khrapak, A. Ivlev, G. Morfill, S. Zhdanov, and H. Thomas, "Scattering in the attractive yukawa potential: Application to the ion-drag force in complex plasmas," *IEEE Transactions on Plasma Science* **32** (2004) 555 .

[136] S. A. Khrapak, A. V. Ivlev, and G. E. Morfill, "Momentum transfer in complex plasmas," *Phys. Rev.* **E70** (2004) 056405.

[137] J. L. Feng, M. Kaplinghat, and H.-B. Yu, "Halo Shape and Relic Density Exclusions of Sommerfeld-Enhanced Dark Matter Explanations of Cosmic Ray Excesses," *Phys. Rev. Lett.* **104** (2010) 151301, `arXiv:0911.0422 [hep-ph]`.

[138] M. Vogelsberger and J. Zavala, "Direct Detection of Self-Interacting Dark Matter," *Mon. Not. R. Astron. Soc.* **430** (2013) 1722, `arXiv:1211.1377 [astro-ph.CO]`.

[139] J. Hisano, S. Matsumoto, M. Nagai, O. Saito, and M. Senami, "Non-Perturbative Effect on Thermal Relic Abundance of Dark Matter," *Phys. Lett.* **B646** (2007) 34, `arXiv:hep-ph/0610249 [hep-ph]`.

[140] A. Hryczuk, R. Iengo, and P. Ullio, "Relic Densities Including Sommerfeld Enhancements in the MSSM," *J. High Energy Phys.* **1103** (2011) 069, `arXiv:1010.2172 [hep-ph]`.

[141] LEP2 SUSY Working Group, ALEPH, DELPHI, L3 and OPAL experiments, "Charginos, Large m0." LEPSUSYWG/01-03.1.

[142] LEP2 SUSY Working Group, ALEPH, DELPHI, L3 and OPAL experiments, "Charginos, at Small DM." LEPSUSYWG/02-04.1.

[143] J. F. Hennawi and J. P. Ostriker, "Observational Constraints on the Self Interacting Dark Matter Scenario and the Growth of Supermassive Black Holes," *Astrophys. J.* **572** (2002) 41, `arXiv:astro-ph/0108203 [astro-ph]`.

[144] T. Tanaka and Z. Haiman, "The Assembly of Supermassive Black Holes at High Redshifts," *Astrophys. J.* **696** (2009) 1798, `arXiv:0807.4702 [astro-ph]`.

[145] D. J. Mortlock, S. J. Warren, B. P. Venemans, M. Patel, P. C. Hewett, *et al.*, "A Luminous Quasar at a Redshift of z = 7.085," *Nature* **474** (2011) 616, `arXiv:1106.6088 [astro-ph.CO]`.

[146] K. Gultekin, D. O. Richstone, K. Gebhardt, T. R. Lauer, S. Tremaine, *et al.*, "The M-sigma and M-L Relations in Galactic Bulges and Determinations of their Intrinsic Scatter," *Astrophys. J.* **698** (2009) 198, `arXiv:0903.4897 [astro-ph.GA]`.

[147] A. Beifiori, S. Courteau, E. Corsini, and Y. Zhu, "On the Correlations between Galaxy Properties and Supermassive Black Hole Mass," *Mon. Not. R. Astron. Soc.* **419** (2012) 2497, `arXiv:1109.6265 [astro-ph.CO]`.

[148] K. Abazajian, M. Acero, S. Agarwalla, A. Aguilar-Arevalo, C. Albright, *et al.*, "Light Sterile Neutrinos: A White Paper," `arXiv:1204.5379 [hep-ph]`.

[149] D. E. Kaplan, G. Z. Krnjaic, K. R. Rehermann, and C. M. Wells, "Atomic Dark Matter," *J. Cosmol. Astropart. Phys.* **1005** (2010) 021, `arXiv:0909.0753 [hep-ph]`.

[150] F.-Y. Cyr-Racine and K. Sigurdson, "Cosmology of Atomic Dark Matter," *Phys. Rev.* **D87** (2013) 103515, `arXiv:1209.5752 [astro-ph.CO]`.

[151] J. M. Cline, Z. Liu, G. Moore, and W. Xue, "Scattering Properties of Dark Atoms and Molecules," *Phys. Rev.* **D89** (2014) 043514, `arXiv:1311.6468 [hep-ph]`.

[152] F. Kahlhoefer, K. Schmidt-Hoberg, M. T. Frandsen, and S. Sarkar, "Colliding Clusters and Dark Matter Self-Interactions," *Mon. Not. R. Astron. Soc.* **437** (2014) 2865, `arXiv:1308.3419 [astro-ph.CO]`.

[153] J. Fan, A. Katz, L. Randall, and M. Reece, "Double-Disk Dark Matter," *Phys. Dark Univ.* **2** (2013) 139, `arXiv:1303.1521 [astro-ph.CO]`.

[154] S. Tulin, H.-B. Yu, and K. M. Zurek, "Resonant Dark Forces and Small Scale Structure," `arXiv:1210.0900 [hep-ph]`.

[155] S. Cassel, "Sommerfeld Factor for Arbitrary Partial Wave Processes," *J. Phys.* **G37** (2010) 105009, `arXiv:0903.5307 [hep-ph]`.

[156] A. Hindmarsh, "ODEPACK, A Systematized Collection of ODE Solvers," in *IMACS Transactions on Scientific Computation*, R. S. et al., ed., vol. 1, pp. 55–64. North-Holland, Amsterdam, 1983.

[157] K. Radhakrishnan and A. C. Hindmarsh, "Description and Use of LSODE, the Livermore Solver for Ordinary Differential Equations," Tech. Rep. UCRL-ID-113855, LLNL, December, 1993.

# Part II

# Fluctuations in Cosmology

Since the discovery of the acceleration of the universe [1, 2], the standard cosmological model—with cosmological constant $\Lambda$, cold dark matter, and approximately scale-free primordial perturbations ($\Lambda$CDM)—has provided an excellent fit to a wide variety of data. However, a problem lurks in the future. As the universe empties out, it approaches a de Sitter phase. The Hubble parameter in de Sitter is constant and related to the cosmological constant by $H = \sqrt{\Lambda/3}$. A stationary observer is surrounded by a cosmological horizon at a distance $R = H^{-1}$. Quantum field theory (QFT) in curved spacetime describes a unique state that is both de Sitter invariant and Hadamard (well-behaved at short distances), called the Euclidean (or Bunch-Davies [3, 4]) vacuum for a free, massive scalar field or the Hartle-Hawking vacuum [5] for an interacting scalar field. A particle detector sensitive to a field in the Hartle-Hawking vacuum will detect thermal Gibbons-Hawking radiation with a temperature $T = H/2\pi$ [6]. Each horizon-sized patch (which we will henceforth simply call a patch) of de Sitter can be associated with an entropy equal to the area of the horizon in Planck units, $S = 3\pi/G\Lambda$ ($S \sim 10^{122}$ for the measured value of $\Lambda$). In horizon complementarity, the quantum state of each patch can be described by a density operator defined on a Hilbert space of dimension $\dim \mathcal{H} = e^S$ [7, 8].

Conventional wisdom holds that the Hartle-Hawking vacuum experiences fluctuations, which may be thought of as being either quantum or thermal, since a patch is a quantum system at a fixed temperature. These fluctuations play several important roles in modern cosmological models. During inflation, when the metric is approximately de Sitter, fluctuations seed the density perturbations responsible for the cosmic microwave background (CMB) anisotropies and large-scale structure [9–11]. Eternal inflation (either stochastic [12–14] or in a landscape of vacua [15–19]) makes use of fluctuations upward in energy density, often described as uptunneling [20, 21]. Finally, the phenomena of Poincaré recurrences [22] and Boltzmann fluctuations can be problematic features of long-lived de Sitter phases. In particular, there is a nonzero rate to fluctuate into any particular local macroscopic configuration of matter allowed by conservation laws, including conscious creatures without any supporting environment (known as Boltzmann brains [23–26]) or for that matter to observers in precisely the macrocondition we find ourselves in at the present moment. Such a scenario implies that our memories and impressions of the past are unlikely to correlate with actual events, but rather to arise from random fluctuations. An empirically viable theory should predict that observable data correlates to the external environment in reliable ways, so we seek theories that avoid Boltzmann brain domination.

In Chapter 3, we attempt to alleviate the Boltzmann brain problem through the instability of the Standard Model electroweak vacuum [27]. The Higgs potential drops below the electroweak vacuum at large field values, so it is possible that Boltzmann brain production is inhibited if the decay rate of the electroweak vacuum is large enough. Otherwise, we must choose a measure on which to calculate the rate Boltzmann brains, and any measure that admits a large number of them

is unacceptable.

Upon further investigation into the nature of fluctuations in de Sitter space, we unveil a deeper problem with the conventional understanding and argue that fluctuations do not occur at all under certain circumstances. The Hartle-Hawking vacuum is stationary, and there is no sense in which fluctuations exist. The observational outcomes of measurements on a quantum mechanical system exhibit quantum fluctuations, but these fluctuations are not inherently the same as classical stochastic fluctuations. In Chapter 4, we present our case against fluctuations in the de Sitter vacuum and comment on the impact it has on widely-accepted theories that take the existence of fluctuations for granted [28].

# Chapter 3

# Can the Higgs Boson Save Us from the Menace of the Boltzmann Brains?

## 3.1   Introduction

The troublesome Boltzmann brain (BB) problem has nothing to do with speculative ideas about eternal inflation or the cosmological multiverse; it is a difficulty of known physics, or at least the simplest interpretation thereof (a constant vacuum energy, QFT in curved spacetime). It is therefore worth asking whether there can be any escape from the BB challenge within known physics.

The simplest solution is if our current vacuum state is unstable and can decay into a different vacuum before BBs form [25]. Within the Standard Model (SM), sufficiently rapid decay is possible if the Higgs field has another vacuum with a lower energy density. Interestingly, renormalization-group calculations using current measurements of SM parameters indicate that the Higgs is susceptible to decay to a larger expectation value [29–42]. We point out that the decay rate might be fast enough to avoid the BB problem, but only if the mass of the top quark is near 178 GeV, a bit larger than conventionally believed. In the absence of a large top mass or new physics, BBs can only be avoided by choosing a particular cosmological measure (see *e.g.* [43–48]). In particular, we argue that local measures (referring to individual causal patches, rather than the entire multiverse) can solve the problem. This result provides empirical support for horizon complementarity [8, 49], the idea that only the part of the universe accessible to a single observer is physically relevant.

## 3.2   Higgs Potential and Decay Rates

Let us begin by reviewing the stability of the Higgs potential, which depends on the behavior of the potential at large field values $\phi = |\Phi|$, where $\Phi$ is the electroweak (EW) Higgs doublet. We assume
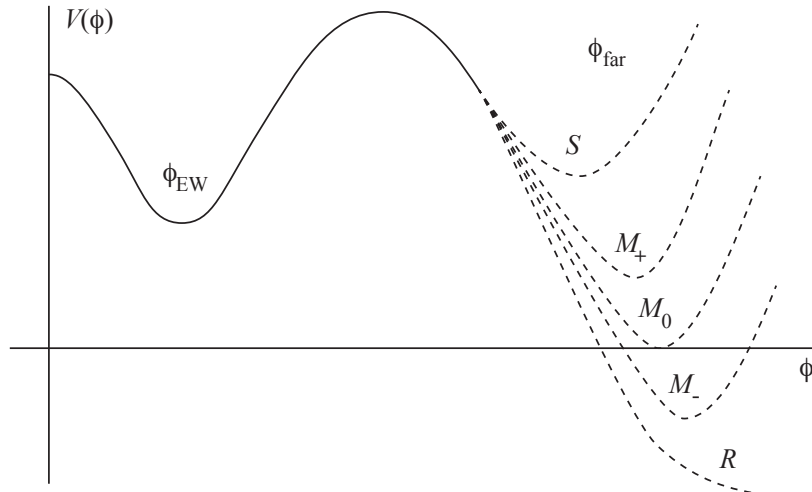
Figure 3.1: Schematic of the Higgs potential. Our current electroweak vacuum is at $\phi_{EW}$, and the far vacuum at $\phi_{far}$ is portrayed for different scenarios: stable, metastable, or runaway. Note that the explicit form of the potential is not gauge invariant [50], but the tunneling rate and vacuum energy at minima are physical quantities [51, 52].

the standard $\Lambda$CDM cosmology and no new physics below the Planck scale. The only two vacua are our present one (the electroweak vacuum $\phi_{EW}$) and a possible "far vacuum" at $\phi_{far}$, as portrayed in Fig. 3.1. How the universe evolves depends on the value $\Lambda_{far}$ of the cosmological constant in the far vacuum, where $\Lambda_i = 8\pi G V(\phi_i)$ and $V(\phi_{EW}) \approx (2.3 \times 10^{-3}\,\mathrm{eV})^4$. If $\Lambda_{far} < \Lambda_{EW}$, it is possible to tunnel from $\phi_{EW}$ to $\phi_{far}$ with a vacuum decay rate $\Gamma_{decay}$.

There are several values to which we would like to compare $\Gamma_{decay}$. There is the rate $\Gamma_{fast}$ that is so rapid our vacuum should have already decayed; the rate $\Gamma_{perc} \sim H^4$, below which the phase transition does not percolate; the rate $\Gamma_{BB}$ at which BBs are created; and $\Gamma_{decay} \to 0$ for which our vacuum becomes stable. Given the precision of the measured parameters, however, we cannot distinguish between $\Gamma_{fast}$ and $\Gamma_{perc}$, nor between $\Gamma_{BB}$ and 0. Similarly, the parameter space for which the far vacuum is de Sitter but lower energy than our current vacuum is negligibly small. We are therefore interested in two simple questions: is the bubble nucleation rate greater than zero (metastability), and is it fast enough to percolate?

To be more quantitative, we consider the full structure of the effective potential

$$V_{eff}(\phi) = -\frac{1}{2}m^2\phi^2 + \frac{1}{4}\lambda\phi^4 + \Delta V(\phi) \;, \tag{3.1}$$

where $\Delta V$ includes radiative corrections from summing 1PI diagrams with vanishing external momenta [53]. There is also a $\phi$-independent energy density that should be included, but its effects are negligible at the scales we are interested in for stability [33]. The effective potential is known to two loops in the $\overline{\text{MS}}$ renormalization scheme [54, 55]. The loop approximation is nearly invariant with respect to the renormalization scale $\mu$ if $\mu$ is chosen to minimize the size of radiative correc-

tions [31, 56]. Logarithmic terms in $\Delta V$ have the form $\ln(\phi^2/\mu^2)$, so the choice $\mu = \phi$ avoids large logarithms at large $\phi$. To work consistently at next-to-next-to-leading order (NNLO), the effective potential needs to be improved using the three-loop renormalization group equations with two-loop matching at the electroweak scale. This procedure correctly resums logarithm contributions [57–59]. Recent NNLO calculations of the electroweak threshold corrections can be found in [40–42]. The most relevant SM parameters for vacuum decay are $\alpha_s(M_Z)$ (the strong coupling evaluated at the $Z$ pole mass), the top pole mass $M_t$, and the Higgs pole mass $M_h$.

For $\phi \gg \phi_{\text{EW}}$, we may neglect the $m^2\phi^2$ term and write the effective potential as $V_{\text{eff}} = \frac{1}{4}\lambda_{\text{eff}}(\phi)\phi^4$ [31, 33], so that the stability bound is set by requiring $\lambda_{\text{eff}} = 0$ at its minimum. The dividing line between stability and metastability is [42]

$$M_t(\text{GeV}) = 171.4 + 0.5(M_h - 125.7) + 357.1(\alpha_s(M_Z) - 0.1184) \pm 0.2 \ , \tag{3.2}$$

where the uncertainty comes from higher order perturbative corrections (and does not include uncertainties in $M_h$ and $\alpha_s$). If the top pole mass is above this value, the electroweak vacuum decays via bubble nucleation.

Nucleation proceeds via instantons with tree-level Euclidean action $S_0$ and radiative correction $\Delta S$. The action is determined from the bounce solution [60] with a characteristic size $R$. Gravitational corrections also become relevant for $R^{-1} \gtrsim 10^{17}$ GeV [61]. Using the bare potential $\frac{1}{4}\lambda(\phi)\phi^4$ for large $\phi$, we obtain $S_0 = 8\pi^2/3|\lambda(\mu)|$. The decay rate per unit volume is then

$$\Gamma_{\text{decay}} = \frac{1}{R^4} \exp\left[ -\frac{8\pi^2}{3|\lambda(\mu)|} - \Delta S(\mu R) \right] \ , \tag{3.3}$$

where the correction $\Delta S$ has been computed to one loop [34]. The size of the bounce $R$ will be that which maximizes the decay rate, and $\mu \approx R^{-1}$ is set to minimize the size of the radiative corrections. The dividing line between percolation and non-percolation is [36]

$$M_t(\text{GeV}) = 178.2 + 0.3(M_h - 125.7) + 397.7(\alpha_s(M_Z) - 0.1184) \pm 1.2 \ , \tag{3.4}$$

where the last term is a theoretical error.

The bounds from (3.2) and (3.4) are shown in Fig. 3.2, with $\alpha_s(M_Z) = 0.1184 \pm 0.0007$ set to its world average value [64]. The dotted lines near the bounds represent the $1\sigma$ deviation in $\alpha_s$. Elliptical contours represent measurements on the Higgs mass and top mass. The Higgs mass $M_h = 125.66 \pm 0.34$ GeV is obtained from a simple average [65] of measurements from CMS [66, 67] and ATLAS [68, 69], fitting peaks in the $h \to \gamma\gamma$ and $h \to ZZ \to 4l$ channels. We use the top mass average of $M_t = 173.20 \pm 0.87$ GeV from the Tevatron Electroweak Working Group [62], which is consistent with measurements from CMS [70] and ATLAS [71]. These measurements indicate that
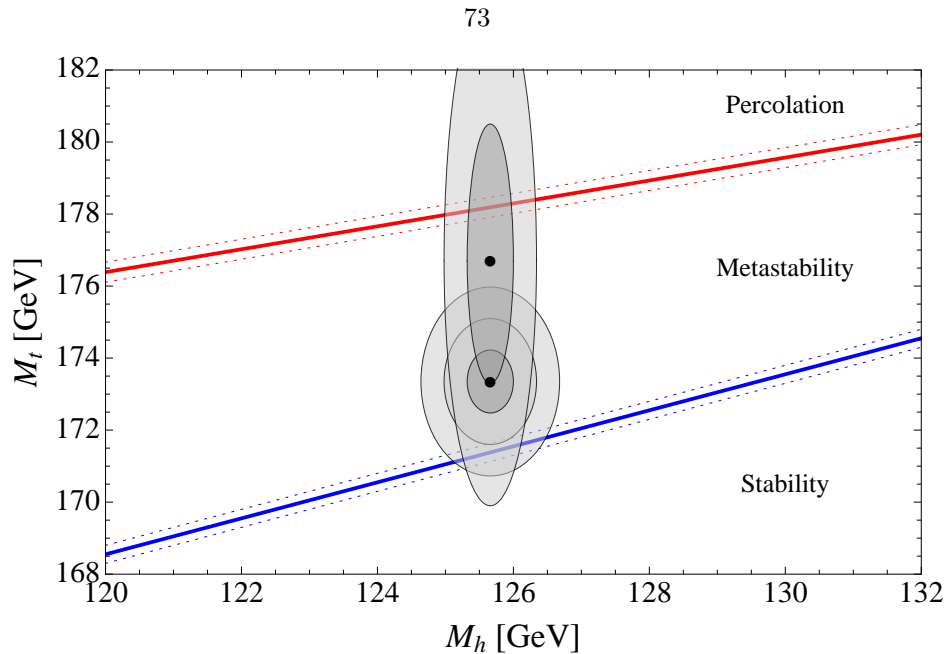
Figure 3.2: Stability regions for the electroweak vacuum. The lower blue line is the stability bound in (3.2), and the upper red line is the percolation bound in (3.4). The smaller contours show the $1\sigma$, $2\sigma$, and $3\sigma$ regions, using top mass measurements from the Tevatron [62]. The larger contours show the $1\sigma$ and $2\sigma$ regions, using an alternative determination of the top pole mass from CMS [63]. The only region that is empirically viable (free of Boltzmann Brains, not already decayed) in a measure-independent way is the upper line, suggesting a top pole mass of $\sim 178$ GeV.

the electroweak vacuum is metastable, entering into the stability region above the $2\sigma$ level.

There are concerns regarding the methods used to extract the mass of the top [39]. The top mass parameter that is used in the reconstruction of collider events is not necessarily the pole mass that is needed in the stability calculations. Furthermore, the top is a confined object that does not exist as an asymptotic state, and non-perturbative effects introduce ambiguities in defining the pole mass. A way to combat these issues is to extract the $\overline{\text{MS}}$ top mass from the total cross section and use the relation between the $\overline{\text{MS}}$ mass and the pole mass [39, 72]. CMS performed this analysis to find a top pole mass of $M_t = 176.7\,^{+3.8}_{-3.4}$ GeV [63]. While the errors are much larger than the other recent top mass measurements, the quoted value is higher, pushing the electroweak vacuum towards larger decay rates, as shown in Fig. 3.2.

## 3.3   Cosmological Measures

We wish to compare the predicted number of BBs to the number of ordinary observers (OOs) in our universe. We assume that BBs fluctuate into existence in a future de Sitter phase with some fixed rate per four-volume, $\Gamma_{\text{BB}}$. This rate depends on the details of what kinds of fluctuations are considered, but typical numbers are of the form $\Gamma_{\text{BB}} \sim \exp(-10^x)$, where $x$ is between 10 and 100. For reasonable physical parameters, the precise value of $\Gamma_{\text{BB}}$ will be irrelevant. Our universe is

plausibly infinite both in space and in time (toward the future), so we need a way of regularizing the numbers of OOs and BBs: a cosmological measure. Studies of the cosmological measure problem are usually carried out in the context of eternal inflation. We assume there was no early inflationary phase, so we consider slight modifications of previous proposals. A "typical" implementation of high-energy eternal inflation would not alter our conclusions, although specific models that would are certainly possible; for our purposes, such a solution counts as "new physics."

If the far vacuum from Fig. 3.1 has $\Lambda_{\text{far}} > 0$, it will be locally de Sitter. In that case, there will be thermal fluctuations between the two vacua for all eternity, including uptunneling [20, 21]. Over sufficiently large timescales, we expect to see equilibrium statistics, and BBs will dominate. The interesting cases are, therefore, when $\Lambda_{\text{far}} = 0$ or when $\Lambda_{\text{far}} < 0$. The first case, which could be enforced by supersymmetry, represents a terminal Minkowski vacuum, in which no further fluctuations occur. The other case is $\Lambda_{\text{far}} < 0$, by which we include the possibility of a runaway, where there is no vacuum below the Planck scale. In either case, we expect a crunch to a singularity in finite time, so such vacua are also thought of as terminal. We will speak as if spacetime ends at the bubble wall, although it is actually a bit later than that (it is possible that a better description of such cases includes a quantum "bounce" back to a spacetime description [73, 74], but we will not consider that possibility here).

One approach to constructing a measure is to start with some spacelike three-volume $\Sigma_0$ defined at early times, as shown in Fig. 3.3. We then define a family of hypersurfaces $\Sigma_\lambda$ by extending initially orthogonal geodesics with proper time $\tau$ into the future from $\Sigma_0$. Each $\Sigma_\lambda$ is the set of all points at some constant parameter $\lambda$, perhaps with some appropriate algorithm to smooth the surfaces, where $\lambda$ is a function of $\tau$. We calculate the number of OOs and BBs in the four-volume between $\Sigma_0$ and $\Sigma_\lambda$ and take the limit $\lambda \to \infty$.

Taking $\lambda = \tau$ gives the **proper-time measure**, which naïvely counts the spacetime volume [75–77]. If the decay rate $\Gamma_{\text{decay}}$ to the far vacuum is sufficiently fast that the phase transition percolates, we spend relatively little time in the electroweak vacuum, and BBs are not produced. If the transition does not percolate, an infinite amount of volume in the electroweak vacuum is produced; in that case, BBs necessarily dominate OOs. To achieve percolation, the expected lifetime of the electroweak vacuum is of order the actual age of our universe, $\Gamma_{\text{decay}} \gtrsim H^4$ [25]. In the context of eternal inflation, the proper-time measure has phenomenological problems, such as the youngness paradox [77, 78], so other measures are generally considered.

An alternative is the **scale-factor-cutoff measure**, which sets $\lambda$ equal to the scale-factor time along a geodesic congruence, $\lambda = \int H(\tau) \, d\tau = \ln a$ [26, 79–81]. In this case, the total four-volume living in the electroweak vacuum in the region between the initial hypersurface $\Sigma_0$ and a later hypersurface $\Sigma_\lambda$ is

$$U_{\text{EW}}(\lambda) = \frac{1}{H(3 - \kappa)} e^{(3-\kappa)\lambda} V_0 \, , \tag{3.5}$$
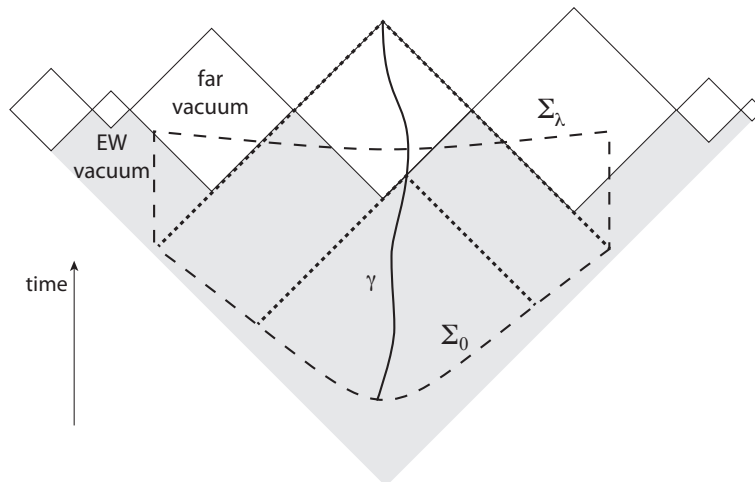
Figure 3.3: Conformal spacetime diagram for our universe. The shaded region is our electroweak vacuum. Diamonds at the top of the diagram are terminal Minkowski vacua; if $\Lambda_{\text{far}} < 0$, the bottom boundaries of those diamonds represent singularities, and the diamonds themselves are absent. Dashed lines depict an initial region $\Sigma_0$ evolving into a later one $\Sigma_\lambda$. Dotted lines represent the causal patch of the geodesic $\gamma$, depending on whether $\gamma$ ends at the bubble wall or extends into Minkowski space.

where $V_0$ is the three-volume of $\Sigma_0$ and $\kappa = (4\pi/3)H^{-4}\Gamma_{\text{decay}}$ is the decay probability in a Hubble four-volume. We see that spacetime volume increases without bound unless $\kappa > 3$, which is just the condition for percolation. The number of BBs, $N_{\text{BB}}(\lambda) = U_{\text{EW}}(\lambda)\Gamma_{\text{BB}}$, therefore also grows without bound and will ultimately dominate over OOs. The scale-factor-cutoff measure recovers the same answer as the proper-time measure for our problem: BBs dominate unless $\Gamma_{\text{decay}} \gtrsim H^4$. This kind of problem is likely to be generic for "global" measures that integrate over a comoving volume of spacetime.

We therefore turn to "local" measures, which restrict attention to a single observer. A standard example is the **causal patch measure** [77,82]. The causal patch of a timelike geodesic $\gamma$ extending from $\Sigma_0$ into the future is the intersection of the future of $\Sigma_0$ with the interior of the past light cone of the futuremost point of $\gamma$. For our problem we can start with any geodesic orthogonal to $\Sigma_0$ and compare the number of OOs to BBs inside the causal patch. If $\Lambda_{\text{far}} < 0$, the interior of the bubble rapidly crunches to a singularity, ending the geodesic $\gamma$. In that case we simply want to know whether the geodesic is likely to hit a bubble wall before it observes the formation of a BB. Therefore, the BB problem is avoided as long as $\Gamma_{\text{decay}} > \Gamma_{\text{BB}}$. If on the other hand $\Lambda_{\text{far}} = 0$, the geodesic enters an asymptotically Minkowski region, and the spacetime volume (in either vacuum) inside the causal patch becomes infinite [83]. In that case, BBs will dominate.

To sum up: if the bubble nucleation rate is fast enough that the transition percolates, there is no BB problem. Otherwise, BBs do dominate according to the global measures we considered and also

for the causal patch measure with a Minkowski far vacuum. If $\Lambda_{\mathrm{far}} < 0$, the causal patch measure offers a solution to the BB problem if $\Gamma_{\mathrm{decay}} > \Gamma_{\mathrm{BB}}$, which is easy to satisfy.

## 3.4 Conclusions

$\Lambda$CDM is only viable if BBs are avoided. There are three possibilities. The simplest possibility is if the decay rate of the electroweak vacuum is comparable to the current age of the universe. We have seen that this scenario can be accomplished without new physics if the top pole mass is $M_t \sim 178$ GeV, given the measured Higgs mass. This mass is $5.6\sigma$ larger than the consensus Tevatron/LHC value, although a different determination method might change this result. It is interesting that the precise value of the top mass plays such an important role in cosmology.

Another possibility is new physics. Heavy scalar singlets tend to promote stability [84, 85], while fermions with large Yukawa couplings promote instability. For example, a fourth generation with a heavy quark [30] or right-handed neutrinos with a see-saw mechanism [38, 86] can destabilize the Higgs potential. The effects of new particles are model dependent, and a complete analysis is needed to definitively comment on a particular model. Alternatively, cosmic acceleration could be due to an ephemeral effect such as quintessence or modified gravity.

The final alternative is to invoke an appropriate cosmological measure. We have argued that global measures generally do not help, but BBs can be avoided in the causal patch measure with a $\Lambda_{\mathrm{far}} < 0$ terminal vacuum if $\Gamma_{\mathrm{decay}} > \Gamma_{\mathrm{BB}}$. This criterion amounts to the demand that the potential is in the metastable region, consistent with current measured parameters. The causal-patch measure is justified in part by complementarity, which instructs us to treat physics outside the horizon as encoded in information on the horizon itself. If neither new physics nor a heavy top quark leads to rapid decay of the universe, the success of $\Lambda$CDM may be taken as empirical support for complementarity, adding another clue to our understanding of quantum gravity.

# Chapter 4

# De Sitter Space without Quantum Fluctuations

## 4.1  Introduction

Despite the general acceptance of viewing the de Sitter vacuum as a thermal system subject to fluctuations, we will argue that some of this conventional wisdom is wrong. Although a patch in the Hartle-Hawking vacuum is in a thermal state, it does not experience fluctuations in any meaningful sense. The density operator in the patch takes the form $\hat{\rho} \sim e^{-\beta \hat{H}}$, where $\beta = 1/T$ and $\hat{H}$ is the static Hamiltonian. The state is stationary; there is no time dependence of any sort. While it is true that an out-of-equilibrium particle detector inside the patch would detect thermal radiation, there are no such particle detectors floating around in the Hartle-Hawking vacuum. In fact, any particle detector placed in the vacuum would equilibrate, reaching a stationary state with thermal occupation numbers [87].

Quantum fluctuations are not dynamical processes inherent to a system, but instead reflect the statistical nature of measurement outcomes. Making a definite measurement requires an out-of-equilibrium, low-entropy detection apparatus that interacts with an environment to induce decoherence. Quantum variables are not equivalent to classical stochastic variables. They may behave similarly when measured repeatedly over time, in which case it is sensible to identify the nonzero variance of a quantum-mechanical observable with the physical fluctuations of a classical variable. In a truly stationary state, however, there are no fluctuations that decohere. We conclude that systems in such a state—including, in particular, the Hartle-Hawking vacuum—never fluctuate into lower-entropy states, including false vacua or configurations with Boltzmann brains.

Although our universe, today or during inflation, is of course not in the vacuum, the cosmic no-hair theorem [88–90] implies that any patch in an expanding universe with a positive cosmological constant will asymptote to the vacuum. Within QFT in curved spacetime, the Boltzmann brain problem is thus eliminated: a patch in eternal de Sitter can form only a finite (and small)

number of brains on its way to the vacuum. At the same time, the standard story of inflationary perturbations remains intact: decoherence is accompanied by copious production of entropy during reheating. Our analysis of quantum fluctuations only calls into question the idea of dynamical transitions from stationary states to states with lower entropy. We point out that the stochastic approximation in slow-roll eternal inflation [12–14] makes use of such transitions to describe putative upward fluctuations of the inflation field. Our picture rules out such fluctuations and may therefore change the conventional understanding of the conditions required for eternal inflation to occur. In particular, eternal inflation is no longer an inevitable consequence of monomial inflation potentials like $V = m^2\varphi^2$.

The cosmic no-hair theorem is given in the context of QFT in curved spacetime. Once quantum gravity is included, we need to be more careful. If we accept the notion of horizon complementarity [8, 49, 91, 92], we should not use local QFT to simultaneously describe locations separated by a horizon. Rather, we should treat each patch of eternal de Sitter space, together with its horizon, as a closed, finite-dimensional quantum system. The system is not stationary, so it must undergo Poincaré recurrences as well as fluctuations, including into configurations we would describe as Boltzmann brains. We suggest the terminology "Boltzmann fluctuations" to describe these true dynamical processes, which can occur because the system never truly settles into the vacuum. Alternatively, there might be a higher-entropy vacuum to which the system can decay, in which case the false de Sitter vacuum patch can be thought of as an open subsystem embedded in a larger theory. If the higher-entropy vacuum is de Sitter, then the full system still has a finite-dimensional Hilbert space, subject to Poincaré recurrences and fluctuations. If there is a Minkowski vacuum with potentially infinite entropy, the larger theory has an infinite-dimensional Hilbert space. Here, we argue that the QFT analysis applies, and the patch rapidly approaches the vacuum and becomes quiescent, with only a finite number of fluctuations along the way.

This chapter is organized as follows:

- In §4.2 we define what is meant by "quantum fluctuations" and argue that they are absent in stationary quantum states. Quantum fluctuations in the traditional sense only appear when an out-of-equilibrium measuring apparatus interacts with a quantum system, which results in time-dependent branching of the wave function. In contrast, "Boltzmann fluctuations" are true statistical fluctuations.

- In §4.3 we examine eternal de Sitter space in or near the unique Hartle-Hawking vacuum. We first describe the system using QFT in a fixed background. Because the Hartle-Hawking vacuum is stationary, we argue that there are no fluctuations, despite the fact that an out-of-equilibrium detector (of which there are none present) would measure a nonzero temperature. The cosmic no-hair theorem ensures that all states evolve toward the vacuum, so the system

must settle down to a state that is free of fluctuations. In the context of horizon complementarity, however, each horizon volume can be treated as a system described by a finite-dimensional Hilbert space, and the cosmic no-hair theorem does not apply. If de Sitter space in horizon complementarity is eternal, there will be recurrences and Boltzmann fluctuations, and the conventional picture is recovered.

- In §4.4, we turn to models that contain false de Sitter vacua. In semiclassical quantum gravity, or in complementarity in a landscape that includes a Minkowski vacuum, the dynamics occur in an infinite-dimensional Hilbert space. The situation is then similar to QFT in global de Sitter, where each patch can relax to a stationary quantum state, free of fluctuations. In complementarity without a Minkowski vacuum, when all vacua are de Sitter, there will still be quantum and Boltzmann fluctuations, since the total Hilbert space is finite-dimensional.

- In §4.5, we discuss the ramifications of this analysis. First, the conventional Boltzmann brain problem is greatly ameliorated. Even with horizon complementarity, there are no fluctuations in the vacuum to lower-entropy states as long as the larger Hilbert space is infinite dimensional. Similarly, we do not expect uptunneling to higher-energy vacua, which dramatically alters the picture of eternal inflation on a landscape. The standard picture of density fluctuations from inflation remains unchanged, but the understanding of stochastic eternal inflation is significantly different. Finally, we note that these results depend crucially on one's preferred version of quantum mechanics.

## 4.2    Quantum Fluctuations vs. Boltzmann Fluctuations

One way of thinking about the nature of quantum fluctuations is to consider an observable represented by a self-adjoint operator $\widehat{\mathcal{O}}$. If a state $|\Psi\rangle$ is not an eigenstate of $\widehat{\mathcal{O}}$, then the variance

$$(\Delta\widehat{\mathcal{O}})^2_\Psi = \langle\widehat{\mathcal{O}}^2\rangle_\Psi - \langle\widehat{\mathcal{O}}\rangle^2_\Psi \tag{4.1}$$

will be strictly positive. Hence, $\widehat{\mathcal{O}}$ does not have a definite value. However, a nonzero variance is not a statement about the *dynamics* of the state, which may well be stationary; it is merely a statement about the distribution of measurement outcomes. In this section we review some basic concepts to clarify the meaning of "quantum fluctuations" and the role of measuring devices.

### 4.2.1    Decoherence and Everettian Worlds

Let us rehearse the standard understanding of quantum measurement and decoherence in the Everett formulation [93, 94]. Consider a Hilbert space that factors into an apparatus $A$ that may observe a

system $S$:

$$\mathcal{H} = \mathcal{H}_S \otimes \mathcal{H}_A . \tag{4.2}$$

The Schmidt decomposition theorem allows us to write an arbitrary state as

$$|\Psi\rangle = \sum_n c_n |s_n\rangle |a_n\rangle , \tag{4.3}$$

where the $|s_n\rangle$ form an orthonormal basis for the system and $|a_n\rangle$ are orthogonal states of the apparatus. We assume that $\dim \mathcal{H}_S < \dim \mathcal{H}_A$, and the sum over $n$ runs up to $\dim \mathcal{H}_S$. The bipartite form of (4.3) is unique up to degeneracies in the coefficients $|c_n|$ (for simplicity, we assume there are no degeneracies throughout the remainder of this chapter). Although the Schmidt decomposition identifies a unique basis, there is no mechanism in place to ensure that the system and apparatus states are ones that appropriately describe actual measurements. Interactions between the system/apparatus and the environment are crucial for using decoherence to solve the measurement problem.

Incorporating the environment $E$, the Hilbert space is

$$\mathcal{H} = \mathcal{H}_S \otimes \mathcal{H}_A \otimes \mathcal{H}_E . \tag{4.4}$$

It may be possible to write a state in the full Hilbert space using a generalized Schmidt decomposition

$$|\Psi\rangle = \sum_n c_n |s_n\rangle |a_n\rangle |e_n\rangle , \tag{4.5}$$

where $|s_n\rangle$ are system basis states; $|a_n\rangle$ are linearly independent, normalized apparatus states; and $|e_n\rangle$ are mutually noncollinear, normalized environment states. The triorthogonal uniqueness theorem [95] guarantees that the form of this tripartite decomposition, if it exists, is unique. Observations are restricted to the system and apparatus, so predictions of the outcomes of measurements are encoded in the reduced density matrix for the system and apparatus, found by tracing out the unobserved degrees of freedom of the environment from the full density matrix $\rho = |\Psi\rangle\langle\Psi|$:

$$\begin{aligned} \rho_{SA} &= \text{Tr}_E |\Psi\rangle\langle\Psi| \\ &= \sum_{m,n} c_m c_n^* \langle e_n | e_m\rangle |s_m\rangle |a_m\rangle \langle s_n| \langle a_n| . \end{aligned} \tag{4.6}$$

In order for this formalism to describe a quantum state that splits into independent Everettian branches or "worlds," several requirements must be satisfied. First, decoherence must occur—there must be no quantum interference between the different worlds, so observers on one branch evolve independently of the existence of other branches. The absence of interference between states in

$\mathcal{H}_S \otimes \mathcal{H}_A$ requires that the reduced density matrix (4.6) be diagonal, *i.e.*, that the environment states associated with different branches be orthogonal.

Any density matrix is diagonal in some basis, but that basis might not be a physically viable one, nor one that is in the tripartite form of (4.5), where measurement outcomes are accurately reflected in the state of the apparatus. The second requirement is therefore that there must exist a basis of apparatus "pointer states" in which decoherence naturally occurs through the dynamical diagonalization of $\rho_{SA}$ in this preferred basis [93, 96–99]. A precise characterization of the pointer states is subtle and context-dependent, but roughly corresponds to states of the apparatus that are macroscopically robust (stable). Any interactions between the apparatus and environment should have a minimal effect on the system-apparatus correlations. In principle, we can deduce the pointer states by writing the Hamiltonian as a sum of system/apparatus, environment, and interaction terms:

$$\hat{H} = \hat{H}_{SA} \otimes \mathbb{1}_E + \mathbb{1}_{SA} \otimes \hat{H}_E + H_I \ . \tag{4.7}$$

The pointer states $|a_n\rangle$ are those whose projectors $\hat{P}_n = |a_n\rangle\langle a_n|$ commute with the interaction Hamiltonian,

$$[\hat{H}_I, \hat{P}_n] = 0 \ . \tag{4.8}$$

In practice, the fact that interactions are local in space implies that pointer states for macroscopic objects are those with definite spatial configurations. For instance, if a large object (a billiard ball, a planet, a cat) is in a quantum superposition of two different position eigenstates, interactions with the environment (the air in a room, the cosmic background radiation) will rapidly cause those two possibilities to decohere, creating separate branches of the wave function.

The final feature that is important to describe branching is an arrow of time. We conventionally imagine that worlds split via decoherence as time passes but almost never merge together, because we implicitly assume that the universe is very far from equilibrium and has evolved from a lower-entropy state in the past. In the present context, "low entropy" means that subsystems begin in a particular state of little or no entanglement, as in (4.9). As we demonstrate in the next subsection, dynamical interactions between apparatus and environment naturally increase the amount of entanglement, leading to branching and generating entropy.[1] The standard picture of decoherence and branching is specific to the far-from-equilibrium situation. Near equilibrium, decoherence can arise through rare fluctuations, but is not tied to quantum measurements, as we discuss in §4.2.3.

---

[1] For the purposes of this chapter, we are concerned with only the von Neumann entropy from entanglements. There is also the thermodynamic entropy associated with a mixed thermal density matrix, which sets an upper bound on the von Neumann entropy. As the quantum system thermalizes, the von Neumann entropy approaches the thermodynamic entropy [100].

## 4.2.2 Quantum Fluctuations

We can use the decoherence program from the previous section to understand the nature of quantum fluctuations. For clarity in the following example, let us identify states in $S$, $A$, and $E$ explicitly with subscripts. In the case of real-world quantum measurement, we posit that there is initially no entanglement between any of the factors:

$$|\Psi(t_0)\rangle = |\sigma_*\rangle_S |a_R\rangle_A |e_*\rangle_E \ . \tag{4.9}$$

The initial state (denoted by an asterisk) of the system can be arbitrary; but the measuring apparatus must be in a specific "ready" state (denoted by the subscript $R$). For definiteness, imagine that the system is a single qubit with basis states $\{|+\rangle_S, |-\rangle_S\}$. The apparatus should begin in a ready state and record the results of repeated measurements of the system. We take the apparatus state to be a tensor product of a number of registers (at least one for each measurement we want to perform), where each register is a qutrit with three basis states $\{|+\rangle_A, |-\rangle_A, |0\rangle_A\}$. The ready state of the apparatus is $|a_R\rangle_A = |000\cdots\rangle_A$, and a measurement correlates one of the registers with the state of the system. That is, under unitary evolution we record a measurement in the first register via

$$|+\rangle_S |000\cdots\rangle_A \to |+\rangle_S |+00\cdots\rangle_A \ , \tag{4.10}$$

$$|-\rangle_S |000\cdots\rangle_A \to |-\rangle_S |-00\cdots\rangle_A \ . \tag{4.11}$$

If the apparatus does not start in the ready state, we cannot be confident that it will end up correctly correlated with the state of the system. Since unitary evolution must be reversible, there can be no valid evolution that takes $|+\rangle_S |\psi\rangle_A$ to $|+\rangle_S |+\rangle_A$ for every possible $|\psi\rangle_A$, for example.

Imagine that the system starts in a superposition, so the state takes the form

$$|\Psi(t_0)\rangle = (\alpha |+\rangle_S + \beta |-\rangle_S) |000\cdots\rangle_A |e_*\rangle_E \ . \tag{4.12}$$

The first step in the evolution is premeasurement, which correlates the apparatus with the system:

$$|\Psi(t_1)\rangle = (\alpha |+\rangle_S |+00\cdots\rangle_A + \beta |-\rangle_S |-00\cdots\rangle_A) |e_*\rangle_E \ . \tag{4.13}$$

The second step is decoherence, in which the apparatus becomes entangled with the environment:

$$|\Psi(t_2)\rangle = \alpha |+\rangle_S |+00\cdots\rangle_A |e_+\rangle_E + \beta |-\rangle_S |-00\cdots\rangle_A |e_-\rangle_E \ . \tag{4.14}$$

Next, we reset in order to perform the measurement again, which means returning the system to its original state. Generally, the environment states will also evolve during this operation. We leave

the apparatus unchanged in order to keep a record of the prior measurement outcomes:

$$|\Psi(t_3)\rangle = \alpha \, |\sigma_*\rangle_S \, |+00\cdots\rangle_A \, |\tilde{e}_+\rangle_E + \beta \, |\sigma_*\rangle_S \, |-00\cdots\rangle_A \, |\tilde{e}_-\rangle_E \ . \tag{4.15}$$

Finally, we repeat the entire procedure, this time recording the measurement outcome in the second register of the apparatus. After one more iteration of premeasurement and decoherence, we end up with

$$\begin{aligned}
|\Psi(t_4)\rangle = {} & \alpha^2 \, |+\rangle_S \, |++0\cdots\rangle_A \, |e_{++}\rangle_E \\
& + \alpha\beta \, |+\rangle_S \, |-+0\cdots\rangle_A \, |e_{-+}\rangle_E \\
& + \alpha\beta \, |-\rangle_S \, |+-0\cdots\rangle_A \, |e_{+-}\rangle_E \\
& + \beta^2 \, |-\rangle_S \, |--0\cdots\rangle_A \, |e_{--}\rangle_E \ .
\end{aligned} \tag{4.16}$$

At this point the wave function consists of four different decoherent branches, provided that all of the environment states are approximately orthogonal, $\langle e_\mu | \, e_\nu \rangle_E \approx 0$.

The statement "we observe quantum fluctuations" is equivalent to the observation that the history of each individual decoherent branch is one in which the state of the apparatus experiences a time series of observational outcomes, bouncing between $|+\rangle$ and $|-\rangle$. On a randomly chosen branch, the history will exhibit fluctuations between the two outcomes, and all macroscopic objects are robust and physically well-defined (pointer states) by construction. Schrödinger cat superpositions are not allowed, and different worlds or branches must evolve separately.

We see that obtaining the standard measurement outcomes requires both the apparatus to be initially in its ready state and the three Hilbert space factors (system/apparatus/environment) to be initially unentangled. These conditions highlight the crucial role of entropy production in the branching of the wave function and thus in the existence of quantum fluctuations. The reduced density matrix $\rho_{SA}$ has a von Neumann entropy

$$S_{SA} = \mathrm{Tr}\,\rho_{SA} \log \rho_{SA} \ . \tag{4.17}$$

Since the state as a whole is pure in our example, all of the entropy comes from the entanglement between $SA$ and $E$. In the initial state (4.12), there is no entanglement, and $S_{SA} = 0$. The entropy increases as the state evolves into two branches (4.14) and again as it evolves into four branches (4.16). Since the entropy of the pure state vanishes, the entropy of the environment equals that of the system/apparatus factor and increases as well. Without entropy production, there are no quantum fluctuations.

Now consider what happens if the entire wave function describing the system, apparatus, and

environment (*i.e.*, the whole universe) begins in an energy eigenstate. We assume there are interaction terms in the Hamiltonian that connect the different factors of the Hilbert space. An energy eigenstate obeys

$$\hat{H} \left| \Psi_n \right\rangle = E_n \left| \Psi_n \right\rangle \ , \tag{4.18}$$

where $\hat{H}$ is the full Hamiltonian. Because the wave function is in an energy eigenstate, its time evolution just takes the form of multiplication by an overall time-dependent phase:

$$\left| \Psi_n(t) \right\rangle = e^{-iE_n(t-t_0)} \left| E_n \right\rangle \ . \tag{4.19}$$

The overall phase factor does not affect any of the observable properties of the state; therefore, it is sensible to refer to such a state as "stationary," and its associated density operator

$$\rho_\Psi = \left| \Psi_n(t) \right\rangle \left\langle \Psi_n(t) \right| = \left| E_n \right\rangle \left\langle E_n \right| \tag{4.20}$$

is manifestly time independent. Another example of stationary density operator is that of a thermal state with temperature $\beta^{-1}$:

$$\rho \sim \exp(-\beta\hat{H}) = \sum_n e^{-\beta E_n} \left| E_n \right\rangle \left\langle E_n \right| \ . \tag{4.21}$$

Indeed, any density matrix diagonal in the energy eigenbasis will be stationary.

In a stationary state, none of the behavior we characterized as "quantum fluctuations"—branching of the wave function into a set of histories with stochastic measurement outcomes over time—is present. In fact, there is no time dependence at all.[2] Certainly, the variance of an observable $\hat{O}$ can be positive in a stationary state, but that variance only leads to fluctuations if the observable is actually measured. Doing so requires an apparatus that is not itself stationary. Indeed, the apparatus must start in a specific ready state, a condition that we may describe as low entropy. If a quantum state describes the whole universe (as it does in cosmology), and this state is stationary, then it cannot undergo quantum fluctuations, because nothing can actually change as time passes. For a thermal state in particular, it will be the case that a particle detector beginning in its ready state would detect thermally fluctuating particles; but if all we have to use as a detector is a part of the stationary system itself, it will simply remain stationary, just as the rest of the quantum state does.

---

[2]Even in stationary states, one can define an effective evolution with respect to correlations with a clock subsystem [101]. The effective time parameter $\tau$ has nothing to do with the ordinary coordinate time $t$; all such time evolutions are present at every moment of (ordinary) time. From this perspective, a large number of Boltzmann brains and similar fluctuations actually exist at every moment in an apparently stationary spacetime. Such a conclusion would apply to Minkowski spacetime as well as to de Sitter, in conflict with the conventional understanding that the appearance of quantum fluctuations in de Sitter depends on the Gibbons-Hawking temperature (but see [102]). This kind of effective evolution is fundamentally different from the ordinary evolution studied in this chapter.

## 4.2.3   Boltzmann Fluctuations

There is an important difference between a quantum-mechanical thermal state and one in classical statistical mechanics. Classically, a state in thermal equilibrium has a uniform temperature in space that is also constant in time. However, this description is macroscopic and obtained by coarse graining. Any realization of such a system with nonzero temperature has a microstate that is time-dependent. For instance, the atoms and molecules in a box of gas are individually moving, even if the temperature and density are constant. The system will therefore undergo rare fluctuations to nonequilibrium states. The probability of observing such a fluctuation to a state with entropy $\Delta S$ lower than equilibrium scales as $\sim e^{-\Delta S}$. To avoid confusion, we will refer to such events in which the evolution of the microstate causes a reduction in entropy as "Boltzmann fluctuations," to distinguish them from "quantum fluctuations" where the wave function branches, which increase von Neumann entropy.

In quantum mechanics, individual energy eigenstates are stationary, in contrast with classical states of nonzero energy. Stationary quantum states will not experience Boltzmann fluctuations. A closed system in a mixed thermal state has a density operator $\rho \sim e^{-\beta \hat{H}}$, which is stationary; therefore, we expect no Boltzmann fluctuations there as well. In Appendix 4.A we verify this conclusion using the decoherent histories formalism. We show that Boltzmann fluctuations will occur in finite-dimensional Hilbert spaces if the initial density matrix is nonstationary, but are absent when the density matrix is stationary.

However, we most commonly encounter thermal density matrices after tracing over environmental degrees of freedom. In that case the remaining system is not closed, and we need to be a bit more careful. Consider a decomposition of a closed quantum system into a set of macroscopically observable system variables and an environment:

$$\mathcal{H} = \mathcal{H}_S \otimes \mathcal{H}_E \tag{4.22}$$

(we have absorbed the apparatus that appears in (4.4) into our definition of the macroscopic system). The environment includes local but microscopic variables (such as the positions and momenta of individual gas molecules, as opposed to macroscopic fluid variables such as temperature and pressure), as well as causally disconnected degrees of freedom (such as modes outside a cosmological horizon). Expectation values of macroscopic observables in a pure state $|\Psi\rangle \in \mathcal{H}$ are encoded in the reduced density matrix $\rho_S = \mathrm{Tr}_E |\Psi\rangle\langle\Psi|$, with entropy given by $S_S = \mathrm{Tr}\,\rho_S \log \rho_S$. While the evolution of the pure state $|\Psi\rangle$ is unitary, that of $\rho_S$ is generally not. It is described by a Lindblad equation [103], which allows for transfer of information between the macroscopic system and the environment:

$$\dot{\rho}_S = i[\hat{H}_*, \rho_S] + \sum_n \left( \hat{L}_n \rho_S \hat{L}_n^\dagger - \frac{1}{2} \hat{L}_n^\dagger \hat{L}_n \rho_S - \frac{1}{2} \rho_S \hat{L}_n^\dagger \hat{L}_n \right) . \tag{4.23}$$

$$\begin{pmatrix} x & & & & & \\ & 0 & & & & \\ & & 0 & & & \\ & & & 0 & & \\ & & & & 0 & \\ & & & & & 0 & \\ & & & & & & 0 \end{pmatrix} \rightarrow \begin{pmatrix} x & & & & & \\ & x & & & & \\ & & x & & & \\ & & & 0 & & \\ & & & & 0 & \\ & & & & & 0 \end{pmatrix} \rightarrow \begin{pmatrix} \cdot & \cdot & \cdot & \cdot & \cdot & \cdot & \cdot & \cdot & \cdot \\ \cdot & \cdot & \cdot & \cdot & \cdot & \cdot & \cdot & \cdot & \cdot \\ \cdot & \cdot & \cdot & \cdot & \cdot & \cdot & \cdot & \cdot & \cdot \\ \cdot & \cdot & \cdot & \cdot & \cdot & \cdot & \cdot & \cdot & \cdot \\ \cdot & \cdot & \cdot & \cdot & \cdot & \cdot & \cdot & \cdot & \cdot \\ \cdot & \cdot & \cdot & \cdot & \cdot & \cdot & \cdot & \cdot & \cdot \\ \cdot & \cdot & \cdot & \cdot & \cdot & \cdot & \cdot & \cdot & \cdot \end{pmatrix} \rightarrow \begin{pmatrix} x & \vline & 0 \\ \hline & \cdot & \cdot & \cdot & \cdot & \cdot & \cdot \\ & \cdot & \cdot & \cdot & \cdot & \cdot & \cdot \\ 0 & \cdot & \cdot & \cdot & \cdot & \cdot & \cdot \\ & \cdot & \cdot & \cdot & \cdot & \cdot & \cdot \\ & \cdot & \cdot & \cdot & \cdot & \cdot & \cdot \\ & \cdot & \cdot & \cdot & \cdot & \cdot & \cdot \end{pmatrix}$$
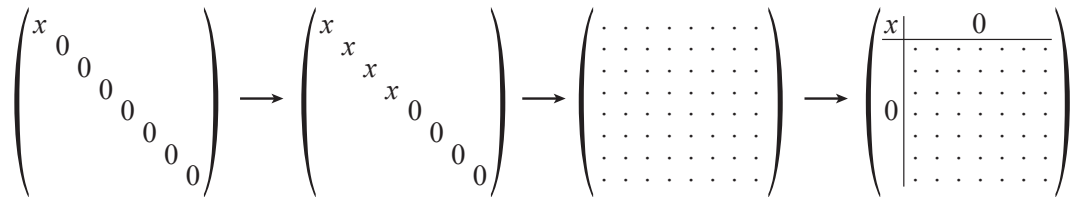
Figure 4.1: Schematic evolution of a reduced density matrix in the pointer basis. The density matrix on the left represents a low-entropy situation, where only a few states are represented in the wave function. There are no off-diagonal terms, since the pointer states rapidly decohere. The second matrix represents the situation after the wave function has branched a few times. In the third matrix, the system has reached equilibrium; the density matrix would be diagonal in an energy eigenbasis, but in the pointer basis, decoherence has disappeared and the off-diagonal terms are nonzero. The last matrix represents a Boltzmann fluctuation in which one pointer state has fluctuated into existence by decohering with respect to the other states.

The Lindblad operators $\hat{L}_n$ characterize the non-unitary part of the evolution of the system as induced by interactions with the environment, and will depend on the specific setup being studied. The Hermitian operator $\hat{H}_*$ is not necessarily equal to the self-interaction Hamiltonian of the system alone; it captures the part of the entire Hamiltonian that induces unitary evolution on the reduced density matrix, including possible renormalization effects due to interaction with the environment. A system far from equilibrium will generally exhibit dissipation and entropy increase (see *e.g.* [104]), and we may define a dissipation timescale on which the system will approach a stationary state.

On much longer timescales, however, even systems with approximately-stationary reduced density matrices can experience decoherence and transitions to lower-entropy states, in precise analogy with Boltzmann fluctuations in classical statistical mechanics. In §4.1 we provide a schematic representation of the evolution of the reduced density matrix, written in the pointer basis. The first two entries show the splitting of branches of the wave function starting from a low-entropy configuration, as described for example by the transition from (4.12) to (4.14) and to (4.16). The state branches and decoheres, remaining diagonal in the pointer basis. Eventually, it approaches equilibrium and becomes diagonal in the energy eigenbasis; by that point, the off-diagonal elements in the pointer basis are comparable to the diagonal ones, and the pointer states are no longer decoherent. From equilibrium, there can be rare fluctuations (if the total Hilbert space is finite-dimensional) to lower-entropy configurations where one branch has once again decohered from the rest, as shown in the last entry.

Crucially, the existence of such fluctuations depends on the dimensionality $d_E$ of the Hilbert space $\mathcal{H}_E$ of the environment (assumed to be larger than the dimensionality of the system's Hilbert space $\mathcal{H}_S$). For finite $d_E$, Hilbert space is bounded, and one can derive a quantum version of the Poincaré recurrence theorem [22]; for infinite $d_E$, the recurrence time goes to infinity, and excitations in the

system can dissipate into the environment and never come back. Zurek [105] has shown that, under reasonable assumptions concerning the initial wave function and the distribution of eigenvalues, the correlation amplitudes governing off-diagonal elements in the reduced density matrix will have an average of zero and experience fluctuations with a magnitude that scales as

$$\Delta \sim d_E^{-1/2} \ . \tag{4.24}$$

In a finite-dimensional Hilbert space, Boltzmann fluctuations are inevitable; however, in an infinite-dimensional space, the system can settle into equilibrium and stay there forever. The reduced density matrix corresponding to the latter asymptotes to a stationary form, free of Boltzmann fluctuations.

This discussion presumes that the branching structure of the wave function can be discerned from the form of the reduced density matrix for the macroscopic variables $\mathcal{H}_S$. In general, we cannot tell what states of a quantum system are actually realized on different branches simply by looking at its reduced density matrix.[3] For example, we might have a single qubit that takes on different states on three different branches of the wave function, specified by three mutually orthogonal environment states:

$$|\Psi\rangle = \frac{1}{\sqrt{2}} |+z\rangle_S |e_\uparrow\rangle_E + \frac{1}{2} |+x\rangle_S |e_\rightarrow\rangle_E - \frac{1}{2} |-x\rangle_S |e_\leftarrow\rangle_E \ . \tag{4.25}$$

The reduced density matrix for the qubit is

$$\rho_S = \frac{1}{2} |+z\rangle_S \langle +z| + \frac{1}{4} |+x\rangle_S \langle +x| + \frac{1}{4} |-x\rangle_S \langle -x| \tag{4.26}$$

$$= \frac{3}{4} |+z\rangle_S \langle +z| + \frac{1}{4} |-z\rangle_S \langle -z| \ . \tag{4.27}$$

In the last line, the existence of three branches is completely obscured; the reduced density matrix does not reveal which states of the system exist as part of distinct worlds.

Thus, the reduced density matrix alone is not enough information to reveal what is truly happening inside a system. Indeed, it is possible to construct a stationary reduced density matrix from an appropriate mixture of nonstationary states by tracing out the environment. Therefore, the fact that a reduced density matrix is stationary does not suffice to conclude that there are no dynamical processes occurring on distinct branches within the system that it describes; for that, it is necessary to consider the full quantum state. When we discuss the thermal nature of a patch of de Sitter space in §4.3.1, we have the benefit of knowing the full state of the de Sitter vacuum, allowing us to circumvent this issue and draw conclusions about the (lack of) dynamics in a patch.

---

[3]We thank Alan Guth, Charles Bennett, and Jess Reidel for discussions on this point.

## 4.3 Single de Sitter Vacua

We now apply these ideas to de Sitter cosmology—specifically, to the case of a unique vacuum with $\Lambda > 0$. In the Hartle-Hawking vacuum, the quantum state of any one causal patch is described by a thermal reduced density matrix. As emphasized in §4.2.3 above, we cannot claim that the patch is stationary on the sole basis of its reduced density matrix; however, given that we know the full vacuum state, we argue that the patch is indeed stationary. Were we to observe the patch, we would see fluctuations, but in the absence of an external observing device, nothing fluctuates. In particular, there are no decohered branches of the wave function containing time-series records of fluctuating observables. This picture does not apply if horizon complementarity is valid; in this case the entire Hilbert space is finite-dimensional, and unless it starts there, the state cannot asymptote to the vacuum as $t \to \infty$. In complementarity, we expect Boltzmann fluctuations and Poincaré recurrences.

### 4.3.1 Eternal de Sitter

Let us recall some basic properties of quantum fields in de Sitter space [87, 106]. De Sitter space is the unique maximally symmetric spacetime with positive curvature. In 4D, it has a scalar curvature $12H^2$ and satisfies the Einstein equations with a cosmological constant $\Lambda = 3H^2$, where $H^{-1}$ is the radius of de Sitter space. Consider a massive[4], noninteracting scalar field $\varphi$, which satisfies the Klein-Gordon equation

$$(\Box - m^2)\varphi = 0 \tag{4.28}$$

in the de Sitter metric. In order to quantize fields in de Sitter space, we must first choose a coordinate system. There are numerous possibilities, but we narrow the scope to flat coordinates and static coordinates, as they are used most often in the literature.

In flat coordinates, the metric reads

$$ds^2 = \frac{1}{H^2\tau^2} \left(-d\tau^2 + dx_i dx^i\right) \ , \tag{4.29}$$

which has the form of a flat, expanding Friedmann-Robertson-Walker metric with a constant Hubble parameter $H$ and conformal time $\tau$. In these coordinates, there is no timelike Killing vector to provide a sensible prescription for defining modes of $\varphi$. Since there is translational and rotational invariance among the spatial directions, we are still able to separate the mode solutions with wave number $\vec{k}$ as

$$f(\tau)e^{i\vec{k}\cdot\vec{x}} \tag{4.30}$$

_____

[4]We do not consider the massless case, since there is no (vacuum) state that is invariant under the full de Sitter group [107], which is problematic for the cosmic no-hair theorem in §4.3.2.

for some function $f$. Thus, we may attempt to define modes in the asymptotic regions of de Sitter, $\mathcal{I}^\pm$, by analogy with Minkowski space. Because of this analogy, the vacuum defined by these modes will have the same symmetries as the free field Minkowski vacuum. Unfortunately, the asymptotic regions are not static in an expanding universe, so we are left to define modes in the adiabatic approximation for a universe that has an infinitely slow expansion. The Euclidean vacuum, formed from the adiabatic modes, is invariant under the de Sitter group, and thus does not change with time. Although de Sitter invariance alone does not define a unique state, the Euclidean vacuum is the unique de Sitter-invariant Hadamard[5] state for a massive, noninteracting scalar field [107, 109–113].

In static coordinates the metric becomes

$$ds^2 = -\left(1 - H^2 r^2\right) dt^2 + \left(1 - H^2 r^2\right)^{-1} dr^2 + r^2 \, d\Omega^2 \ . \tag{4.31}$$

These coordinates give a timelike Killing vector $-\partial_t$ that points toward the future (past) in the northern (southern) causal diamond, and we may use this Killing vector to define modes. Following [114], the mode expansions for the southern and northern diamonds of de Sitter space are

$$\varphi^S = \int_0^\infty d\omega \sum_{j=-\infty}^\infty \left[ a_{\omega j}^S \varphi_{\omega j}^S + \left(a_{\omega j}^S\right)^\dagger \left(\varphi_{\omega j}^S\right)^* \right] \tag{4.32}$$

$$\varphi^N = \int_0^\infty d\omega \sum_{j=-\infty}^\infty \left[ a_{\omega j}^N \varphi_{\omega j}^N + \left(a_{\omega j}^N\right)^\dagger \left(\varphi_{\omega j}^N\right)^* \right] \ , \tag{4.33}$$

where $\omega$ is the mode frequency. The operators $a_{\omega j}^N$ and $\left(a_{\omega j}^S\right)^\dagger$ are annihilation operators in the northern and southern diamonds. The Euclidean vacuum is

$$|\Omega\rangle = \prod_{\omega=0}^\infty \prod_{j=-\infty}^\infty \left(1 - e^{-2\pi\omega}\right)^{1/2} \exp\left[ e^{-\pi\omega} \left(a_{\omega j}^N\right)^\dagger a_{\omega j}^S \right] |S\rangle \otimes |N\rangle \ , \tag{4.34}$$

where $|S\rangle$ and $|N\rangle$ are the southern and northern no-particle vacua. Ignoring gravitational back-reaction, the static Hamiltonian associated with the northern modes is

$$\hat{H}_N = \int_0^\infty d\omega \sum_{j=-\infty}^\infty \left(a_{\omega j}^N\right)^\dagger a_{\omega j}^N \, \omega \ , \tag{4.35}$$

and the reduced density matrix in the northern diamond is

$$\rho_N = \mathrm{Tr}_S \, |\Omega\rangle\langle\Omega| = \left[ \prod_\omega (1 - e^{-2\pi\omega}) \right] e^{-\beta \hat{H}_N} \ , \tag{4.36}$$

which is a thermal density matrix with temperature $T = 1/\beta$.

---

[5]Without the Hadamard condition [108], there are a continuum of de Sitter-invariant states, known as the $\alpha$ vacua, which are related to one another via Bogoliubov transformations [107].

If the universe is in the Euclidean vacuum, the reduced density matrix describing the area inside a causal horizon is thermal. In §4.2.3, we argued that a subsystem with a thermal density matrix may still evolve into one with a Boltzmann fluctuation. In the case of the Euclidean vacuum, however, we have both the reduced density matrix $\rho_N$ and the full quantum state $|\Omega\rangle$. From an examination of (4.34), we see that the modes of a given frequency $\omega$ in the northern diamond are in a one-to-one correspondence with the modes in the southern diamond. By tracing out the southern diamond to construct $\rho_N$, we know precisely which correlations we are discarding, mode by mode. Furthermore, there is no interaction Hamiltonian between the northern and southern diamonds, since the diamonds are not in causal contact. The entanglement structure is not disrupted by the separate evolution in each diamond, so dynamical processes akin to the one shown in the last panel of Fig. 4.1 are forbidden. Then the reduced density matrix of each diamond is truly stationary, and no Boltzmann fluctuations are possible in either diamond.

We have argued that there are no Boltzmann fluctuations in the de Sitter vacuum. It remains to determine whether the universe may actually be described by the de Sitter vacuum. Accordingly, the rest of our analysis consists of understanding the conditions under which the quantum state takes on this stationary vacuum form in different models.

## 4.3.2 Cosmic No-Hair

We turn now to situations, like that of our universe today, in which the universe is not in the vacuum but rather evolving in time. We will see that, though there may be fluctuations initially if the state is very far from the vacuum, the state will quickly approach the vacuum on time scales proportional to the inverse of the Hubble parameter, after which no fluctuations will arise.

We begin with the classical form of the cosmic no-hair theorem, which states that, given a positive vacuum energy density (*i.e.*, a positive cosmological constant $\Lambda$), the metric evolves toward that of de Sitter space [88]. Physically, excitations of de Sitter (including matter and radiation fields with substantial energy densities) redshift away across the horizon, so every causal patch relaxes to the vacuum.

The physical intuition behind the cosmic no-hair theorem extends to quantum fields in curved spacetime. For generic states, the expectation value of a massive scalar field $\varphi$ decays exponentially in time:

$$\langle\varphi(x)\rangle_\psi = \mathcal{O}(e^{-M|\tau|}) , \tag{4.37}$$

for a decay constant $M > 0$ and proper time $\tau$ between the point $x$ and some reference point at $\tau \to \infty$ [89]. Higher $n$-point correlation functions at large separations decay as well. The vacuum is stable against perturbations and is an attractor state for local operators, whose expectation values in a generic state will approach the expectation values in the vacuum in the asymptotic region.

A quantum-gravitational version of the no-hair theorem would presumably yield analogous results for the graviton field $h_{\mu\nu}$, but a scalar field can stand in as a proxy in order to make calculations manageable. Although we have focused on a free scalar field theory to write an explicit form of the Euclidean vacuum and the reduced density matrix, the graviton has self interactions, so the analysis needs to be extended to an interacting scalar theory with a Hartle-Hawking vacuum. For renormalizable interactions, the cosmic no-hair theorem still holds at an arbitrary number of loops, for arbitrary $n$-point functions, and for $D \geq 2$. Furthermore, $M$ does not receive any radiative corrections. The results of [89, 90] show that the decay constant for massive[6] scalar fields is

$$M = \begin{cases} \frac{3}{2}H & \text{for } m > \frac{3}{2}H \\ \frac{3}{2}H - \sqrt{\frac{9}{4}H^2 - m^2} & \text{for } 0 < m \leq \frac{3}{2}H \ . \end{cases} \tag{4.38}$$

If the universe is in an arbitrary state that is perturbed around the Hartle-Hawking vacuum, the state will approach the vacuum at large spacetime distances exponentially fast, with a decay constant $3H/2$ for large $m$. Once the field correlations have sufficiently decayed, the arguments of §4.2.3 tell us that no fluctuations occur.

### 4.3.3 Complementarity in Eternal de Sitter

Horizon complementarity posits that the spacetime interpretation of a quantum state depends on the viewpoint of a specified observer [8, 49, 91, 92]. In particular, a description in terms of local quantum field theory will not extend smoothly beyond a horizon. Applied to de Sitter space, this philosophy implies that spacetime locality only applies within a cosmological horizon volume, and the corresponding quantum system has a finite-dimensional Hilbert space. The Hilbert space of the patch can be decomposed as a product of bulk and boundary factors [116, 117]:

$$\mathcal{H} = \mathcal{H}_{\text{bulk}} \otimes \mathcal{H}_{\text{boundary}} \tag{4.39}$$

(we ignore a possible factor corresponding to singular spacetime geometries, which will not be important for our analysis).

From the Bekenstein-Hawking relation [118, 119], the entropy associated with the patch is one quarter of the area of the horizon: $S_{\text{dS}} = \mathcal{A}/4$. This entropy is related to the density matrix $\rho \sim e^{-\beta \hat{H}}$ for the patch via $S_{\text{dS}} = \text{Tr}_{\text{boundary}} \rho \ln \rho$, so the patch is thermal even if the system as a whole is in a pure quantum state. The energy spectrum is discrete, with only a finite number of

---

[6]As previously mentioned, the massless case is problematic, since there is no de Sitter-invariant vacuum in the noninteracting limit [107]. Hollands [115] is able to show rigorously only that correlation functions grow no faster than a polynomial function of proper time. The expectation, however, is that these functions should in fact decay, and Hollands presents evidence that the 2-point function does indeed decay, though not exponentially as it does in the massive case.
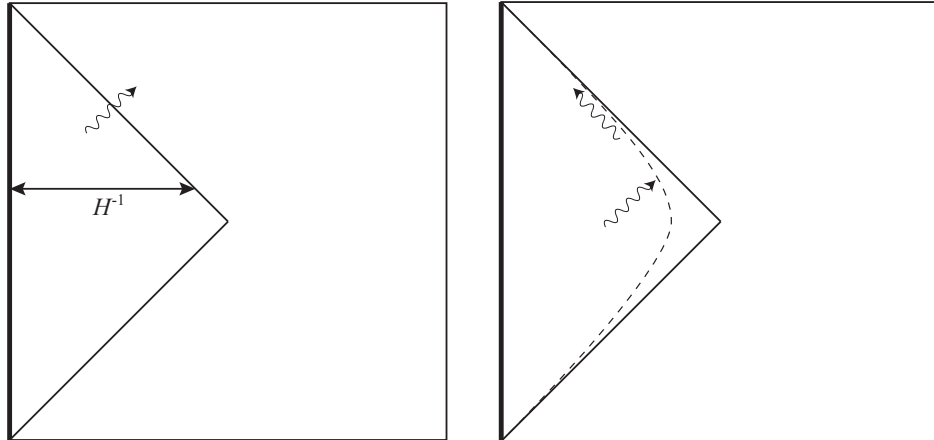
Figure 4.2: Conformal diagrams for de Sitter space in the global (QFT) picture (left) and with horizon complementarity (right). We consider an observer at the north pole, represented by the line on the left boundary and their causal diamond (solid triangle). The wavy line represents excitations of the vacuum approaching the horizon. In QFT in curved spacetime, the excitation exits and the state inside the diamond approaches the Hartle-Hawking vacuum, in accordance with the cosmic no-hair theorems. In contrast, horizon complementarity implies that excitations are effectively absorbed at the stretched horizon (dashed curve just inside the true horizon) and eventually return to the bulk.

eigenvalues with energies less than any given cutoff value [120].

If we interpret the entropy as being the logarithm of the number of quantum states, the horizon patch is analogous to a closed thermal system at a temperature $T$ [7, 8]. Although the relationship $\dim \mathcal{H} = e^S$ holds only at infinite temperature [120], there are compelling reasons (*e.g.*, from black holes) to think that the static Hamiltonian is bounded from above [121].[7] In our discussion of complementarity, we assume that this bound exists and that the dimension of the Hilbert space

$$\dim \mathcal{H} = e^{2S_{\mathrm{dS}}} = \exp(6\pi\Lambda^{-1}) \tag{4.40}$$

is finite (the factor of 2 comes from the fact that the bulk and boundary components have equal dimensionality).

The complementarity picture of eternal de Sitter with a unique vacuum state is therefore very different from the situation of QFT in a de Sitter background discussed in §4.3.1. In the latter, the ability of excitations to leave the horizon and never return depended crucially on the fact that Hilbert space was infinite-dimensional. In complementarity, eternal de Sitter space is a truly closed finite-dimensional system, subject to Poincaré recurrences [22]. Of course, there is a true vacuum state, the lowest-energy eigenstate, that is strictly stationary, but a generic state is nonstationary. We may think of excitations as being absorbed by a stretched horizon with a finite area and eventually being

---

[7]For subtleties involving the use of the static Hamiltonian in quantum gravity, see [122].

emitted back into the bulk, as shown in Fig. 4.2. Boltzmann fluctuations into lower-entropy states (described in §4.2.3) are allowed, in agreement with the conventional picture of a thermal de Sitter patch. As we argue below, this story changes in important ways in theories with more than one metastable vacuum.

## 4.4    Multiple Vacua

In this section we consider theories with more than one metastable potential minimum, at least one of which has $\Lambda > 0$, as portrayed schematically in Fig. 4.3. We consider the existence of fluctuations in both the lowest-energy "true" vacuum and in any higher-energy false vacua. For convenience, we limit our attention to vacua with non-negative energy, $\Lambda \geq 0$. Transitions from vacua with $\Lambda \geq 0$ to those with $\Lambda < 0$ generally result in singular crunches; evolution might continue via quantum gravity effects, but we will not address that possibility here.

### 4.4.1    Semiclassical Quantum Gravity

We first consider semiclassical quantum gravity, by which we mean QFT coupled to a classical (but dynamical) spacetime background. Coleman studied false vacua in this context and calculated the rate at which a higher-energy vacuum would decay to a lower-energy state via bubble nucleation [60, 123]. It is useful to consider an analogous problem in one-dimensional quantum mechanics, in which a single particle moves in a potential $V(x)$ of the same schematic form as shown in Fig. 4.3, with a global (true) minimum at $x_T$ and a local (false) minimum at $x_F$. Then, one can calculate the transition amplitude using the path integral defined with respect to Euclidean time $T$:

$$\left\langle x_T \right| e^{-HT} \left| x_F \right\rangle = N \int [dx] e^{-S_E[x(T)]} \; , \tag{4.41}$$

where $H$ is the Hamiltonian and $S_E$ is the Euclidean action, while the states $|x_T\rangle$ and $|x_F\rangle$ are position eigenstates. This quantity can be calculated using instanton methods and represents the amplitude for finding the particle at position $x_T$, given that it started at position $x_F$—something that might be of relevance to an observer measuring the position of the particle. An analogous field theory calculation can be used to calculate the rate of from one field configuration $|\varphi_1(x)\rangle$ to another $|\varphi_2(x)\rangle$, including the tunneling rate from one vacuum to another.

Our interest, however, is not in what an out-of-equilibrium observer with a field-value detection device would measure, but in how quantum states evolve in isolated patches of de Sitter space. Eigenstates of the field operator $\hat{\varphi}(x)$ are not energy eigenstates; therefore, we need to be careful when we use terms such as "false vacuum" and "true vacuum" to refer to quantum states rather than field values. For some purposes it is useful to study eigenstates of a perturbative Hamiltonian
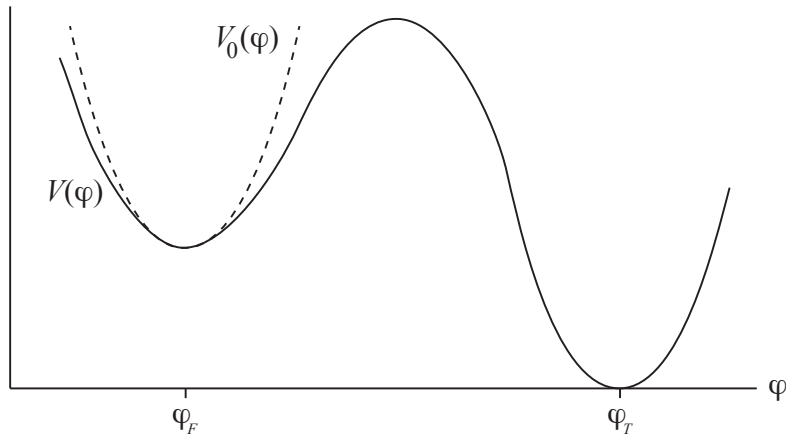
Figure 4.3: A scalar field potential with multiple local minima. The global minimum corresponds to the true-vacuum value $\varphi_T$ (which may have $\Lambda = 0$ or $\Lambda > 0$), and for simplicity we have portrayed a single false-vacuum value $\varphi_F$. The dashed line represents the perturbative Hamiltonian for the false vacuum, in which the potential is given by a local approximation to the true potential in the vicinity of $\varphi_F$.

constructed by approximating the potential in the vicinity of one local minimum, as shown for $\varphi_F$ in Fig. 4.3. In that case the results from §4.3.1, where we studied QFT in a fixed de Sitter background, are relevant.

Consider first the true vacuum quantum state $|0\rangle$ of the full theory. A generic homogeneous field value $\varphi_*$ will have some nonzero overlap with this state, $\langle \varphi_* | 0 \rangle \neq 0$, but the field will be mostly localized near the global minimum value $\varphi_T$. While it is difficult to rigorously prove a version of the cosmic no-hair theorem for this interacting theory, we intuitively expect the physics in this case to mirror that of QFT with a unique de Sitter vacuum. Namely, excitations above the lowest-energy state will dissipate outside the horizon, and each local patch will approach the vacuum state $|0\rangle$. This state is stationary, and we expect no quantum or Boltzmann fluctuations. Since we are dealing with QFT, the Hilbert space is infinite-dimensional, and there are no recurrences.

We also do not expect uptunneling to a higher-energy vacuum from the true vacuum state for the same reason (energy eigenstates are stationary and do not fluctuate). This assertion might seem to be in tension with the existence of instantons that contribute a nonzero amplitude to processes analogous to (4.41), but such a counterargument confuses field values with quantum states. Although there are instanton solutions, their role is to shift the value of the vacuum energy in the true vacuum from what one would compute in a local approximation to the effective potential near $\varphi_T$. The situation is analogous to that of the QCD vacuum, where instantons connecting vacua of different winding numbers provide a shift in energy that depends on the value of $\theta_{\text{QCD}}$. Instantons are important for calculating energy eigenvalues, but once the quantum system is in a stationary state such as the vacuum $|0\rangle$, they do not describe true dynamical transitions. The local perturbative

vacuum will be unstable to uptunneling via instantons, but that is not the true nonperturbative vacuum into which the system settles.

Next, we turn to false vacua. A semiclassical state with $\langle \varphi \rangle = \varphi_F$ is not strictly a vacuum state, or indeed any form of energy eigenstate, as it will decay via tunneling. We may nevertheless consider the energy eigenstates of the perturbative Hamiltonian, obtained by locally approximating the potential in the vicinity of $\varphi_F$, as shown in Fig. 4.3. These are not energy eigenstates of the full Hamiltonian, but their dynamics are well-described by a combination of processes near the false-vacuum value plus decays via bubble nucleation. We may think of the "false de Sitter vacuum state" as the Hartle-Hawking vacuum state of this perturbative Hamiltonian. Once again, we expect excitations of such a state to rapidly dissipate by leaving the horizon, and the configuration will become quiescent with respect to perturbative fluctuations. We refer to such states as "quiescent" rather than "stationary," since they are not true eigenstates but nevertheless do not exhibit thermal fluctuations.

We are left with two kinds of possible non-perturbative processes to consider: downtunneling to lower-energy vacua and uptunneling to higher-energy vacua. First, we examine downtunneling. In the conventional picture of false-vacuum decay, a small bubble of true vacuum nucleates and grows at nearly the speed of light. This picture is clearly a semiclassical description of a single branch of the wave function, rather than a full treatment of the quantum state. We can decompose the Hilbert space into the product of the state of a smooth background field $\varphi_\lambda(x)$ and small-scale fluctuations:

$$\mathcal{H} = \mathcal{H}_{\varphi_\lambda} \otimes \mathcal{H}_{\delta\varphi} \ . \tag{4.42}$$

Here, $\lambda$ is a length scale used to smooth the field. The factor $\mathcal{H}_{\varphi_\lambda}$ includes configurations with bubbles of different sizes and locations, as well as completely homogeneous configurations. When a bubble nucleates, some of the energy density that was in the potential for $\varphi$ gets converted into fluctuation modes. Therefore, a reduced density matrix for the background field obtained by tracing over $\mathcal{H}_{\delta\varphi}$ will exhibit decoherence, as the fluctuations produced by bubbles in different locations will generically be orthogonal to each other. In that sense, the semiclassical configurations described by bubble nucleation correspond to truly distinct branches of the wave function. With that single caveat, we agree with the standard picture of downtunneling to lower-energy vacua.

Different cases of interest for bubble nucleation are shown in Fig. 4.4. An observer at the north pole in the de Sitter diagram could witness the nucleation of a bubble to a lower-energy de Sitter vacuum, or to a Minkowski vacuum (the triangular "hat"), or avoid seeing bubbles at all. The probability of seeing a bubble along any specified geodesic asymptotes to 1, but for a sufficiently small nucleation rate, the physical volume of space remaining in the false vacuum grows with time.
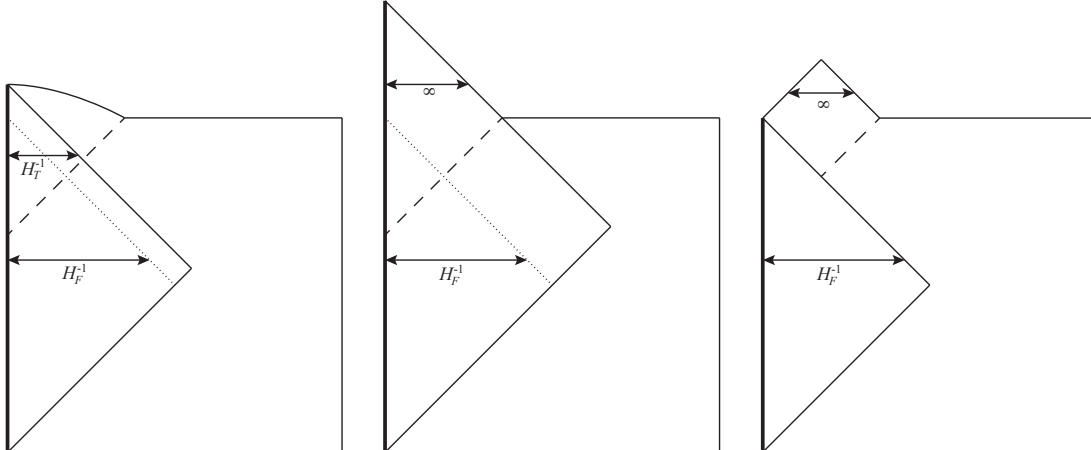
Figure 4.4: Conformal diagrams for de Sitter space with a false vacuum. The first two diagrams show the effect of a bubble (dashed line) nucleating within the northern-hemisphere causal patch, leading to lower-energy de Sitter (left) and Minkowski (middle), while the third shows a false-vacuum region that does not experience any bubbles (right). $H_F^{-1}$ and $H_T^{-1}$ are the Hubble radii of the false and true vacua, with the latter being infinite in the Minkowski case. In both cases the true horizon is larger than the Hubble radius in the false vacuum; in the left-hand diagram, it becomes equal to the horizon in the true vacuum, while on the right it becomes infinitely large. In either of these cases, excitations can leave the apparent horizon in the false vacuum while remaining inside the true horizon. On the right, the observer at the North pole remains in the false vacuum state forever, although there are bubbles outside their horizon.

Next we turn to uptunneling from one false-vacuum state to another of even higher energy.[8] In the true vacuum, we could straightforwardly argue that the spirit of the cosmic no-hair theorem is obeyed: excitations leave the horizon and the system approaches its lowest-energy eigenstate. In the false vacuum, the argument is not so clean, since there are no true energy eigenstates to approach. Nevertheless, the physical situation is quite similar. The Hilbert space is still infinite-dimensional, so we do not expect recurrences, and excitations within a patch can readily leave the horizon, leaving us in the perturbative vacuum. In that state, however, there will still be a nonzero amplitude for the nonperturbative process describing uptunneling. Uptunneling represents a decrease rather than an increase of entropy, so it must necessarily be a Boltzmann fluctuation rather than a simple branching of the wave function.

By itself, this result might seem puzzling. We have claimed that a system near the lowest-energy minimum in the potential settles into a true stationary vacuum state with no possibility of uptunneling, while there can be uptunneling from a false vacuum. These claims can be reconciled by considering a limit in which the barrier between false and true vacuum becomes infinitely large. In that case, transitions from the false to true vacua are suppressed, and the behavior of the false vacuum should increasingly resemble our picture of the true vacuum. In particular, rather than

---

[8]We thank Stefan Leichenauer and Paul Steinhardt for discussions of these issues.

staying in the perturbative vacuum (from which there can be uptunneling), we expect the system to evolve to what we might call a "semi-perturbative vacuum"—a quiescent state in which the field is concentrated near the false vacuum, but also has some support on field values corresponding to potential minima of higher energies. The timescale over which the perturbative vacuum relaxes to a semi-perturbative vacuum (presumably with slightly smaller effective cosmological constant) will be governed by the barrier-penetration factor connecting the false vacuum to higher-energy minima. That factor also governs the rate for uptunneling to such minima. Therefore, we expect a relatively short window in which uptunneling can happen before the state relaxes, after which the rate of uptunneling falls to zero.

While these results are not rigorous, they provide a strong indication that false-vacuum states in semiclassical quantum gravity either decay or asymptote to quiescent states that are free of fluctuations.

## 4.4.2 Complementarity in a Landscape

We now consider theories with multiple vacua, each labeled by a field expectation value $\varphi_i$, in the context of horizon complementarity. In this case the Hilbert space appropriate to a single vacuum (4.39) is promoted to a direct sum, with one term for each semiclassical patch geometry:

$$\mathcal{H} = \bigoplus_i \mathcal{H}^{(i)}_{\text{bulk}} \otimes \mathcal{H}^{(i)}_{\text{boundary}} \ . \tag{4.43}$$

The structure is similar to that of Fock space [116, 117]. The dimensionality of the entire Hilbert space is the sum of the dimensions of each term, $\dim \mathcal{H}^{(i)} = e^{2S^{(i)}_{\text{dS}}} = \exp(6\pi \Lambda_i^{-1})$. There are two cases of interest: the finite-dimensional case where every vacuum has $\Lambda > 0$, and the infinite-dimensional case where there is at least one vacuum with $\Lambda = 0$ (as mentioned previously, we do not consider vacua with $\Lambda < 0$, as transitions into them lead to singularities).

If all vacua have $\Lambda > 0$, the situation is very similar to the single-vacuum case discussed in §4.3.3. Exact energy eigenstates, including the lowest-energy vacuum state, will be stationary, and no fluctuations will occur. The vacuum will feature a de Sitter semiclassical geometry with the field value concentrated near the true minimum, although it will not be a field eigenstate. Generic states, however, will not be stationary, and in a finite-dimensional Hilbert space there is no room for excitations to dissipate outside the horizon, so recurrences are expected.

Now consider theories with at least one vacuum having $\Lambda = 0$, as might be expected in supersymmetric or string theories. The future development of the spacetime includes census-taker observers living in a Minkowski "hat" [124, 125], as shown in the middle and right diagrams of Fig. 4.4. The Hilbert space of the full theory is then infinite dimensional, and such observers have access, in principle, to an infinite amount of information.

From (4.24), the rate of Boltzmann fluctuations goes to zero (and the timescale for recurrences goes to infinity) for infinite-dimensional Hilbert spaces, where $\Lambda_T = 0$. Of course, there are no fluctuations in the true Minkowski vacuum. But we can make a stronger statement: the rate of fluctuations will asymptote to zero even in the false vacua. The intuition is that states with excitations around false-vacuum geometries are more likely to decay than the vacuum states themselves. So time evolution will skew the population of false vacua towards states that are stationary except for the possibility of decay by bubble nucleation, *i.e.* quiescent in the sense of the previous subsection. After a high-energy vacuum decays to a lower-energy one, transient excitations will allow for the existence of Boltzmann fluctuations, but the excited states will again preferentially decay. The surviving configurations will become effectively stationary, and the fluctuation rate will asymptote to zero, rather than to a nonzero constant. We therefore expect only a finite (and presumably small) number of fluctuations in a landscape of vacua that includes a Minkowski vacuum.

This intuition can be bolstered by an analogy to one-dimensional quantum mechanics in the presence of a barrier. Consider once again a particle of mass $m$ and energy $E$ moving in a potential $V(x)$ schematically similar to the false-vacuum potential shown in Fig. 4.3. The particle can escape the well by tunneling through the barrier. A wave packet initially in the potential well will leak out, and the WKB approximation relates the wave functions on either side of the potential:

$$\frac{\psi(x_e)}{\psi(x_0)} = \exp\left(-\frac{1}{\hbar}\int_{x_0(E)}^{x_e(E)} \sqrt{2m(V(x)-E)}dx\right) \equiv e^{-\gamma/2} \ , \qquad (4.44)$$

where $x_0(E)$ and $x_e(E)$ are the starting and ending points for the region where the particle "has negative energy," so $V(x_0(E)) = V(x_e(E)) = E$. The escape probability is simply $e^{-\gamma}$, and the tunneling rate is given by the product of this probability with some characteristic frequency:

$$R = f(E)e^{-\gamma} \ . \qquad (4.45)$$

The classic barrier penetration problem considers a square-well potential, in which the bound particle has a position-independent momentum, $p(E) = \sqrt{2m(E-V)}$, and a characteristic "collision frequency", $f(E) = p(E)/(2mx_0)$. Here, we assume a more general potential, so the momentum is a function of both $E$ and $x$, and the frequency will be given by some integral over positions inside the well. The exact expression is not important for us—we assume only that the frequency is an increasing function of $E$, $f'(E) > 0$. Then, the energy dependence of the tunneling rate is

$$\frac{dR}{dE} = f'(E)e^{-\gamma} - \frac{2}{\hbar}f(E)e^{-\gamma}\int_{x_0(E)}^{x_e(E)} \left[-\frac{2}{\sqrt{2m(V(x)-E)}}\right] \ , \qquad (4.46)$$

which is manifestly positive (we have used the fact that $V(x_0) - E = V(x_e) - E = 0$ to eliminate

the terms which arise from varying the limits of integration).

This simple exercise demonstrates an intuitively sensible result: among states trapped behind a barrier, those with higher energy tunnel out more quickly. In the case of the cosmological false vacuum, the analogous statement is that excited states of the perturbative Hamiltonian undergo false-vacuum decay more rapidly.

In complementarity, we see that only in the case of a Minkowski true vacuum can recurrences and fluctuations be avoided entirely. A version of this phenomenon—the crucial difference in the long-term quantum evolution of landscapes with and without $\Lambda = 0$ vacua—has been previously noted in a slightly different context [117, 126]. There, it was pointed out that quantum measurements in a false-vacuum state will decohere by becoming entangled with environment degrees of freedom, but they must eventually recohere if the total Hilbert space is finite-dimensional. In infinite-dimensional Hilbert spaces, in contrast, decoherence can persist forever. This argument is analogous to our own, in that such models are largely free of Boltzmann fluctuations.

## 4.5 Consequences

### 4.5.1 Boltzmann Brains

In the conventional picture, because de Sitter space has a temperature, it experiences thermal fluctuations that lower the entropy by $\Delta S$ with a finite rate proportional to $e^{-\Delta S}$. If the Hartle-Hawking vacuum is eternal, then all fluctuations that fit within a horizon volume are produced an infinite number of times inside each such volume. Such fluctuations could contain conscious observers like ourselves [22–24]. Due to the exponential suppression of lower-entropy states, the fluctuations containing observers—even the ones that contain exact copies of our own brains—that occurred most frequently would look entirely unlike the world we observe. In particular, fluctuations containing the room that the reader is currently in would be vastly more likely than fluctuations containing all of Earth, let alone the entire observable universe, and the momentary coalescence of the reader's brain thinking the precise thoughts they are having right now out of thermal equilibrium would be likelier still. If this conclusion were correct, we would not be able to trust our memories or our (supposed) observations, a solution inconducive to the practice of science.

We have argued, however, that this situation is less generic in de Sitter cosmologies than is often supposed.[9] The appearance of Boltzmann brains is avoided in the context of QFT in eternal de Sitter space or in a landscape with a terminal Minkowski vacuum (with or without complementarity). In these cases, the dimension of the Hilbert space is infinite, so the recurrence time also goes to infinity, and the (possibly false) de Sitter vacuum becomes quiescent. If the horizon volume is initially in

---

[9]For related work that questions the validity of Boltzmann brains for decoherence-based reasons, see [102, 127, 128]. For the need for Hilbert space to be infinite-dimensional, see [129].

an excited state (as it is if the dark energy is a positive cosmological constant), then the cosmic no-hair theorem dictates that correlations fall off exponentially with time as the excitations leave the horizon. The total number of Boltzmann brains will thus be finite and presumably small, given the vast exponential suppression of macroscopic fluctuations. Thus, if enough observers are produced before de Sitter space approaches the vacuum (*e.g.*, in a period of structure formation) the vast majority of observers can, in fact, trust their memories and observations. This conclusion opens the door for many multiverse models that might have been discounted because of a Boltzmann brain problem, and could help resolve potential tensions with low-energy physics [27].

### 4.5.2    Landscape Eternal Inflation

Another kind of fluctuation into a lower-entropy state that is often invoked in de Sitter cosmology is uptunneling from one de Sitter vacuum state to another one of higher energy [20,21]. Processes such as this can be crucial for populating an entire landscape of vacua, starting from a state concentrated on any particular field value.

Uptunneling is conceptually very similar to the standard picture of a fluctuation into a Boltzmann brain: a vacuum in a thermal state undergoes a transition to a lower-entropy configuration with probability $e^{-\Delta S}$. The situation is the time-reverse of the well-known process of vacuum decay, which results in the production of particles and an increase in entropy. The analysis presented in this chapter leads to an analogous conclusion to that of the last subsection: if the total Hilbert space is infinite-dimensional, excitations around any particular false vacuum will dissipate. As discussed in §4.4, the system will relax to a (perturbative, semi-perturbative, or true) vacuum state, not a state of definite field value. The state becomes quiescent, and the rate of Boltzmann fluctuations asymptotes to zero.

Note that eternal inflation is still conceivable: uptunneling is suppressed, but downtunneling proceeds as usual, and different branches of the wave function will correspond to different distributions of bubbles in a semiclassical spacetime background. If the field starts out in a metastable vacuum, then the portion of it that remains there (on any one branch) is rewarded with greater volume production. Almost every world line will intersect a bubble of lower-energy vacuum, but if the tunneling rate is low enough to avoid percolation, the physical volume remaining in the high-energy vacuum grows without bound, as depicted in the rightmost diagram in Fig. 4.4. In this sense inflation continues forever.

On the other hand, it is clear that the details of eternal inflation in a landscape of vacua will change. In particular, the conclusions of the previous section suggest a reinterpretation of the rate equations for eternal inflation that relate the probabilities of transitions between different vacua [26, 116, 130]. Consider the simple landscape of Fig. 4.3, with minima located at field values $\varphi_F$ and $\varphi_T$, respectively. In the standard presentation, *e.g.* [130], the rate equations for a two-minimum

landscape read

$$\frac{dp_f}{d\tau} = -\kappa_f p_f + \kappa_t p_t \ , \qquad \frac{dp_t}{d\tau} = -\kappa_t p_t + \kappa_f p_f \ , \qquad (4.47)$$

where $\kappa_f$ and $\kappa_t$ are transition probabilities per unit proper time. The usual interpretation is that $\kappa_f$ ($\kappa_t$) represents the probability to transition from the false (true) vacuum to the true (false) one. But we have argued that, in the long-time limit, the probability to transition from the true to a false vacuum falls to zero. However, both the true and the false vacuum states have nonzero overlap with the states of any definite field value, so heuristically we may think of the true vacuum, for example, as containing an exponentially small piece with field value near $\varphi_F$. The rate equations should essentially be interpreted as probabilities to transition between states of definite field value in an (unrealistic) idealization where an observer is measuring the value of the field at regular intervals. In the real universe, where there is no external observer and the wave function evolves unitarily, the state simply evolves toward the true vacuum as time passes. Quantum fluctuations in de Sitter space do not provide a dynamical mechanism for populating an entire landscape with actual semiclassical geometries centered on different vacua and living on different branches of the wave function.

With horizon complementarity, this picture changes somewhat. If the true vacuum is de Sitter, Hilbert space is finite-dimensional, and Boltzmann fluctuations will lead to true transitions between states concentrated at different minima of the potential. If the true vacuum is Minkowski, on the other hand, Hilbert space is infinite-dimensional, and the above discussion is once again valid.

### 4.5.3   Inflationary Perturbations

The absence of quantum fluctuations in de Sitter space might seem to call into question the standard picture of the origin of density perturbations in inflation. In this case, however, the conventional wisdom gets the right answer; our approach leaves the standard predictions for density and tensor fluctuations from inflation essentially unaltered. The basic point is that the quantum state of light fields can remain coherent during inflation itself, but then experience decoherence and branching of the wave function when entropy is generated at reheating.

We can describe the Hilbert space during inflation as a product of the quantum states of the large-scale homogeneous background $\varphi(t)$ (macroscopic) perturbations and the small-scale (microscopic) perturbations:

$$\mathcal{H} = \mathcal{H}_{\varphi(t)} \otimes \mathcal{H}_{\mathrm{macro}} \otimes \mathcal{H}_{\mathrm{micro}} \ . \qquad (4.48)$$

The small-scale perturbations, including the specific microstates of individual photons and other particles, are unobservable, in the same way that individual atoms and molecules are unobservable in an ordinary box of gas. They serve as an environment we can trace over to understand the state of the observable large-scale perturbations. During inflation, the overall quantum state approaches

a factorizable form, as excitations dissipate and perturbations approach their lowest-energy states:

$$|\Psi_{\text{inflation}}\rangle = |\varphi(t)\rangle \otimes |0\rangle_{\text{macro}} \otimes |0\rangle_{\text{micro}} \ . \tag{4.49}$$

The state $|0\rangle_{\text{macro}}$ has a nonzero variance for the field operator $\varphi$, as calculated in standard treatments, but its quantum coherence is maintained.[10]

At reheating, however, entropy is generated. Energy in the inflaton is converted into a dense, hot plasma with many degrees of freedom. The specific form of the microscopic perturbations will depend on the state of the macroscopic perturbations; these factors become entangled, producing a state of the form

$$|\Psi_{\text{reheating}}\rangle = |\varphi(t)\rangle \otimes \left[ \sum_i |\delta\varphi_i\rangle_{\text{macro}} \otimes \left( \sum_\mu |\delta\varphi_{i,\mu}\rangle_{\text{micro}} \right) \right] \ . \tag{4.50}$$

Tracing over the microscopic fluctuations leaves a mixed-state density matrix for the macroscopic fluctuations, inducing decoherence [131–135]. By this process, the unique quantum state of the inflaton field evolves into a large number of decohered branches, each with a specific pattern of perturbations such as we observe in the CMB, with statistics given by the Born rule. In effect, reheating acts as an explicit measurement process. We therefore expect that the standard calculations of scalar and tensor fluctuations in any given inflationary model are unaffected by the considerations in this chapter.

### 4.5.4 Stochastic Eternal Inflation

We next turn to the possibility of eternal inflation in a slow-roll potential, as distinguished from a landscape of false vacua. The traditional approach to this scenario makes use of the stochastic approximation, which treats the inflaton field value in the slow-roll regime as a stochastic variable, undergoing a random walk [12–14]; for recent treatments see [136–138]. Consider the case of a power-law potential,

$$V(\varphi) = \frac{\lambda\varphi^{2n}}{2nM_{\text{pl}}^{2n-4}} \ . \tag{4.51}$$

In a single Hubble time, the expectation value of the field decreases by

$$\Delta\varphi = \frac{nM_{\text{pl}}^2}{4\pi\varphi} \ , \tag{4.52}$$

---

[10]One might imagine that decoherence occurs because modes become super-Hubble-sized, and we should trace over degrees of freedom outside the horizon. This reasoning is not quite right, as such modes could (and often do) later re-enter the observable universe; they become larger than the Hubble radius during inflation but never leave the true horizon.

but the dispersion of perturbations around this value is

$$\Delta^2 = \left\langle \delta\varphi^2 \right\rangle = \frac{H^3}{4\pi^2} t \; . \tag{4.53}$$

In a Hubble time $H^{-1}$, we have $\Delta = H/2\pi$.

Now comes the critical step. In the stochastic approximation, one asserts that $\Delta$ represents an RMS fluctuation amplitude

$$|\delta\varphi| = \frac{H}{2\pi} \; , \tag{4.54}$$

and that the effective value of the inflaton in a given Hubble patch should be treated as a random variable drawn from a distribution with this amplitude. Above a critical field value,

$$\varphi^* = \lambda^{-1/(2n+2)} M_{\mathrm{pl}} \; , \tag{4.55}$$

the fluctuations dominate, $|\delta\varphi| \gg \Delta\varphi$. In this picture, to an excellent approximation, $\varphi$ undergoes a random walk with time step $H^{-1}$ and step size $|\delta\varphi|$. Causality dictates that each horizon area undergoes these fluctuations independently. For every Hubble time, when a horizon volume grows by a factor $e^3 \sim 20$, the field value in approximately 10 of the new horizon volumes is larger than its parent. In fact, this statement is a much stronger condition than what is required for eternal inflation. It suffices for only one of these volumes to move upward on the potential: $|\delta\varphi| \approx \mathcal{O}\left(\Delta\varphi/20\right)$.

The stochastic-approximation approach to eternal inflation differs sharply from the analysis presented in this chapter. As we have argued in §4.2, quantum fluctuations in closed systems near equilibrium cannot be treated as classical random variables. Fluctuations $\delta\varphi$ only become real when they evolve into different decoherent branches of the wave function and generate entropy. For the perturbations we observe in the CMB, this entropy source is provided by reheating. But precisely in the slow-roll regime, where the stochastic inflation story is invoked, there is no entropy production, no measurement or decoherence, and no branching of the wave function. All that happens during a Hubble time is a decrease in the classical field expectation value, $\Delta\varphi$. There is no quantum-dominated regime; the field simply rolls down its potential.

A more honest approach to eternal inflation would be to take the quantum nature of the dynamics seriously, and investigate the evolution of the wave function describing the coupled background and perturbations; we hope to study this more carefully in future work. Nevertheless, it is possible to draw some qualitative conclusions by considering the evolution of a wave packet in field space representing the homogeneous mode. If the initial state of the field has support near a local maximum of the potential, inflation is plausibly eternal: part of the wave packet will roll down the potential, eventually couple to perturbation modes, and experience decoherence, while part will remain near the maximum and continue to inflate. In contrast, if the field is slowly rolling down a monotonic
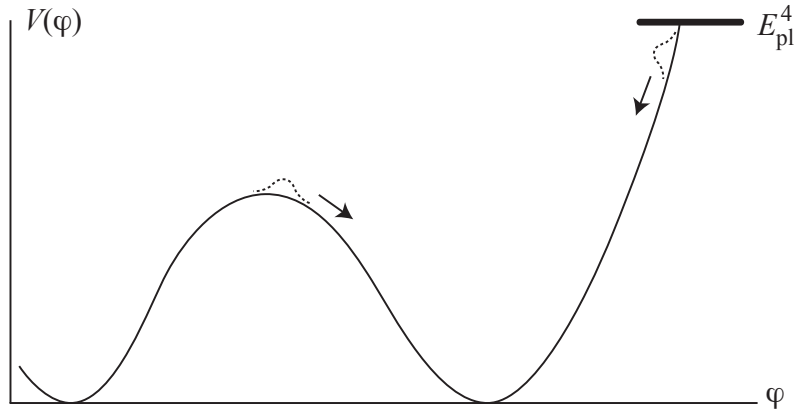
Figure 4.5: Potential supporting different kinds of inflation. Dashed lines are schematic representations of two different initial quantum states for the field. If the field begins at the right edge near the Planck cutoff, we expect it to evolve smoothly to the non-inflationary regime at the bottom of the potential. In contrast, if it begins at the top of a hill, it is plausible to imagine that part of the wave function remains in an inflationary state for arbitrarily long periods of time (although the amplitude for that branch of the wave function will be monotonically decreasing).

portion of the potential—as expected for a polynomial potential with a Planck-scale energy density cutoff—it will reach the bottom of the potential, and the inflationary phase will end in a finite time and after a finite number of $e$-folds. These two possibilities are portrayed in Fig. 4.5. We note that the simplest inflaton potentials, monomial power-laws $V(\varphi) \sim \varphi^n$, do not have saddle points and should thus avoid eternal inflation given a Planck-scale cutoff (the recent BICEP2 detection [139] of large-scale B-mode polarization in the CMB, if interpreted as a tensor/scalar ratio $r \sim 0.2$, is well fit by an $m^2 \varphi^2$ potential).

For a field on the monotonic portion of the potential, one might object that, even once the field has rolled down, some portion of the wave function will always remain arbitrarily close to the maximum allowed value of the potential, $e.g.$ the Planck-scale cutoff, just as a wave packet is supported throughout all of space despite being concentrated around a single point. This reasoning is correct, but it does not imply that there are some portions of the wave function where the end of inflation is postponed. The problem with this interpretation was already noted in §4.4.1 and §4.5.2: states of definite field value are not the same as states of definite energy density. In the slow-roll approximation, the cosmic no-hair theorem acts to bring the inflaton field to the appropriate vacuum state—a state of energy density corresponding perturbatively to de Sitter space with the appropriate cosmological constant. Each such state has nonzero overlap with the states of definite field value, but the cosmic no-hair theorem guarantees (to the extent that the slow-roll approximation is valid, so that no entropy is produced) that the field is driven into the appropriate false vacuum state, and then rolls smoothly to states with lower and lower energy density until the point that inflation ends. Again, there is negligible entropy production, no quantum fluctuations, and no branching during

this period—the inflaton remains in a single coherent state until reheating occurs.

To gain intuition for the points we make above, it is useful to consider applying the stochastic approximation to a free massive scalar field in eternal de Sitter space itself. At the minimum of the potential $V = m^2\varphi^2/2$, it is clear that the classical change $\Delta\varphi$ vanishes while the quantum variance $\delta\varphi$ does not, so the system is automatically in the quantum-dominated regime. If the stochastic approximation is applied, we expect occasional fluctuations of the field to very large values, leading to rapid inflation in those regions but not in others. In other words, if the stochastic picture is valid, one is led to the conclusion that de Sitter space with a massive scalar field has a runaway instability, in contrast with the usual view that there is a lowest-energy eigenstate with a stable semiclassical geometry (*cf.* [140]). In light of the above, we interpret this purported instability differently: it indicates a problem with the stochastic approximation, not with de Sitter space itself. The vacuum state of the scalar field is not a state of definite field value, although it is centered around the minimum of the potential. Rather, the state has overlap with all field values, at least up to a potential Planck-scale energy density cutoff. But we do not interpret the de Sitter vacuum as an unstable superposition of different field values expanding at different rates. Instead, we say that the field is in a single state, the vacuum, with a definite energy density given by the cosmological constant $\Lambda$.

### 4.5.5 Other Formulations of Quantum Mechanics

Throughout this chapter we have worked in the context of the Everett/Many-Worlds formulation of quantum mechanics, in which a single wave function evolves unitarily in Hilbert space according to the Schrödinger equation. Interestingly, our conclusions could be dramatically altered in other formulations. We will not explore these possibilities in detail here, but we briefly mention two alternatives.

One is a hidden-variable theory, such as the de Broglie-Bohm model, which augments the wave function by a hidden configuration space [141, 142]. Quantum fluctuations represent a real difference in knowledge of the system between merely knowing the wave function and also knowing the point in configuration space. What we think of as a stationary thermal state in the Everett approach would be more closely analogous to a thermal distribution function in classical statistical mechanics; while the density operator is stationary, the underlying state could still be evolving in time. We would therefore observe quantum fluctuations even in equilibrium. Although hidden-variable approaches to QFT are still under development [143, 144], it seems reasonable to imagine that such a theory would feature true, dynamical fluctuations in de Sitter space.

Another alternative is a stochastic dynamical-collapse theory, such as the Ghirardi-Rimini-Weber (GRW) model [145, 146]. Set in the context of nonrelativistic, many-particle quantum mechanics, the state of each particle has a fixed probability per unit time of spontaneously collapsing to a

localized position. Entanglement between particles induces an effective, ongoing "measurement" of macroscopic systems. Again, there is not a well-developed GRW model for QFT in de Sitter space, but the philosophy of the approach leads us to expect that a thermal state would experience true fluctuations. It seems we are dealing with one of the rare cases in which one's favorite formulation of quantum mechanics can drastically affect one's expectation for how observable quantities evolve.

## 4.6   Conclusions

Quantum variables are not equivalent to classical stochastic variables. They are related by the appearance of quantum fluctuations, which require entropy generation, decoherence, and branching of the wave function. In stationary states, entropy is not generated, and the wave function remains fixed; therefore, there are no quantum fluctuations, and treating a quantum field as a classical stochastic field is inappropriate. We have argued that this shift in thinking has important consequences for the cosmology of de Sitter space, since de Sitter regions tend to approach a stationary thermal state. In particular, if the true Hilbert space is infinite-dimensional (as is the case in QFT in curved spacetime or in horizon complementarity in the presence of a Minkowski vacuum), de Sitter vacua settle down and do not fluctuate. There are no Boltzmann brains in such states, relieving a major problem for many multiverse cosmological models. On the other hand, we also predict there is neither uptunneling to higher-energy vacua nor stochastic fluctuations up a slow-roll potential, implying that eternal inflation is much less generic than often supposed. A better understanding of complementarity and the correct formulation of quantum mechanics will help establish what happens in the real universe.

# Appendix

## 4.A   Boltzmann Fluctuations via Decoherent Histories

The appearance of decoherent Boltzmann fluctuations in time-dependent states (and their absence in stationary states) can be made explicit by using the formalism of decoherent (or consistent) histories [147–152]. It allows us to ask when two possible histories of a quantum system actually decohere from each other and can be assigned probabilities, which corresponds, in our case, to the existence of a physical fluctuation. Consider an operator $P_F$ that projects a state onto a subspace corresponding to a particular kind of fluctuation—it may be a Boltzmann brain or an uptunneling to a false vacuum (nothing that we will say relies on the details of what kind of fluctuation we are considering; in particular, we do not need to worry about what counts as a "brain"). If an external observer has a fluctuation-detection apparatus, the probability of observing such a fluctuation in a state $|\Psi\rangle$ is $p(F) = ||P_F |\Psi\rangle||^2$. But we are interested in dynamical fluctuations in closed systems without any external observers, so this quantity is beside the point. What matters to us is whether a history in which the system fluctuates into $F$ decoheres with one in which there is no such fluctuation, corresponding to the projection operator $P_N = \mathbb{1} - P_F$.

Start with a closed system described by a density operator $\rho(t_0)$ at an initial time $t_0$. We want to consider possible coarse-grained histories of the system, described by sequences of projection operators $\{P_\alpha\}$. These operators partition the state of the system at some time into mutually exclusive alternatives and obey

$$\sum_\alpha P_\alpha = \mathbb{1} \ , \qquad P_\alpha P_\beta = \delta_{\alpha\beta} P_\alpha \ . \tag{4.56}$$

A history is described by a sequence of such alternatives, given by a sequence of projectors at specified times, $\{P^{(1)}_{\vec{\alpha}_1}(t_1), \dots P^{(n)}_{\vec{\alpha}_n}(t_n)\}$. At each time $t_i$, we have a distinct set of projectors $P^{(i)}_\alpha$, and the particular history is described by a vector of specific projectors labeled by $\vec{\alpha}$. The decoherence functional of two histories $\vec{\alpha}$ and $\vec{\alpha}'$ is

$$D(\vec{\alpha}, \vec{\alpha}') = \text{Tr}[P^{(n)}_{\vec{\alpha}_n}(t_n) \cdots P^{(1)}_{\vec{\alpha}_1}(t_1) \rho(t_0) P^{(1)}_{\vec{\alpha}'_1}(t_1) \cdots P^{(n)}_{\vec{\alpha}'_n}(t_n)] \ , \tag{4.57}$$

where the trace is taken over the complete Hilbert space. If the decoherence functional vanishes for two histories, we say that those histories are consistent or decoherent, and they can be treated according to the rules of classical probability theory.

The case of interest to us is relatively simple. Starting with an initial condition at $t_0$, we investigate histories that either do or do not look like the specified fluctuations at $t_1$, so that $\{P_\alpha^{(1)}\} = \{P_F^{(1)}, P_N^{(1)}\}$, and then evolve back to their starting point at a later time $t_2$. The Heisenberg-picture projectors $P_\alpha(t)$ are related to time-independent ones by

$$P_\alpha(t_0 + \Delta t) = e^{i\hat{H}\Delta t} P_\alpha e^{-i\hat{H}\Delta t} \ . \tag{4.58}$$

Defining $\Delta t_1 = t_1 - t_0$ and $\Delta t_2 = t_2 - t_1$, we have

$$D(\vec{\alpha}, \vec{\alpha}') = \text{Tr}[P_{\vec{\alpha}_2} e^{-i\hat{H}\Delta t_2} P_{\vec{\alpha}_1} e^{-i\hat{H}\Delta t_1} \rho(t_0) e^{i\hat{H}\Delta t_1} P_{\vec{\alpha}_1'} e^{i\hat{H}\Delta t_2} P_{\vec{\alpha}_2'}] \ . \tag{4.59}$$

Note from (4.57), (4.56), and the cyclic property of the trace, the histories of interest always end in the same place, $P_{\vec{\alpha}_n}^{(n)} = P_{\vec{\alpha}_n'}^{(n)}$, since $D(\vec{\alpha}, \vec{\alpha}')$ vanishes trivially otherwise. We therefore write the last projector as $P_{\vec{\alpha}_2'} = \delta_{\vec{\alpha}_2, \vec{\alpha}_2'}$. We can express the density matrix and the projectors in the energy eigenbasis:

$$P_{\alpha_1}^{(1)} = \sum_{nm} p_{\alpha_1}^{nm} |E_n\rangle\langle E_m| \ , \tag{4.60}$$

$$P_{\alpha_2}^{(2)} = \sum_{nm} q_{\alpha_2}^{nm} |E_n\rangle\langle E_m| \ , \tag{4.61}$$

$$\rho(t_0) = \sum_{n,m} \rho^{nm} |E_n\rangle\langle E_m| \ . \tag{4.62}$$

Acting the Hamiltonian on the energy eigenstates and summing over Kronecker delta functions, we obtain

$$D(\vec{\alpha}, \vec{\alpha}') = \sum_{n_1, m_1, n_1', m_1'} q_{\vec{\alpha}_2}^{m_1' n_1} p_{\vec{\alpha}_1}^{n_1 m_1} p_{\vec{\alpha}_1'}^{n_1' m_1'} \rho^{m_1 n_1'} e^{-i[(E_{n_1} - E_{m_1'})\Delta t_2 + (E_{m_1} - E_{n_1'})\Delta t_1]} \delta_{\vec{\alpha}_2, \vec{\alpha}_2'} \ . \tag{4.63}$$

For generic values of the energy eigenvalues (*i.e.*, neglecting conspiracies that would make the energy differences all rational multiples of each other), the real and imaginary parts of this expression are almost periodic functions. Following similar logic used to derive the quantum recurrence theorem in Appendix 7.1 of [22], in a finite-dimensional Hilbert space, there will always be times $\Delta t_1$, $\Delta t_2$ such that $|D(\vec{\alpha}, \vec{\alpha}')| < \epsilon$ for any positive $\epsilon$. Moreover, there will always be a $\Delta t_2$ for which the decoherence functional approximately vanishes for any fixed $\Delta t_1$, and vice versa. This result confirms our intuition that time-dependent states will generally exhibit fluctuations into any allowed

configuration, given sufficient time.

Now consider the case where the initial density matrix is stationary, meaning it is diagonal in the energy eigenbasis:

$$\rho^{mn} = r_m \delta^{mn} \ . \tag{4.64}$$

Plugging into (4.63) and changing dummy indices, we get

$$D(\vec{\alpha}, \vec{\alpha}') = \sum_{n,m,\ell} q_{\vec{\alpha}_2}^{mn} p_{\vec{\alpha}_1}^{n\ell} p_{\vec{\alpha}_1'}^{\ell m} r_\ell e^{-i(E_n - E_m)\Delta t_2} \delta_{\vec{\alpha}_2, \vec{\alpha}_2'} \ . \tag{4.65}$$

We want the final projector to be onto the same kind of state we originally started with, since we are asking about the reality of fluctuations in such states. Thus, we have

$$P_{\alpha_2}^{(2)} = \sum_m r_m \, |E_m\rangle\langle E_m| \ , \qquad q_{\alpha_2}^{mn} = r_m \delta^{mn} \tag{4.66}$$

and obtain

$$D(\vec{\alpha}, \vec{\alpha}') = \sum_{n,\ell} p_{\vec{\alpha}_1}^{n\ell} p_{\vec{\alpha}_1'}^{\ell n} r_n r_\ell \delta_{\vec{\alpha}_2, \vec{\alpha}_2'} \ . \tag{4.67}$$

Unlike the generic case, where the initial density matrix and final projector are both stationary, the decoherence functional describing histories with and without fluctuations is some fixed constant, which never evolves to zero. Therefore, even when a projection operator describing some sought-after fluctuation has a nonzero norm when acting on a state, it does not imply that the state actually exhibits such a fluctuation, in the sense that a history in which the configuration appears decoheres from those in which it does not. This example helps illustrate the fundamental difference between quantum fluctuations (which require external observers) and Boltzmann fluctuations (which are dynamical events in time-dependent states).

# Bibliography

[1] **Supernova Search Team** Collaboration, "Observational Evidence from Supernovae for an Accelerating Universe and a Cosmological Constant," *Astron. J.* **116** (1998) 1009, arXiv:astro-ph/9805201 [astro-ph].

[2] **Supernova Cosmology Project** Collaboration, "Measurements of Omega and Lambda from 42 High Redshift Supernovae," *Astrophys. J.* **517** (1999) 565, arXiv:astro-ph/9812133 [astro-ph].

[3] T. Bunch and P. Davies, "Quantum Field Theory in de Sitter Space: Renormalization by Point Splitting," *Proc. Roy. Soc. Lond.* **A360** (1978) 117.

[4] T. Bunch and P. Davies, "Nonconformal Renormalized Stress Tensors in Robertson-Walker Space-Times," *J. Phys.* **A11** (1978) 1315.

[5] J. Hartle and S. Hawking, "Path Integral Derivation of Black Hole Radiance," *Phys. Rev.* **D13** (1976) 2188.

[6] G. Gibbons and S. Hawking, "Cosmological Event Horizons, Thermodynamics, and Particle Creation," *Phys. Rev.* **D15** (1977) 2738.

[7] T. Banks, "Cosmological Breaking of Supersymmetry? Or Little Lambda Goes Back to the Future 2," *Int. J. Mod. Phys.* **A16** (2001) 910, arXiv:hep-th/0007146 [hep-th].

[8] T. Banks and W. Fischler, "M Theory Observables for Cosmological Space-Times," arXiv:hep-th/0102077 [hep-th].

[9] D. H. Lyth and A. R. Liddle, *The Primordial Density Perturbation: Cosmology, Inflation and the Origin of Structure.* Cambridge University Press, Revised edition 2009.

[10] S. Dodelson, *Modern Cosmology.* Academic Press, San Diego, CA, 2003.

[11] D. Baumann, "TASI Lectures on Inflation," arXiv:0907.5424 [hep-th].

[12] A. Vilenkin, "The Birth of Inflationary Universes," *Phys. Rev.* **D27** (1983) 2848.

[13] A. S. Goncharov and A. D. Linde, "Global Structure of the Inflationary Universe," *Zh. Eksp. Teor. Fiz.* **92** (1987) 1137.

[14] A. Goncharov, A. D. Linde, and V. F. Mukhanov, "The Global Structure of the Inflationary Universe," *Int. J. Mod. Phys.* **A2** (1987) 561.

[15] S. Weinberg, "Anthropic Bound on the Cosmological Constant," *Phys. Rev. Lett.* **59** (1987) 2607.

[16] R. Bousso and J. Polchinski, "Quantization of Four Form Fluxes and Dynamical Neutralization of the Cosmological Constant," *J. High Energy Phys.* **0006** (2000) 006, `arXiv:hep-th/0004134 [hep-th]`.

[17] S. Kachru, R. Kallosh, A. D. Linde, and S. P. Trivedi, "De Sitter Vacua in String Theory," *Phys. Rev.* **D68** (2003) 046005, `arXiv:hep-th/0301240 [hep-th]`.

[18] L. Susskind, "The Anthropic Landscape of String Theory," in *The Davis Meeting On Cosmic Inflation*. Mar, 2003. `arXiv:hep-th/0302219 [hep-th]`.

[19] F. Denef and M. R. Douglas, "Distributions of Flux Vacua," *J. High Energy Phys.* **0405** (2004) 072, `arXiv:hep-th/0404116 [hep-th]`.

[20] K.-M. Lee and E. J. Weinberg, "Decay of the True Vacuum in Curved Space-Time," *Phys. Rev.* **D36** (1987) 1088.

[21] A. Aguirre, S. M. Carroll, and M. C. Johnson, "Out of Equilibrium: Understanding Cosmological Evolution to Lower-Entropy States," *J. Cosmol. Astropart. Phys.* **1202** (2012) 024, `arXiv:1108.0417 [hep-th]`.

[22] L. Dyson, M. Kleban, and L. Susskind, "Disturbing Implications of a Cosmological Constant," *J. High Energy Phys.* **0210** (2002) 011, `arXiv:hep-th/0208013 [hep-th]`.

[23] A. Albrecht and L. Sorbo, "Can the Universe Afford Inflation?," *Phys. Rev.* **D70** (2004) 063528, `arXiv:hep-th/0405270 [hep-th]`.

[24] R. Bousso and B. Freivogel, "A Paradox in the Global Description of the Multiverse," *J. High Energy Phys.* **0706** (2007) 018, `arXiv:hep-th/0610132 [hep-th]`.

[25] D. N. Page, "Is Our Universe Likely to Decay within 20 Billion Years?," *Phys. Rev.* **D78** (2008) 063535, `arXiv:hep-th/0610079 [hep-th]`.

[26] A. D. Linde, "Sinks in the Landscape, Boltzmann Brains, and the Cosmological Constant Problem," *J. Cosmol. Astropart. Phys.* **0701** (2007) 022, `arXiv:hep-th/0611043 [hep-th]`.

[27] K. K. Boddy and S. M. Carroll, "Can the Higgs Boson Save Us From the Menace of the Boltzmann Brains?," `arXiv:1308.4686 [hep-ph]`.

[28] K. K. Boddy, S. M. Carroll, and J. Pollack, "De Sitter Space Without Quantum Fluctuations," `arXiv:1405.0298 [hep-th]`.

[29] A. Sirlin and R. Zucchini, "Dependence of the Quartic Coupling h(M) on m(H) and the Possible Onset of New Physics in the Higgs Sector of the Standard Model," *Nucl. Phys.* **B266** (1986) 389.

[30] M. Sher, "Electroweak Higgs Potentials and Vacuum Stability," *Phys. Rep.* **179** (1989) 273.

[31] J. Casas, J. Espinosa, and M. Quiros, "Improved Higgs Mass Stability Bound in the Standard Model and Implications for Supersymmetry," *Phys. Lett.* **B342** (1995) 171, `arXiv:hep-ph/9409458 [hep-ph]`.

[32] J. Espinosa and M. Quiros, "Improved Metastability Bounds on the Standard Model Higgs Mass," *Phys. Lett.* **B353** (1995) 257, `arXiv:hep-ph/9504241 [hep-ph]`.

[33] J. Casas, J. Espinosa, and M. Quiros, "Standard Model Stability Bounds for New Physics within LHC Reach," *Phys. Lett.* **B382** (1996) 374, `arXiv:hep-ph/9603227 [hep-ph]`.

[34] G. Isidori, G. Ridolfi, and A. Strumia, "On the Metastability of the Standard Model Vacuum," *Nucl. Phys.* **B609** (2001) 387, `arXiv:hep-ph/0104016 [hep-ph]`.

[35] J. Espinosa, G. Giudice, and A. Riotto, "Cosmological Implications of the Higgs Mass Measurement," *J. Cosmol. Astropart. Phys.* **0805** (2008) 002, `arXiv:0710.2484 [hep-ph]`.

[36] N. Arkani-Hamed, S. Dubovsky, L. Senatore, and G. Villadoro, "(No) Eternal Inflation and Precision Higgs Physics," *J. High Energy Phys.* **0803** (2008) 075, `arXiv:0801.2399 [hep-ph]`.

[37] J. Ellis, J. Espinosa, G. Giudice, A. Hoecker, and A. Riotto, "The Probable Fate of the Standard Model," *Phys. Lett.* **B679** (2009) 369, `arXiv:0906.0954 [hep-ph]`.

[38] J. Elias-Miro, J. R. Espinosa, G. F. Giudice, G. Isidori, A. Riotto, *et al.*, "Higgs Mass Implications on the Stability of the Electroweak Vacuum," *Phys. Lett.* **B709** (2012) 222, `arXiv:1112.3022 [hep-ph]`.

[39] S. Alekhin, A. Djouadi, and S. Moch, "The Top Quark and Higgs Boson Masses and the Stability of the Electroweak Vacuum," *Phys. Lett.* **B716** (2012) 214, `arXiv:1207.0980 [hep-ph]`.

[40] F. Bezrukov, M. Y. Kalmykov, B. A. Kniehl, and M. Shaposhnikov, "Higgs Boson Mass and New Physics," *J. High Energy Phys.* **1210** (2012) 140, `arXiv:1205.2893 [hep-ph]`.

[41] G. Degrassi, S. Di Vita, J. Elias-Miro, J. R. Espinosa, G. F. Giudice, *et al.*, "Higgs Mass and Vacuum Stability in the Standard Model at NNLO," *J. High Energy Phys.* **1208** (2012) 098, `arXiv:1205.6497 [hep-ph]`.

[42] D. Buttazzo, G. Degrassi, P. P. Giardino, G. F. Giudice, F. Sala, *et al.*, "Investigating the Near-Criticality of the Higgs Boson," `arXiv:1307.3536 [hep-ph]`.

[43] S. Winitzki, "Predictions in Eternal Inflation," *Lect. Notes Phys.* **738** (2008) 157, `arXiv:gr-qc/0612164 [gr-qc]`.

[44] A. Aguirre, S. Gratton, and M. C. Johnson, "Hurdles for Recent Measures in Eternal Inflation," *Phys. Rev.* **D75** (2007) 123501, `arXiv:hep-th/0611221 [hep-th]`.

[45] A. D. Linde, V. Vanchurin, and S. Winitzki, "Stationary Measure in the Multiverse," *J. Cosmol. Astropart. Phys.* **0901** (2009) 031, `arXiv:0812.0005 [hep-th]`.

[46] D. Schwartz-Perlov and A. Vilenkin, "Measures for a Transdimensional Multiverse," *J. Cosmol. Astropart. Phys.* **1006** (2010) 024, `arXiv:1004.4567 [hep-th]`.

[47] B. Freivogel, "Making Predictions in the Multiverse," *Class. Quant. Grav.* **28** (2011) 204007, `arXiv:1105.0244 [hep-th]`.

[48] M. P. Salem, "Bubble Collisions and Measures of the Multiverse," *J. Cosmol. Astropart. Phys.* **1201** (2012) 021, `arXiv:1108.0040 [hep-th]`.

[49] L. Susskind, L. Thorlacius, and J. Uglum, "The Stretched horizon and black hole complementarity," *Phys. Rev.* **D48** (1993) 3743, `arXiv:hep-th/9306069 [hep-th]`.

[50] H. H. Patel and M. J. Ramsey-Musolf, "Baryon Washout, Electroweak Phase Transition, and Perturbation Theory," *J. High Energy Phys.* **1107** (2011) 029, `arXiv:1101.4665 [hep-ph]`.

[51] N. Nielsen, "On the Gauge Dependence of Spontaneous Symmetry Breaking in Gauge Theories," *Nucl. Phys.* **B101** (1975) 173.

[52] R. Fukuda and T. Kugo, "Gauge Invariance in the Effective Action and Potential," *Phys. Rev.* **D13** (1976) 3469.

[53] S. R. Coleman and E. J. Weinberg, "Radiative Corrections as the Origin of Spontaneous Symmetry Breaking," *Phys. Rev.* **D7** (1973) 1888.

[54] C. Ford, I. Jack, and D. Jones, "The Standard Model Effective Potential at Two Loops," *Nucl. Phys.* **B387** (1992) 373, `arXiv:hep-ph/0111190 [hep-ph]`.

[55] S. P. Martin, "Two Loop Effective Potential for a General Renormalizable Theory and Softly Broken Supersymmetry," *Phys. Rev.* **D65** (2002) 116003, `arXiv:hep-ph/0111209 [hep-ph]`.

[56] J. Casas, J. Espinosa, M. Quiros, and A. Riotto, "The Lightest Higgs Boson Mass in the Minimal Supersymmetric Standard Model," *Nucl. Phys.* **B436** (1995) 3, `arXiv:hep-ph/9407389 [hep-ph]`.

[57] B. M. Kastening, "Renormalization Group Improvement of the Effective Potential in Massive phi**4 Theory," *Phys. Lett.* **B283** (1992) 287.

[58] M. Bando, T. Kugo, N. Maekawa, and H. Nakano, "Improving the Effective Potential," *Phys. Lett.* **B301** (1993) 83, `arXiv:hep-ph/9210228 [hep-ph]`.

[59] M. Bando, T. Kugo, N. Maekawa, and H. Nakano, "Improving the Effective Potential: Multimass Scale Case," *Prog. Theor. Phys.* **90** (1993) 405, `arXiv:hep-ph/9210229 [hep-ph]`.

[60] S. R. Coleman, "The Fate of the False Vacuum. 1. Semiclassical Theory," *Phys. Rev.* **D15** (1977) 2929.

[61] G. Isidori, V. S. Rychkov, A. Strumia, and N. Tetradis, "Gravitational Corrections to Standard Model Vacuum Decay," *Phys. Rev.* **D77** (2008) 025034, `arXiv:0712.0242 [hep-ph]`.

[62] **Tevatron Electroweak Working Group, D0** Collaboration, "Combination of CDF and DO Results on the Mass of the Top Quark using up to 8.7 $fb^{-1}$ at the Tevatron," `arXiv:1305.3929 [hep-ex]`.

[63] **CMS** Collaboration, "Determination of the Top-Quark Pole Mass and Strong Coupling Constant from the $t\bar{t}$ Production Cross Section in pp Collisions at $\sqrt{s} = 7$ TeV," *Phys. Lett.* **B728** (2014) 496, `arXiv:1307.1907 [hep-ex]`.

[64] **Particle Data Group** Collaboration, "Review of Particle Physics (RPP)," *Phys. Rev.* **D86** (2012) 010001.

[65] P. P. Giardino, K. Kannike, I. Masina, M. Raidal, and A. Strumia, "The Universal Higgs Fit," `arXiv:1303.3570 [hep-ph]`.

[66] "Updated Measurements of the Higgs Boson at 125 GeV in the Two Photon Decay Channel," Tech. Rep. CMS-PAS-HIG-13-001, CERN, Geneva, 2013.

[67] "Properties of the Higgs-like Boson in the Decay H to ZZ to 4l in pp Collisions at sqrt s =7 and 8 TeV," Tech. Rep. CMS-PAS-HIG-13-002, CERN, Geneva, 2013.

[68] "Measurements of the Properties of the Higgs-like Boson in the Two Photon Decay Channel with the ATLAS Detector using 25 fb$^{-1}$ of Proton-Proton Collision Data," Tech. Rep. ATLAS-CONF-2013-012, CERN, Geneva, Mar, 2013.

[69] "Measurements of the Properties of the Higgs-like Boson in the Four Lepton Decay Channel with the ATLAS Detector using 25 fb1 of Proton-Proton Collision Data," Tech. Rep. ATLAS-CONF-2013-013, CERN, Geneva, Mar, 2013.

[70] **CMS** Collaboration, "Measurement of the Top-Quark Mass in All-Jets $t\bar{t}$ Events in pp Collisions at $\sqrt{s}$=7 TeV," *Eur. Phys. J.* **C74** (2014) 2758, `arXiv:1307.4617 [hep-ex]`.

[71] "Measurement of the top quark mass in dileptonic top quark pair decays with $\sqrt{s} = 7$ tev atlas data," Tech. Rep. ATLAS-CONF-2013-077, CERN, Geneva, Jul, 2013.

[72] F. Jegerlehner, M. Y. Kalmykov, and B. A. Kniehl, "On the Difference Between the Pole and the MSbar Masses of the Top Quark at the Electroweak Scale," *Phys. Lett.* **B722** (2013) 123, `arXiv:1212.4319 [hep-ph]`.

[73] B. Craps, T. Hertog, and N. Turok, "On the Quantum Resolution of Cosmological Singularities using AdS/CFT," *Phys. Rev.* **D86** (2012) 043513, `arXiv:0712.4180 [hep-th]`.

[74] J. Maldacena, "Vacuum Cecay into Anti de Sitter Space," `arXiv:1012.0274 [hep-th]`.

[75] A. D. Linde, "Eternally Existing Self Reproducing Chaotic Inflationary Universe," *Phys. Lett.* **B175** (1986) 395.

[76] A. Vilenkin, "Predictions from Quantum Cosmology," *Phys. Rev. Lett.* **74** (1995) 846, `arXiv:gr-qc/9406010 [gr-qc]`.

[77] R. Bousso, B. Freivogel, and I.-S. Yang, "Boltzmann Babies in the Proper Time Measure," *Phys. Rev.* **D77** (2008) 103514, `arXiv:0712.3324 [hep-th]`.

[78] M. Tegmark, "What does Inflation Really Predict?," *J. Cosmol. Astropart. Phys.* **0504** (2005) 001, `arXiv:astro-ph/0410281 [astro-ph]`.

[79] A. D. Linde and A. Mezhlumian, "Stationary Universe," *Phys. Lett.* **B307** (1993) 25, `arXiv:gr-qc/9304015 [gr-qc]`.

[80] A. D. Linde, D. A. Linde, and A. Mezhlumian, "From the Big Bang Theory to the Theory of a Stationary Universe," *Phys. Rev.* **D49** (1994) 1783, `arXiv:gr-qc/9306035 [gr-qc]`.

[81] A. De Simone, A. H. Guth, A. D. Linde, M. Noorbala, M. P. Salem, *et al.*, "Boltzmann Brains and the Scale-Factor Cutoff Measure of the Multiverse," *Phys. Rev.* **D82** (2010) 063520, `arXiv:0808.3778 [hep-th]`.

[82] R. Bousso, "Holographic Probabilities in Eternal Inflation," *Phys. Rev. Lett.* **97** (2006) 191302, `arXiv:hep-th/0605263 [hep-th]`.

[83] Y. Sekino, S. Shenker, and L. Susskind, "On the Topological Phases of Eternal Inflation," *Phys. Rev.* **D81** (2010) 123515, `arXiv:1003.1347 [hep-th]`.

[84] O. Lebedev, "On Stability of the Electroweak Vacuum and the Higgs Portal," *Eur. Phys. J.* **C72** (2012) 2058, `arXiv:1203.0156 [hep-ph]`.

[85] J. Elias-Miro, J. R. Espinosa, G. F. Giudice, H. M. Lee, and A. Strumia, "Stabilization of the Electroweak Vacuum by a Scalar Threshold Effect," *J. High Energy Phys.* **1206** (2012) 031, `arXiv:1203.0237 [hep-ph]`.

[86] J. Casas, V. Di Clemente, A. Ibarra, and M. Quiros, "Massive Neutrinos and the Higgs Mass Window," *Phys. Rev.* **D62** (2000) 053005, `arXiv:hep-ph/9904295 [hep-ph]`.

[87] M. Spradlin, A. Strominger, and A. Volovich, "Les Houches Lectures on de Sitter Space," `arXiv:hep-th/0110007 [hep-th]`.

[88] R. M. Wald, "Asymptotic Behavior of Homogeneous Cosmological Models in the Presence of a Positive Cosmological Constant," *Phys. Rev.* **D28** (1983) 2118.

[89] S. Hollands, "Correlators, Feynman Diagrams, and Quantum No-Hair in de Sitter Spacetime," *Commun. Math. Phys.* **319** (2013) 1, `arXiv:1010.5367 [gr-qc]`.

[90] D. Marolf and I. A. Morrison, "The IR Stability of de Sitter QFT: Results at All Orders," *Phys. Rev.* **D84** (2011) 044040, `arXiv:1010.5327 [gr-qc]`.

[91] C. R. Stephens, G. 't Hooft, and B. F. Whiting, "Black Hole Evaporation without Information Loss," *Class. Quant. Grav.* **11** (1994) 621, `arXiv:gr-qc/9310006 [gr-qc]`.

[92] M. K. Parikh, I. Savonije, and E. P. Verlinde, "Elliptic de Sitter Space: dS/Z(2)," *Phys. Rev.* **D67** (2003) 064005, `arXiv:hep-th/0209120 [hep-th]`.

[93] M. Schlosshauer, "Decoherence, the Measurement Problem, and Interpretations of Quantum Mechanics," *Rev. Mod. Phys.* **76** (2004) 1267, `arXiv:quant-ph/0312059 [quant-ph]`.

[94] D. Wallace, *The Emergent Multiverse.* Oxford University Press, Oxford, 2012. `http://dx.doi.org/10.1093/acprof:oso/9780199546961.001.0001`.

[95] A. Elby and J. Bub, "Triorthogonal Uniqueness Theorem and Its Relevance to the Interpretation of Quantum Mechanics," *Phys. Rev.* **49** (1994) 4213.

[96] W. Zurek, "Pointer Basis of Quantum Apparatus: Into What Mixture Does the Wave Packet Collapse?," *Phys. Rev.* **D24** (1981) 1516.

[97] W. H. Zurek, "Preferred states, predictability, classicality and the environment-induced decoherence," *Prog. Theor. Phys.* **89** (1993) 281.

[98] W. H. Zurek, "Decoherence, Einselection, and the Existential Interpretation: The Rough Guide," *Phil. Trans. Roy. Soc. Lond.* **A356** (1998) 1793, `arXiv:quant-ph/9805065 [quant-ph]`.

[99] W. H. Zurek, "Decoherence, Einselection, and the Quantum Origins of the Classical," *Rev. Mod. Phys.* **75** (2003) 715, `arXiv:quant-ph/0105127`.

[100] S. Khlebnikov and M. Kruczenski, "Thermalization of Isolated Quantum Systems," `arXiv:1312.4612 [cond-mat.stat-mech]`.

[101] D. N. Page and W. K. Wootters, "Evolution without Evolution: Dynamics Described by Stationary Observables," *Phys. Rev.* **D27** (1983) 2885.

[102] M. Davenport and K. D. Olum, "Are There Boltzmann Brains in the Vacuum?," `arXiv:1008.0808 [hep-th]`.

[103] G. Lindblad, "On the Generators of Quantum Dynamical Semigroups," *Commun. Math. Phys.* **48** (1976) 119.

[104] F. Marquardt and A. Püttmann, "Introduction to Dissipation and Decoherence in Quantum Systems," `arXiv:0809.4403 [quant-ph]`.

[105] W. Zurek, "Environment Induced Superselection Rules," *Phys. Rev.* **D26** (1982) 1862.

[106] N. D. Birrell and P. C. W. Davies, *Quantum Fields in Curved Space*. Cambridge Monographs on Mathematical Physics. Cambridge University Press, 1984. First published 1982. Reprinted 1989, 1992, 1994.

[107] B. Allen, "Vacuum States in de Sitter Space," *Phys. Rev.* **D32** (1985) 3136.

[108] P. Candelas and D. Raine, "General Relativistic Quantum Field Theory-An Exactly Soluble Model," *Phys. Rev.* **D12** (1975) 965.

[109] J. Géhéniau and C. Schomblond *Acad. R. Belg. Bull. Cl. Sci.* **54** (1968) 1147.

[110] C. Schomblond and P. Spindel, "Unicity Conditions of the Scalar Field Propagator Delta(1)(x,y) in de Sitter Universe," *Annales Poincare Phys. Theor.* **25** (1976) 67.

[111] N. Chernikov and E. Tagirov, "Quantum Theory of Scalar Fields in de Sitter Space-Time," *Annales Poincare Phys. Theor.* **A9** (1968) 109.

[112] E. Tagirov, "Consequences of Field Quantization in de Sitter Type Cosmological Models," *Annals Phys.* **76** (1973) 561.

[113] E. Mottola, "Particle Creation in de Sitter Space," *Phys. Rev.* **D31** (1985) 754.

[114] R. Bousso, A. Maloney, and A. Strominger, "Conformal Vacua and Entropy in de Sitter Space," *Phys. Rev.* **D65** (2002) 104039, `arXiv:hep-th/0112218 [hep-th]`.

[115] S. Hollands, "Massless Interacting Quantum Fields in de Sitter Spacetime," *Annales Henri Poincare* **13** (2012) 1039, `arXiv:1105.1996 [gr-qc]`.

[116] Y. Nomura, "Physical Theories, Eternal Inflation, and Quantum Universe," *J. High Energy Phys.* **1111** (2011) 063, `arXiv:1104.2324 [hep-th]`.

[117] Y. Nomura, "Quantum Mechanics, Spacetime Locality, and Gravity," *Found. Phys.* **43** (2013) 978, `arXiv:1110.4630 [hep-th]`.

[118] J. D. Bekenstein, "Black Holes and Entropy," *Phys. Rev.* **D7** (1973) 2333.

[119] S. Hawking, "Gravitational Radiation from Colliding Black Holes," *Phys. Rev. Lett.* **26** (1971) 1344.

[120] N. Goheer, M. Kleban, and L. Susskind, "The Trouble with de Sitter Space," *J. High Energy Phys.* **0307** (2003) 056, `arXiv:hep-th/0212209 [hep-th]`.

[121] T. Banks, "Some Thoughts on the Quantum Theory of Stable de Sitter Space," `arXiv:hep-th/0503066 [hep-th]`.

[122] S. B. Giddings and D. Marolf, "A Global Picture of Quantum de Sitter Space," *Phys. Rev.* **D76** (2007) 064023, `arXiv:0705.1178 [hep-th]`.

[123] S. R. Coleman and F. De Luccia, "Gravitational Effects on and of Vacuum Decay," *Phys. Rev.* **D21** (1980) 3305.

[124] L. Susskind, "The Census Taker's Hat," `arXiv:0710.1129 [hep-th]`.

[125] Y. Sekino and L. Susskind, "Census Taking in the Hat: FRW/CFT Duality," *Phys. Rev.* **D80** (2009) 083531, `arXiv:0908.3844 [hep-th]`.

[126] R. Bousso and L. Susskind, "The Multiverse Interpretation of Quantum Mechanics," *Phys. Rev.* **D85** (2012) 045007, `arXiv:1105.3796 [hep-th]`.

[127] I. Gott, J. Richard, "Boltzmann Brains: I'd Rather See Than Be One," `arXiv:0802.0233 [gr-qc]`.

[128] S. Aaronson, "The Ghost in the Quantum Turing Machine," `arXiv:1306.0159 [quant-ph]`.

[129] S. M. Carroll, "What if Time Really Exists?," `arXiv:0811.3772 [gr-qc]`.

[130] J. Garriga and A. Vilenkin, "Recycling Universe," *Phys. Rev.* **D57** (1998) 2230, `arXiv:astro-ph/9707292 [astro-ph]`.

[131] D. Polarski and A. A. Starobinsky, "Semiclassicality and Decoherence of Cosmological Perturbations," *Class. Quant. Grav.* **13** (1996) 377, `arXiv:gr-qc/9504030 [gr-qc]`.

[132] F. C. Lombardo and D. Lopez Nacir, "Decoherence during Inflation: The Generation of Classical Inhomogeneities," *Phys. Rev.* **D72** (2005) 063506, `arXiv:gr-qc/0506051 [gr-qc]`.

[133] P. Martineau, "On the Decoherence of Primordial Fluctuations during Inflation," *Class. Quant. Grav.* **24** (2007) 5817, `arXiv:astro-ph/0601134 [astro-ph]`.

[134] C. P. Burgess, R. Holman, and D. Hoover, "Decoherence of Inflationary Primordial Fluctuations," *Phys. Rev.* **D77** (2008) 063534, `arXiv:astro-ph/0601646 [astro-ph]`.

[135] C. Kiefer, I. Lohmar, D. Polarski, and A. A. Starobinsky, "Pointer States for Primordial Fluctuations in Inflationary Cosmology," *Class. Quant. Grav.* **24** (2007) 1699, `arXiv:astro-ph/0610700 [astro-ph]`.

[136] P. Creminelli, S. Dubovsky, A. Nicolis, L. Senatore, and M. Zaldarriaga, "The Phase Transition to Slow-Roll Eternal Inflation," *J. High Energy Phys.* **0809** (2008) 036, `arXiv:0802.1067 [hep-th]`.

[137] S. Dubovsky, L. Senatore, and G. Villadoro, "Universality of the Volume Bound in Slow-Roll Eternal Inflation," *J. High Energy Phys.* **1205** (2012) 035, `arXiv:1111.1725 [hep-th]`.

[138] E. J. Martinec and W. E. Moore, "Modeling Quantum Gravity Effects in Inflation," `arXiv:1401.7681 [hep-th]`.

[139] **BICEP2** Collaboration, "BICEP2 I: Detection Of B-mode Polarization at Degree Angular Scales," `arXiv:1403.3985 [astro-ph.CO]`.

[140] R. Bousso, "Proliferation of de Sitter space," *Phys. Rev.* **D58** (1998) 083511, `arXiv:hep-th/9805081 [hep-th]`.

[141] D. Bohm, "A Suggested Interpretation of the Quantum Theory in Terms of Hidden Variables. 1.," *Phys. Rev.* **85** (1952) 166.

[142] D. Bohm, "A Suggested Interpretation of the Quantum Theory in Terms of Hidden Variables. 2.," *Phys. Rev.* **85** (1952) 180.

[143] D. Durr, S. Goldstein, R. Tumulka, and N. Zanghi, "Bohmian Mechanics and Quantum Field Theory," *Phys. Rev. Lett.* **93** (2004) 090402, `arXiv:quant-ph/0303156 [quant-ph]`.

[144] W. Struyve, "Pilot-Wave Theory and Quantum Fields," *Rept. Prog. Phys.* **73** (2010) 106001, `arXiv:0707.3685 [quant-ph]`.

[145] G. Ghirardi, A. Rimini, and T. Weber, "A Model for a Unified Quantum Description of Macroscopic and Microscopic Systems," in *Quantum Probability and Applications II*, pp. 223–232. Springer, 1985.

[146] G. Ghirardi, A. Rimini, and T. Weber, "Unified Dynamics for Microscopic and Macroscopic Systems," *Phys. Rev.* **D34** (1986) 470.

[147] R. B. Griffiths, "Consistent Histories and the Interpretation of Quantum Mechanics," *J. Statist. Phys.* **36** (1984) 219.

[148] R. Omnes, "Consistent Interpretations of Quantum Mechanics," *Rev. Mod. Phys.* **64** (1992) 339.

[149] M. Gell-Mann and J. B. Hartle, "Classical Equations for Quantum Systems," *Phys. Rev.* **D47** (1993) 3345, `arXiv:gr-qc/9210010 [gr-qc]`.

[150] J. B. Hartle, "The Quantum Mechanics of Closed Systems," `arXiv:gr-qc/9210006 [gr-qc]`.

[151] J. Halliwell, "A Review of the Decoherent Histories Approach to Quantum Mechanics," *Annals N.Y. Acad. Sci.* **755** (1995) 726, `arXiv:gr-qc/9407040 [gr-qc]`.

[152] J. B. Hartle, R. Laflamme, and D. Marolf, "Conservation Laws in the Quantum Mechanics of Closed Systems," *Phys. Rev.* **D51** (1995) 7007, `arXiv:gr-qc/9410006 [gr-qc]`.